Università della Calabria

Facoltà di Ingegneria

SCUOLA DI DOTTORATO "PITAGORA"
IN SCIENZE INGEGNERISTICHE

Tesi di Dottorato – XXV Ciclo

Sviluppo di modelli multibody avanzati per la dinamica delle ruote dentate.

Relatore
Prof. Domenico Mundo
UNIVERSITA' DELLA CALABRIA

Co-relatore
Prof. Wim Desmet
KATHOLIEKE UNIVERSITEIT LEUVEN

Candidato
Antonio Palermo

Anno Accademico 2011/2012

Università della Calabria

Facoltà di Ingegneria

SCUOLA DI DOTTORATO "PITAGORA"
IN SCIENZE INGEGNERISTICHE

PhD Dissertation – 25th Issue

Development of advanced multibody models for gear dynamics.

Promotor
Prof. Domenico Mundo
UNIVERSITA' DELLA CALABRIA

Co-promotor
Prof. Wim Desmet
KATHOLIEKE UNIVERSITEIT LEUVEN

Candidato
Antonio Palermo

Academic Year 2011/2012

Table of Contents

***Nota sui contenuti**: Tutte le figure riprodotte da articoli disponibili in letteratura hanno ricevuto l'autorizzazione dai detentori dei diritti di copyright, gratuita o a pagamento, alla riproduzione e diffusione nella presente tesi di dottorato.*

***Note on contents**: All the figures reproduced from papers available in the literature obtained authorisation from Copyright owners, for free or purchased, for reproduction and diffusion within the present PhD dissertation.*

Prefazione

La presente tesi di dottorato rappresenta per me una espressione della mia passione per l'Ingegneria Meccanica. Le trasmissioni sono ovunque nell'industria meccancia, spaziando da applicazioni ad alta precisione ad applicazioni ad elevatissima coppia e velocita'. Dal mio punto di vista, la "miscela" di Meccanica Applicata e di Costruzione di Macchine rende le ruote dentate dei componenti affascinanti: precise relazioni geometriche giocano un ruolo fondamentale in quel complesso processo che l'ingranamento rappresenta, mentre deformazioni locali (contatto) e globali (denti, corpi ruota, struttura di supporto) impongono deviazioni sui requisiti geometrici da raggiungere per un ingranamento fluido. Inevitabili errori di lavorazione e di assemblaggio peggiorano la situazione. In tale contesto, il progettista di trasmissioni deve prestare attenzione ad una vasta serie di aspetti ingegneristici in modo da assicurarsi che la trasmissione svolga il proprio lavoro in maniera affidabile, silenziosa ed energeticamente efficiente. Non ero al corrente di tali sfide progettuali all'inizio del dottorato su questo tema di ricerca. Fortunatamente ho potuto contare sul supporto di supervisori esperti, che mi hanno aiutato lungo l'intero percorso di ricerca applicata e che continuano a farlo.

Il mio primo ringraziamento va al Prof. Domenico Mundo, a cui devo la possibilita' di iniziare il lavoro sulle trasmissioni durante la tesi specialistica presso l'azienda LMS Italiana di Torino e di continuare con il dottorato al meglio nel suo contesto di collaborazioni e nella sua rete di contatti. Egli ha sempre creduto che le mie capacita' fossero appropriate per proseguire tali studi e mi ha garantito indipendenza nel prendere le decisioni, dopo avermi consigliato in base alla sua esperienza.

Sono molto grato a Rabah Hadjit e a Sergio Lentini dal periodo in LMS Italiana, i quali mi hanno introdotto al tema delle trasmissioni con innumerevoli discussioni riguardanti le finezze dell'ingranamento. L'intero ufficio della divisione Engineering Services (ES) di Torino e' stato per me l'ambiente perfetto per lavorare e fruire dell'amicizia con tutti i compagni di squadra: Paola, Valerio, Paolo, Giancarlo, Brizzio e il mio collega tesista Stefano.

In particolare, Rabah ha rappresentato per me una guida speciale. Egli si e' sempre preoccupato di migliorare le mie capacita' condividendo la sua esperienza da specialista e supportandomi nello svolgere corsi di formazione.

Ricordero' il periodo negli Stati Uniti a lavoro nell'ufficio LMS ES di Troy, l'accoglienza della Vigilia di Natale con i bimbi e i buoni pranzi che Cristina ha preparato ad Ann Arbor.

Un altro ringraziamento speciale va al Prof. Wim Desmet, il mio supervisore alla KULeuven. Egli e' un uomo estremamente occupato, comunque il suo impegno (a prescindere se a notte fonda o nei weekend) e la sua grande esperienza rendono le sue valutazioni esaurienti e acute. Egli e' sempre stato disponibile nei momenti cruciali del mio percorso di Dottorato e ha provvisto direzioni avvedute qualora mi trovassi ad un "incrocio" importante. Gli sono anche grato per la fiducia che ripone nelle mie capacita' e per avermi consentito di intraprendere un percorso di doppio dottorato che continuera' alla KULeuven. Bert Pluymers e' stato il suo collaboratore complementare, che ha sempre organizzato i miei piani di reclutamento, grazie Bert.

Sono molto grato a Peter Mas e ad Herman Van der Auweraer, che, in qualita' di direttore dell'innovazione per la divisione ES e di direttore della ricerca aziendale, hanno considerato il mio lavoro di ricerca utile per l'azienda e continuano a supportare i miei periodi di ricerca presso LMS International. Un grazie speciale, sempre in LMS, va anche a Jan Deleener, per le sue valutazioni durante le attivita' all'ES division, e a Stijn Donders, il quale ha sempre rappresentato un punto di riferimento sebbene non coinvolto direttamente nelle mie attivita'. Stijn, grazie anche per aver partecipato alla mia discussione di dottorato interna all'Unical. Molti altri ringraziamenti saranno necessari alla fine della campagna sperimentale che stiamo attualmente svolgendo a Leuven.

Un ringraziamento speciale va anche ad un revisore altrettanto speciale e aggiuntivo: il Prof. David Dooner dell'Universita' di Puerto Rico in Mayagüez. Grazie per le valutazioni dettagliate e i consigli rivolti al prosieguo delle attivita'.

Preface

This dissertation represents for me an expression of the passion and joy I feel for Mechanical Engineering. Transmissions are everywhere in mechanical industry, ranging in applications from tiny precision to huge torque and speed. The mix of Applied Mechanics and Machine Design make gears a fascinating component from my point of view: strict geometry relationships play a crucial role in the complex process of gear meshing; local (contact) and global (teeth, gear bodies and supporting structure) deformations cause deviations on the geometric requirements to be achieved for smooth meshing. Unavoidable manufacturing and assembly errors then make things worse. In this environment, the transmission designer needs to pay attention to a wide range of engineering aspects to make sure that the transmission does its job in a reliable, quiet and energy efficient way. I was not aware of all these challenges, when I started the PhD in this research field. Fortunately I could count on the support of expert advisors who were able to help me throughout my applied research path, and continue to do so.

My first thanks goes to Prof. Domenico Mundo, who gave me the chance to start the work on transmissions during my Master Thesis within the company LMS Italiana in Torino and to continue with the PhD in the perfect frame of his collaborations and network of contacts. He also always believed in my skills to undertake these studies and provided me with freedom in taking decisions after his experienced advice.

I am very grateful to Rabah Hadjit and Sergio Lentini from the period in LMS Italiana, who introduced me to the topic of transmissions with countless discussions on the fine aspects of gear meshing. The whole Engineering Services (ES) office in Torino has been for me the perfect environment to work and enjoy a very friendly relationship with all the teammates: Paola, Valerio, Paolo, Giancarlo, Brizzio and my colleague Stefano.

In particular, Rabah has been for me a special mentor. He always took care of improving my skills by sharing his wide and specialised experience and by supporting my training activities. I will remember the US period working together in the LMS ES Troy office, the warmth of that Christmas Eve with the kids and the tasty lunches which Cristina has prepared in Ann Arbor.

Another very special thanks goes to Prof. Wim Desmet, my PhD advisor at KULeuven. He is an extremely busy man, however his commitment (no matter how late in the night or in the weekend) and his great experience make his feedbacks thorough and acute. He was always available in crucial moments of my PhD path and provided wise directions whenever I was at an important “crossroad”. I am grateful to him also for believing in my skills and allowing me to undertake a dual PhD programme which will now continue at KULeuven. Bert Pluymers has been his complementary collaborator, who always promptly arranged my HR plan, thank you Bert.

I am very grateful to Peter Mas and Herman Van der Auweraer, who, as Innovation Director for the ES division and Corporate Research Director respectively, considered my research work valuable for the company and continue supporting my research periods at LMS International. Special thanks in the LMS crew also go to Jan Deleener, for his constant feedback during activities at ES division, and to Stijn Donders, who although not directly involved in my research activities always represented a reference point to rely on. Stijn, thank you also for attending my internal PhD discussion at Unical. Many more acknowledgements will be required at the end of the gear experimental activities we are currently undertaking in Leuven.

A special acknowledgement goes also to a special and additional reviewer of this PhD dissertation: Prof. David Dooner from University of Puerto Rico at Mayagüez. Thank you for providing thorough feedback and hints for future research.

Sommario esteso

Il lavoro di tesi e' incentrato sullo sviluppo di una metodologia multibody che permetta di simulare la risposta dinamica di una trasmissione come sistema completo, considerando gli effetti di contatto non-lineari e tridimensionali sull'ingranamento delle ruote dentate.

In particolare, le ruote dentate facenti parte della trasmissione non sono analizzate in maniera isolata, bensi' risentono delle condizioni operative istantanee derivanti dalle deformazioni strutturali e dalle interazioni della trasmissione con il generatore e l'utilizzatore della potenza meccanica. Tali condizioni operative sono espresse, per tutti gli ingranaggi della trasmissione, in termini di disallineamenti istantanei e coppia trasmessa istantanea.

Lo sviluppo della metodologia e' stato svolto in collaborazione con la Katholieke Universiteit Leuven e l'azienda LMS International, entrambe situate nella citta' di Leuven (Belgio).

La tesi ha inizio con un capitolo introduttivo, prosegue con la discussione dello stato dell'arte, illustra attraverso tre capitoli di dettaglio la metodologia sviluppata, presenta i risultati numerici per due tipici casi di studio e termina con le conclusioni.

L'introduzione illustra sinteticamente le problematiche legate alla dinamica delle trasmissioni di potenza, le necessita' del contesto industriale di riferimento, la traiettoria di ricerca seguita durante il periodo di dottorato e i contributi sostanziali apportati dalla metodologia sviluppata. Tali contributi sono identificati nella possibilita' di evitare i costi computazionali imposti dalle dettagliate simulazioni di contatto, di modellare quindi in maniera dettagliata ed efficiente carichi dinamici e disallineamenti dinamici strettamente connessi alle vibrazioni e alla durabilita' delle trasmissioni meccaniche, e infine di calcolare tali quantita' fisiche attraverso una metodologia tale da poter essere utilizzata per un generico sistema meccanico rappresentato in ambiente multibody.

Il capitolo relativo allo stato dell'arte identifica tre classi principali di modellazione adottate per la dinamica delle trasmissioni meccaniche e ne analizza le relative applicazioni nei principali campi industriali, identificando punti di forza e di debolezza per ciascuna delle classi. Le tre classi analizzate includono modelli

analitici (da mono- a tri-dimensionali), modelli agli Elementi Finiti (statici e dinamici) e modelli multibody (a corpo-ruota rigido e flessibile). Le applicazioni riguardano il calcolo delle vibrazioni ai fini del comfort acustico e della durabilita' delle trasmissioni nel campo automobilistico, eolico e aeronautico. Si evidenzia come in tali applicazioni le trasmissioni rappresentino sistemi critici per il successo commmerciale dei prodotti (campo automobilistico ed eolico) o per la sicurezza degli utilizzatori (campo aeronautico).

Il primo capitolo di dettaglio (Cap. 3) analizza le motivazioni teoriche su cui si fondano le ipotesi alla base della metodologia proposta. L'Errore di Trasmissione e' identificato come l'indicatore quantitativo principale per il calcolo delle vibrazioni della trasmissione. Subito dopo sono discussi i contributi della flessibilita' dei denti e dei disallineamenti all'Errore di Trasmissione. Tale discussione fornice il substrato per comprendere come le modifiche microgeometriche delle superfici dei denti possano ridurre in maniera significativa le vibrazioni e migliorare la distribuzione delle pressioni di contatto. Sulla base delle motivazioni teoriche, la metodologia proposta permette di calcolare la rigidezza di ingranamento statica (per un range di condizioni operative) prima della simulazione dinamica e di ridurre i relativi tempi di calcolo in modo notevole, grazie alla semplice interpolazione di tale rigidezza in funzione delle condizioni operative istantanee.

Il secondo capitolo di dettaglio (Cap. 4) fornisce la formulazione matematica alla base della metodologia proposta.

Il terzo capitolo di dettaglio (Cap. 5) illustra in maniera quantitativa la sensibilita' dell'Errore di Trasmissione rispetto alle variazioni della coppia applicata, di interasse e del disallineamento angolare nel piano d'azione. Appare necessario da tale analisi includere gli effetti di tali variazioni per ottenere una risposta dinamica che sia accurata.

Il capitolo sui casi di studio mostra come la discussione condotta nei capitoli precedenti sia correttamente rintracciabile nei risultati forniti dalla metodologia proposta. Il primo caso di studio analizzato e' quello di una coppia di ruote dentate elicoidali che presentano modifiche microgeometriche della superficie dei denti ottimizzate. La variabilita' dell'Errore di Trasmissione risulta minima nelle condizioni operative di ottimo e degrada allontanandosi da tali condizioni. A bassa velocita' di rotazione i risultati dinamici convergono verso i risultati delle simulazioni statiche. Il secondo caso di studio analizzato e' un rotismo

epicicloidale a tre pianeti elicoidali. I risultati mostrano come sia necessario modellare gli effetti tridimensionali del contatto al fine di catturare correttamente la risposta dinamica del rotismo.

Abstract

This PhD dissertation focuses on the development of a multibody methodology to simulate the dynamic behaviour of geared transmissions. A key feature of the proposed methodology is the capability of accounting for detailed gear contact in system-level dynamics, such that the gears are coupled to the supporting structural elements and are affected by the mutual interactions. The formulation is suited for general multibody models where internal and external, spur and helical gears are used. Given the complexity of the meshing process, an efficient approach for accurately describing gear contact is adopted: firstly, a three-dimensional static contact problem is solved and results are stored in multivariate look-up tables for a range of operating conditions; subsequently, the dynamic simulation is launched and the look-up tables are interpolated using instantaneous values for the operating conditions, thus overcoming the need for solving a new contact problem at each time step of the simulation. A structured overview of the motivations for the proposed simulation technique is provided in the body of the dissertation and results for two cases of study are discussed.

Nomenclature

Symbol	*Description*
$\square_i$	*Subscript indicating the gear number (i=1,2) – unless otherwise stated*
$\square_r$	*Subscript indicating the reference frame – unless otherwise stated*
O_i, O_r	*Frame origins*
$\boldsymbol{x_i}$	*x axes unit vectors pointing towards each other*
$\boldsymbol{z_i}$	*z axes unit vectors towards the material pointing same direction*
$\boldsymbol{y_i}$	*y axes unit vectors obtained as $\boldsymbol{z_i}$ cross $\boldsymbol{x_i}$*
$\boldsymbol{x_r}$	
$\boldsymbol{z_r}$	*Reference frame fixed to gear 1 carrier, initially overlapping on frame 1*
$\boldsymbol{y_r}$	
DTE	*Dynamic Transmission Error on the operating pitch circle in the transverse reference plane*
DTE_r	*DTE due to relative rotation of the gears*
DTE_t	*DTE due to relative translation of the gears*
r_{poi}	*Operating pitch radius*
r_{pi}	*Pitch radius*
$\boldsymbol{CD}$	*Centre distance vector pointing from O_1 to O_2*
θ_i	*Rotation angle*
z_i	*Teeth number*
ω_i	*Angular velocity around $\boldsymbol{z_r}$ axis*
$\boldsymbol{v_{21}}$	*Relative velocity vector*
$\boldsymbol{F}$	*Normal contact force vector*
$\boldsymbol{F_{tt}}$	*Tangential contact force vector (tangent to base circles in the transverse plane)*
$\boldsymbol{F_r}$	*Radial contact force vector*
$\boldsymbol{F_{tt}}$	*Tangential contact force vector*
$\boldsymbol{F_{tn}}$	*Normal contact force in the transverse plane vector*
$\boldsymbol{F_a}$	*Axial contact force vector*
ϕ_t	*Operating transverse pressure angle*
ϕ_n	*Operating normal pressure angle*
$\boldsymbol{T}$	*Transformation vector to obtain $\boldsymbol{F}$ magnitude from F_{tt}*
F_{tt_k}	*Elastic component of F_{tt}*
F_{tt_c}	*Damping component of F_{tt}*
k	*Equivalent mesh stiffness along the tangential direction*
c	*Viscous damping coefficient*
$\boldsymbol{C}$	*Contact point coordinates vector*

$\boldsymbol{q_1}$	*Translations vector of frame 1*
FW_a	*Active (contacting) face width*
$[\boldsymbol{s}]$	$\boldsymbol{CD}$ *Scaling matrix for operating pitch point calculation*
$\boldsymbol{O_z}$	*Offset vector for axial positioning of* $\boldsymbol{C}$
FW_i	*Face width*
θ_{ip}	*Angular pitch of gear i*
θ_{is}	*Initial angular position of gear i*
CD_{xy_r}	*Centre distance projection on the reference transverse plane*
β	*Helix angle*
r_{bi}	*Base radius of gear i*
$\boldsymbol{LOA_r}$	*Line of Action unit vector in the reference frame*
$\boldsymbol{OLOA_r}$	*Offline Line of Action unit vector in the reference frame*
$\boldsymbol{POA_r}$	*Plane of action in the reference frame*
α_i	*Angular misalignment in the plane of action (angle)*
M	*Relative angular misalignment in the plane of action (slope coefficient)*
$\boldsymbol{\omega_{12}}$	*Relative angular velocity around* $\boldsymbol{z_r}$ *axis*
DTE_M	*DTE component due to angular misalignment*
F_{tt_n}	*Nominal value of* F_{tt}
T_{i_n}	*Nominal value of Torque applied to gear i*
T_i	*Torque interpolated from look-up tables using instantaneous operating conditions*
DTE_{el}	*Elastic component of DTE*
b	*Circular backlash (arc length) at the theoretical pitch circle*
sp	*Shuttling parameter (normalized axial component of* $\boldsymbol{C}$*)*

Chapter 1.

Introduction

The use of gears is widespread in the mechanical industry. Gears accomplish the same fundamental task for rotations as levers do for translations. Gears can transmit the rotation of a driving shaft to a driven shaft to make it rotate either faster or slower. Faster rotation results in a torque reduction, slower rotation results in a torque multiplication. Reduction or multiplication of rotational speed or torque can be accomplished with an extremely high variety of gear shapes, arrangements and sizes. Alongside of this fundamental task, gears grant high efficiency and high power density for a wide range of speeds and torques. Applications span from the everyday life to the very dedicated solutions. Tiny and precise gears exert their charm by ticking the time in watches. Commonly unnoticed gears are shifted when driving. Gears taller than a person bear huge loads in wind turbines, marine and industrial machinery. Complex arrangements of gears in helicopters bridge the tens of thousands of revolutions per minute for the jet engine to the hundreds for the rotor. Additional arguments on the key role which is covered by gears in mechanical systems can be found in a recent editorial of the Journal of Mechanical Design [1], where gears are also reported after a survey to be the icon perceived as being the most representative of Mechanical Engineering. This happens to be also because gears have a long tradition in mechanics. World's earliest known use of epicyclic metallic gears dates already in the first hundred years Before Christ. The finding in 1901 is from the Antikythera mechanism, which was lying on the seabed near the homonymous Greek island, and which has recently been understood [2][3] and reproduced (*Figure 1.1*).

Figure 1.1 – Main fragment of the Antikythera mechanism, dated circa 100 B.C. (left); modern watch reconstruction, dated 2012 by Hublot (right).

It is moreover known that less sophisticated and wooden gears were already used by earlier civilizations.

In spite of the long track of gear applications and usage, the complex phenomena which are involved in the meshing process still constitute an actual research topic. The field of investigation of this dissertation is bounded to involute parallel spur and helical gears having (nearly) involute teeth. The focus is on the dynamic behaviour of power transmissions, where several challenges need to be addressed nowadays for increased acoustic comfort, durability and efficiency. Precise geometric conditions are required to achieve conjugate action for the tooth profiles and therefore a constant instantaneous velocity ratio. Manufacturing and assembly errors, together with deflections and thermal distortions disturb reaching conjugate action. It turns out that teeth rarely possess involute profiles, since deliberate tooth microgeometry modifications are required to compensate for deviations from the ideal case. Tooth microgeometry modifications are a key factor for determining if a proper transmission has been designed and manufactured. Procedures for designing both gear macrogeometry and microgeometry have been reported to be a kind of “black art”, due to the vast amount of geometry associated with the process and the empirical experience privilege of gear manufacturers. A strong focus from the ‘50s up to date has been directed towards accurate modelling of gear meshing and tooth contact to

establish proper macro- and microgeometry design and manufacturing. Modelling provides the important advantages of avoiding the construction of expensive prototypes, evaluating several design possibilities by means of sensitivity analyses, and optimizing the final candidate. Modelling gear meshing requires accounting for multiple contact points which span the different tooth profiles. Steep strain gradients and load-dependent nonlinearities are typical of contact and need to be captured at each contact point. Further complications arise when considering the global deflections of each contacting tooth, which changes the contact handover conditions between subsequent tooth pairs. This substantially affects variability of the meshing stiffness and can be turned at the designers' advantage. The meshing problem is intrinsically three-dimensional when helical gears are considered, and becomes three-dimensional also for spur gears when misalignments are taken into account. From the point of view of a static simulation, there are quite established commercial simulation tools which provide reasonably accurate calculations, but which also proved to fail in important applications. From the point of view of a dynamic simulation, the field is much more open. Structures are becoming lighter and lighter for efficiency reasons and capturing the dynamic coupling between mechanical components is vital for a reliable design. The current context where transmissions operate, and their main application fields, are discussed in the following paragraphs. It is however worthwhile to highlight the biggest challenges. Dynamic meshing loads are the ones which typically cause transmission failures and excessive vibration or noise. Dynamics therefore play a major role for durability and comfort. Correctly accounting for resonance frequencies and the related mode shapes is a fundamental challenge not yet solved. One class of problems is the one addressing meshing dynamics with no loss of contact. In this case, the gear vibration has tonal components related to the meshing frequencies and gears are reported to "whine". These tonal vibrations usually amplify when one meshing frequency matches a resonance frequency for the system. The main challenge here is to simulate the mesh stiffness fluctuations coupled with the dynamic behaviour of the full supporting structure. Especially when gears are part of a planetary set, mutual interactions happen directly between the gears themselves and are tightly affected by the distributed flexibility of the supporting structure. Another class of problems is the one addressing meshing dynamics with loss of contact. Clearance-type nonlinearities here introduce jumps and stability

bifurcations in the response of the transmission. In this case, the gear vibration becomes broadband since impacts excite the system over a broad frequency range and gears are reported to “rattle”. Impact overloads which occur when contact is restored represent the focus for durability. In both cases of gear whine and rattle, important consideration is nowadays devoted to efficiency. Increase in the price of fuels and regulations slashing pollutant emissions drive the motivations. Gear efficiency is mainly related to elasto-hydrodynamic film lubrication and mechanical interactions between the rotating gears and the surrounding fluids. This constitutes another complex branch of study and will not be treated in this dissertation. To close the introduction to the relevance of gear dynamics simulations in transmissions, an observation drawn in the conclusions of a recent PhD dissertation [4] is that the bigger becomes the size of a wind turbine (and its transmission), the more important becomes the detailed design of microgeometry modifications paired with the tuning of flexible global system dynamics.

1.1. Context

The current quest for lighter mechanical transmissions (and structures, more in general) is increasing the mutual coupling between mechanical components in the dynamic response of the system. At the same time, regulations and customers require increased reliability and higher acoustic comfort. As a first example, in the automotive field, hybrid and electric vehicles require special care for transmission design since noise from the internal combustion engine, masking gear whine or rattle, is no longer present. In the wind turbines field, reliability issues on gearboxes motivate related literature [4][5][6] and a dedicated industrial consortium to tackle highly expensive failures by modelling and by condition monitoring [7]. Since global system response simulation is required, accounting for flexible mode shapes of key mechanical components and non-linear gear contact, Finite Element (FE) analysis proves to be computationally too expensive: simulation time on a typical workstation regarding one mesh cycle (one angular tooth pitch rotation) is in the order of hours for a general purpose non-linear FE code and in the order of minutes in the most efficient case of an FE formulation specialized in contact analysis [12]. On the other hand, a variety of fast analytical models is available in the literature for lumped-parameters systems having few

degrees of freedom [8]. Few recent models rely also on a three-dimensional formulation [9][10]. These models, however, do not consider flexible mode shapes of key components such as shafts, carriers and the housing. The conditions discussed above identify multibody modelling as the most appropriate approach to evaluate the global mechanical system behaviour. An efficient multibody approach aimed at including three-dimensional gear contact, while considering flexible mode shapes (excluding the gear blank), is proposed in this dissertation.

1.2. PhD Trajectory

The PhD trajectory presented in this dissertation work has matured from two circumstances. The first consists in the industrial need for capturing system-level dynamics of mechanical power transmissions including detailed gear meshing; the second is due to the scientific relevance of this target in the related state of the art. Initial background and motivation for the addressed problem comes from the Master Thesis period spent by the Author in the company LMS Italiana, Turin (Italy), subsidiary of LMS International, headquartered in Leuven (Belgium). The PhD track aims to two main goals in two phases: the first is the development of an advanced multibody methodology for gear meshing simulation with system-level dynamics; the second is the numerical and experimental validation of the developed methodology. Two collaborations have been set up for both the development and the validation phases of the PhD track. The first is with LMS International to provide simulation capability in the multibody software environment Virtual.Lab Motion. The second is with the PMA division of the Mechanical Engineering Department at the Katholieke Universiteit Leuven, to contribute to the research and development process for the simulation technique. Prof. Wim Desmet, from the latter institution, is the Co-promotor of this dissertation. Within this framework, a dual PhD track has been outlined. The development phase constitutes the research topic for the current PhD programme at the University of Calabria. The validation of the methodology will be added in the PhD programme at the Katholieke Universiteit Leuven. Hereafter a more detailed breakdown of the goals is reported.

Targets for the development phase can be stated as follows:

1) Identify an efficient methodology to model mesh stiffness variability in multibody environment;
2) Keep the formulation modular for a general gear pair which can be spur or helical, external or internal;
3) Keep the complexity of the formulation scalable, to allow performing sensitivity analyses and tuning the computational effort according to the simulation purpose;
4) Decouple gear contact calculations, which represent the most computationally expensive step in the solution, from the dynamic simulation;
5) Include in the dynamic simulation the effects of:
    a. Load-dependent nonlinearities due to contact and tooth microgeometry modifications;
    b. Relative misalignments between the gears;
    c. Instantaneous magnitude, orientation and contact point position for the resultant dynamic contact force;
    d. Contact loss within the backlash.

Targets for the validation phase can be stated as follows:

1) Compare and correlate simulations with measurements of the most relevant gear quantities:
    a. At the sub-system level: on single gear pairs where different microgeometry modifications are applied and under imposed conditions of:
        - Misalignment
        - Applied external torque
        - Rotational speed
    b. At the system level: on a full wind turbine driveline.
2) Compare and correlate simulations with a numerical case study undergoing loss of contact.

For the validation at the sub-system level, a dedicated gear test rig has been designed by the Author to impose the listed conditions and has been manufactured in Leuven. Two families of test gears were also manufactured for extensive validation purposes, spur and helical.

For the validation at the system level, within the collaboration with the Katholieke Universiteit Leuven and LMS International, an agreement has been signed to access the data made available by the USA National Renewable Energy Laboratory (NREL) Gearbox Research Collaborative (GRC) [7]. A multibody model for the transmission has been set up in Virtual.Lab Motion. Investigations are ongoing.

For the numerical validation of contact loss phenomena, several case studies are available in the literature. Two cases appear to be particularly interesting for that purpose. The first case consists of a single gear pair for which the dynamic behaviour is calculated by means of different techniques [11][12]. The second consists in a multi-mesh gear train including a driving gear, an idler gear and a driven gear. Impact of microgeometry modifications is assessed and different simulation techniques are compared [13]. Although contact loss is expected to be observed and studied during the experimental campaign for some of the spur gear pairs, numerical validation for contact loss is likely to bring more insights due to the difficulty of measuring experimentally impact forces. Measurements aiming at a correlation for impact forces will however be performed. The discussion on the validation part ends here, as it represents the part dedicated to the PhD track at the Katholieke Universiteit Leuven. The current dissertation will focus in detail on the developed methodology.

1.3. Contribution to the state of the art

Main contributions to the state of the art can be listed as follows:

1) faster gear meshing simulations, allowing to perform speed-sweep simulations with a large number of gear rotations without the need of linearizing the system (time-domain integration);
2) generalised element to be included as a module in multibody models, enabling the exploitation of other software functionalities for modelling the interacting components;
3) overcome limitations of analytical models, avoiding excessive simplification needed for analytical identification of the equations of motion;

4) overcome limitations of the Finite Element Method in yielding unpractical computational times and a very detailed solution for every analysed configuration of the system;
5) scalability with choosing the main phenomena to be taken into account in the dynamic simulation, thus allowing sensitivity analyses and tuning of simulation complexity based on the final objectives.

The outlined points are further justified and clarified hereafter.

Solving the gear contact problem for each timestep of a speed-sweep dynamic simulation and for all the meshing gears represents a computationally expensive task because of the extremely high amount of timesteps to be calculated. Meshing frequency is in fact equal to the shaft rotation frequency times the number of teeth for the connected gear. This leads to quickly rising frequencies, hence to sampling frequencies for the simulation at least twice as big as the maximum frequency to be analysed. This problem is further complicated when the simulation is already heavy due to mutual interactions between components which include distributed flexibility (housing, shafts, planetary carriers, etc.). A traditional solution to this problem is to linearize the system around one operating condition and perform the speed-sweep in frequency domain. In this way a significant amount of information about the system is lost: load-dependent changes in the mesh stiffness due to tooth microgeometry modifications, variable misalignments and teeth loading due to system dynamics and supporting element resonances, loss of contact and related impacts which may arise in gears or bearings. Basically all the consequences due to deviations from the assumed operating conditions are lost. This assumption is relaxed when using time-integration calculation schemes and all the deviations can intrinsically be taken into account in the simulation.

Having a generalised gear contact element in general-purpose multibody software provides the key feature of very limited constraint in building a model for a mechanical system. Modular “building blocks”, such as rigid bodies, flexible bodies, constraints, joints, force elements, standardized subsystems (e.g. automotive suspension systems, control units, hydraulic systems, etc.) are available in such multibody simulation environment. Including gears in this set of “building blocks” provides versatility to the engineering designer for a vast range of applications. Similar reasons are stated in the literature (reviewed in *Paragraph 2.3*) proposing multibody methodologies. Up to now, there are no reported

multibody formulations as detailed and scalable as the one proposed by the Candidate.

Very efficient analytical formulations for gear contact analysis are available in the literature (reviewed in *Paragraph 2.1*), having different degree of detail. These formulations are tailored to simulate specific application cases which are bounded similarly by specific assumptions (planar motion, concentrated elasticity, particular trends for the mesh stiffness fluctuation, etc.). The assumptions made to simplify the addressed case study are ultimately needed to derive the equations of motion for the system. Simplifying assumptions cannot be generalized for different case studies. Moreover, equations of motion are hard to derive manually when the distributed flexibility of components needs to be included. These limitations are overcome by the proposed methodology.

Finite Element methodologies provide the opportunity of avoiding a-priori approximations and at the same time including the distributed flexibility of the full system (reviewed in *Paragraph 2.2*). The price to pay is however very high: non-linear formulation is needed for capturing gear contact; extremely refined meshes are required for describing tooth microgeometry and capturing the contact stress/strain gradients. An innovative FE formulation has been proposed for avoiding the mesh refinement at contact locations, however the number of degrees of freedom remains prohibitively high for running three-dimensional dynamic simulations. A major drawback for FE simulations is that a complex nonlinear elastic problem needs to be solved for each iteration of the dynamic solution. Decoupling between the computationally expensive contact calculations and the dynamic simulation is introduced by the proposed methodology and solves the issue. Distributed flexibility for the supporting structure can still be included in the simulation efficiently, through the multibody software environment, by means of component mode synthesis (CMS) techniques. Currently it is however not possible to include distributed flexibility for the gear body.

An additional contribution to the state of the art is the capability of scaling the modelling complexity to perform sensitivity analyses or obtaining acceptable simulation times. With this approach it is possible to answer to questions like: do misalignments play a significant role in the dynamics of the transmission? Similar insights can be gained for variation of the resisting load, changes in centre distance, axial positioning of the contact force, etc. Once a sensitivity analysis has been performed, the design of the transmission can be more effective in

solving the identified problems and the final detailed simulation can be set with deeper knowledge of the transmission behaviour.

1.4. Dissertation structure

The current introduction chapter states the rationale and provides an overview on the current needs and challenges faced in the design of mechanical power transmissions.

Chapter 2 is devoted to a more detailed analysis of the current state of the art. The advantages and disadvantages for the methodologies currently available for simulating transmission dynamics are compared. The three classes of models already quoted are addressed: analytical, Finite Element and multibody. Given the current modelling techniques, multibody models appear to have the highest suitability to simulate system-level dynamics in a fully coupled non-linear system. In the same chapter, a special focus is then directed to the main industrial application fields for the proposed simulation technique. Industrial needs in each specific context are discussed.

Chapter 3 presents the theoretical background which motivates the modelling choices undertaken for the formulation of the gear element. In first instance, the overall structure of the element is discussed. Subsequently, the gear Transmission Error (TE) is discussed as the main quantity capable of describing deviations from a perfect transmission of motion. The principal causes of imperfections are discussed together with their effects on the TE. Load-dependent nonlinearities and mesh stiffness fluctuations are evaluated, gear misalignment components are defined and gear microgeometry modifications are explained.

Chapter 4 provides the formulation of the proposed gear multibody element. Firstly, the quantitative estimation of the TE is presented by using the specialized calculation code Load Distribution Program (LDP) from the Ohio State University Gearlab. Subsequently, it is shown how the dynamic contact force can be calculated by using a formulation based on the TE and how instantaneous (namely dynamic) operating conditions can be taken into account. Operating conditions are defined in terms of transmitted load and relative positioning between the gears (misalignments). Moreover the so called shuttling phenomenon and the modelling of backlash are separately treated.

Chapter 5 discusses the advances brought by the proposed simulation methodology by means of numerical examples. Specific phenomena are highlighted through static and dynamic preliminary simulations. Quantitative effects of tooth profile microgeometry modifications are shown for an example gear pair in a range of transmitted loads which include the optimal level. Misalignment sensitivity for the TE variability is shown for a gear pair belonging to an automotive transmission and one belonging to a wind turbine. The already discussed sample gear pair is used to show how tooth lead modifications can decrease the sensitivity to an important misalignment component.

Chapter 6 discusses the application of the proposed gear simulation methodology with all the highlighted phenomena to two case studies. The first case study is a single gear pair, where misalignments and load variations are imposed during the dynamic simulation. The second case study is a planetary stage where the three-dimensional dynamic gear behaviour is discussed with special attention to shuttling phenomena.

The remaining chapters draw the conclusions and provide the references on which the dissertation is based.

Chapter 2.

State of the art

Although gears have been used in mechanical industry for a long time, first systematic research activities aimed towards understanding the meshing started in the ‘50s. References from Tuplin, Reswick, Strauch, Zeman, Abramov, Utagawa highlight the first systematic attempts for understanding the dynamics of spur gears. The reported references mainly come from two important papers from that time, written by Harris [14], later assisted by Munro [15]. The first paper [14] gave a considerable contribution to understanding the main sources of gear meshing vibrations. Harris introduced in his model deliberate profile modifications and showed how such modifications affected what he called “static error” in gear meshing. A first remark of the paper was the explanation on how contact handovers between tooth pairs was the key to understand gear vibration. The “static error”, calculated and measured, showed variability dependent on load. This variability was almost none for a specific load, paving the way for quantitative microgeometry modification. Computational power at the time was only a tiny fraction of what we have available today and thousands of photoelastic stress patterns had to be analysed to gain these insights (leaving a flavour of the needed dedication). A second remark of the paper was that the meshing vibration at resonance (caused by the periodic “static error”) was limited by damping and eventually by loss of contact. The second paper [15], based on the PhD dissertation of Munro, appears to be more refined. The “static error” becomes a “static transmission error”, which is defined for any instantaneous angular position of one gear as “the angular displacement of the mating gear from the position it would occupy if the teeth were rigid and unmodified”. The definition should be complemented by stating that the teeth are also perfectly aligned and spaced, however the idea of TE is nowadays one of the most widely accepted causes for gear vibration. In the paper a lumped-parameters dynamic model for a single gear pair was presented. Nonlinearity due to loss of contact

was also calculated and measured with good qualitative agreement both for TE and tooth loads. Dynamic overloads were observed to be up to six times higher than the nominal applied load.

While addressing the basics of gear dynamics, it is worthwhile to suggest references to become acquainted with the topic. Although dating from the early days for gear dynamics research, the two papers discussed above are very much recommended for anyone who is approaching gear vibration and noise problems. Useful references are also the book on gear noise and vibration by Smith [16], the book on gear geometry by Litvin and Fuentes [17] and the Dudley's handbook on practical gear design [18].

Back to gear meshing modelling, more recent analytical models to study gear vibrations are based on a similar logic: they consider gear bodies rigid and model contact between each gear pair by one or more spring-damper systems aligned along the line of action of the gear pair [8]. These models are loaded with dynamic excitations which can be divided in internal or external, respectively whether they are caused intrinsically by the meshing or are induced by load or displacement fluctuations from the power generator, the power user or the structure supporting the gears as reported by Helsen et al. [19]. Dominant internal or external excitations determine the physical phenomena at the source of vibrations which must be captured by the model. Dion et al. [20] and Ziegler et al. [21] show how external excitations, especially in case of lightly loaded gears, can cause contact loss and repeated teeth impacts. Noise emitted in this case is known as *gear rattle*. It has broadband frequency spectrum and is directly related to gear backlash. Nonlinear behaviour induced by the clearance was observed by Kahraman and Singh [22] and Liu and Parker [13], and it can be captured using time-integration solution schemes. Internal excitation, instead, is usually dominant when teeth do not loose contact and leads to tonal noise known as gear whine. In this case the most important underlying physical phenomenon is mesh stiffness variation with tooth-passing frequency, as pointed out by Ozguven and Houser [23] and Morgan et al. [24]. Physical effects leading to mesh stiffness variability are one first main distinguishing feature between the available techniques. The second one is the level of detail reached for modelling the structure hosting the gears, as it significantly affects the meshing process as it was shown by Harris et al. [25] and Campbell et al. [26]. Both these features have an influence on the number of degrees of freedom required to model the

meshing and to constrain each gear, thus determining the level of detail and complexity of the model. Basic models account only for the rotation of the gears, where contact between each gear pair is modelled by a single spring-damper element [8]. Gear whine applications require variable mesh stiffness to account for the variable number of tooth pairs in contact, including elastic tooth deflections and tooth profile microgeometry modifications as discussed by Umezawa et al. [27] and Cai and Hayashi [28][29]. These models are simplified assuming rigid bodies/supports and one-dimensional modelling for the meshing along the direction of the contact force. Models like the one proposed by Ambarisha and Parker [30] show how bearing and shaft stiffnesses can be included following a lumped approach under the assumption of a motion in the plane orthogonal to the gear axes. However tooth contact areas extend along the axial direction and are influenced by the relative position and orientation of the gears (misalignments). Three-dimensional (3D) analytical models, like the ones by Velex and Ajmi [31] and Eritenel and Parker [32], were developed to account for misalignments. The 3D nature of contact also plays a key role when the axial oscillation of the contact force position (shuttling) becomes an important excitation, as reported by Helsen [19]. Shuttling effects were modelled by Nishino [33] using two spring-damper elements with phased mesh stiffness curves for the same gear pair. Three main drawbacks result from this analytical approach: first, to be able to write the equations of motion, analytical models rely on a significant reduction of the level of detail used to model the geared system; second, gear blanks and the surrounding structure are considered rigid bodies connected by lumped stiffnesses; third, analytical models need to be tailored to the system under study according to the complexity of the problem.

FE techniques can be adopted to model in detail gears interaction and include gear body flexibility, as shown by Kubur et al. [34], Lin et al. [35] and Li [36]. However, extremely refined mesh and non-linear elements are needed to correctly simulate gear contact, with discretisation issues to capture the tooth surface due to microgeometric corrections. As a consequence, simulation time becomes prohibitive, especially when analysing a gear train with dynamic interactions and a high number of revolutions for the gears needs to be simulated, as is the case with speed-sweep analyses. To increase computational efficiency, a special FE formulation has been developed by Vijayakar [87]. Here, contact is solved analytically near teeth surfaces and the resulting loads are

applied to the remaining FE mesh, which can now be much coarser, through interface nodes. Still, calculation times are not suitable for speed-sweep dynamic analyses in 3D. A good compromise between analytical and FE techniques, in terms of level of detail and computational efficiency, is represented by multibody modelling. Multibody elements for gear meshing provide simulation versatility as they can be used to build complex models together with all the other elements already available in multibody software. For the sake of high calculation efficiency, it is possible to retain the assumption of rigid gear blanks and introduce flexibility for key components in the model, such as shafts and gearbox housing, exploiting the benefits of modal reduction techniques [37] like the Craig-Bampton approach [38]. In this view, Cardona [39] developed a 3D multibody element to apply contact forces in the appropriate directions for a variety of gears used in industry. This element however is not considering mesh stiffness fluctuations, misalignments and backlash. A formulation based on a variable mesh stiffness approach, accounting for the actual and variable number of tooth pairs in contact, has been proposed by Ebrahimi and Eberhard [40]. A constant stiffness value is considered for a single tooth, under the assumption that each tooth can undergo a displacement in a direction tangential to the gear blank independently from each other. The same Authors estimated stiffness values with FE calculations and a spur gear pair was analysed in a plane orthogonal to the axes of rotation. Up to date, there are no formulations in literature which allow dynamic system-level simulations with high numbers of revolutions for the gears and where gear contact is modelled with detail in three-dimensions.

2.1. Analytical models

Analytical models have been developed for a vast variety of applications. They started from the early days of gear dynamics research, with a single gear pair and a single degree of freedom, and evolved until today's more refined three-dimensional formulations. Ongoing research is still exploring analytical models since they provide low computational requirements (thanks to their lumped-parameters formulation) and can be tailored to describe in an efficient way specific applications. The latter represents inherently an advantage and a limitation: it requires the user to be an expert in the topic of gear dynamics and to be in possession of sensitive engineering judgement for deciding which degrees

of freedom to take into account and how. Critical approximations are moreover to be evaluated for modelling the variable gear mesh stiffness.

2.1.1. One-dimensional models

One-dimensional models are used to assess the rotational vibration around the gear axes. All the translational motions of the gear bodies are excluded from the simulation; therefore this class of models is suitable to perform simulations where translational vibrations have limited effect on the meshing vibrations. The purpose of rotational models, sometimes improperly called “torsional models”, can be either to simulate gear whine or gear rattle. Rotating masses are lumped into inertia moments and associated to the related rotational degrees of freedom. Connectivity between the degrees of freedom is set by means of rotational or translational spring-damper elements. Rotations are in fact usually expressed, in an equivalently way, by using the displacement that they cause along the line of action of the gears. Each displacement represents the TE between the related gears. While detailed discussion of the TE is provided in *Paragraph 3.2*, it is sufficient for the moment to keep the qualitative definition provided in the previous paragraph, which states it as a deviation of the real transmission from the ideal kinematic transmission. First examples whine models can be retrieved in the work by Mahalingam and Bishop [41], where a gear train is analysed and the rotational modes of vibration are discussed along with their natural frequencies. Later models like the one from Ozguven and Houser [23] were aimed towards assessing the dynamic response of the gear mesh by using the Static TE and the average mesh stiffness to generate a forced input and trigger the gear pair vibration. Loss of contact was assumed to happen as soon as the dynamic contact force became negative. Comparison to experimental results for a single spur gear pair showed satisfactory agreement and showed loss of contact when the gear mesh frequency matched the gear pair resonance frequency. Simulating gear vibration by means of forced response does not take into account parametric excitation, since mesh stiffness is not variable with time.

A similar model assuming constant mesh stiffness was used by Kahraman and Singh [22] to deepen the analysis on loss of contact. Clearance-type nonlinearity was included in the model by setting the mesh stiffness equal to zero for values of TE within the backlash range. Jumps in the frequency response for a spur gear

pair were discussed as well as chaotic behaviour and phase plane plots. Two different solution methods were discussed and parametric studies on damping were performed. Limited experimental validation was reached, by comparing to measurements available in literature.

An example of model with time-varying stiffness can be found in the work by Cai [28][29]. The papers started from the results obtained by Umezawa [27][42][43][44][45] and extended the stiffness formulation to account for teeth not belonging to a rack (differently from Umezawa). The formulation used by Cai can be taken as a typical baseline for a rotational analytical model, therefore it is worthwhile to provide more details on the formulation and the results that can be drawn from it. Gears are held by hinges allowing one degree of freedom per gear, which yields only one degree of freedom as soon as the relative rotation is considered. Each rotating mass is represented by inertia moments J_1 and J_2. The single degree of freedom is expressed in terms of relative displacement along the line of action for the gears, where a spring-damper element is acting to represent variable mesh stiffness and losses of the gear pair under a linear viscous assumption. In series with the spring-damper element, profile errors for the meshing teeth are acting through as a displacement-driven excitation. A schematic of the model is represented in Figure 2.1. Therefore, the model makes a distinction between displacements which are due to elastic deflection for each meshing tooth pair and displacements which are due to the microgeometry modifications or manufacturing errors for each tooth profile.

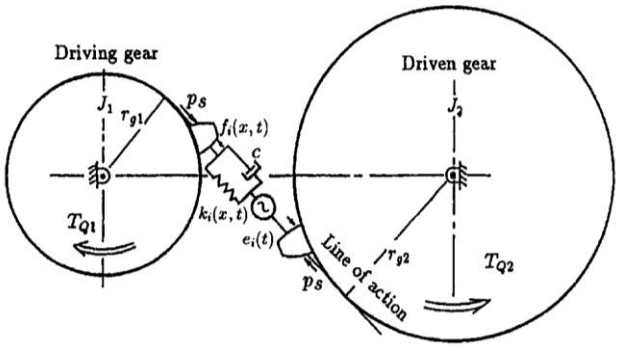

Figure 2.1 – One-dimensional gear pair rotational model used by Cai. Reproduced from [29].

The equation of motion for the dynamic system can be written as:

$$\begin{cases} m\ddot{x} + c\dot{x} + \sum_{i=1}^{I} f_i(x,t) = p_s \\ f_i(x,t) = k_i(x,t)[x_s + x + e_i(t)] \end{cases} \quad (2.1)$$

where $x = x(t)$ represents the dynamic relative displacement on the line of action and the unknown of the differential equation. This dynamic displacement coincides with the dynamic TE between the gears. The term m represents the equivalent mass of the gears obtained after dividing each inertia moment J_i by the related base radius r_i :

$$m = \frac{m_1 m_2}{m_1 + m_2}, \qquad m_i = \frac{J_i}{{r_i}^2}, \ i = 1{,}2 \quad (2.2)$$

The term $f_i(x,t)$ represents the force related to the elastic deflections and the imposed displacements due to profile deviations from the pure involute. The summation accounts for the I pairs of teeth which can engage simultaneously at the given time instant. The terms which determine the elastic force are:

- $k_i(x,t)$ = instantaneous stiffness for the I-th pair of teeth;
- $x_s = p_s/\bar{k}$ = average displacement given by the total contact force p_s which acts on the average total meshing stiffness $\bar{k}$;
- $e_i(t)$ = sum of the profile deviations for the two teeth belonging to the I-th pair.

Emphasis should be placed on the determination of the single tooth pair stiffness $k_i(x,t)$. This value is determined by Cai using the formula suggested by the ISO Standard 6336 for the stiffness at pitch point and an exponential function to approximate the variability during rotation. Substantial approximations are introduced in this step of stiffness estimation. A wide research field addresses this topic, which is not the subject of this PhD dissertation and will not be discussed. Nonetheless, physical mechanisms affecting single tooth pair (and total mesh) stiffness are addressed in *Chapter 3* and considerations about how to determine the mesh stiffness by using the FE method are reported in the next paragraph.

Solving the equation of motion, information can be extracted on the dynamic TE, the single-tooth dynamic loads and the dynamic total contact force, in time or frequency domain.

A model assuming both clearance-type nonlinearity due to backlash and time-varying mesh stiffness was used by Blankenship and Kahraman [46][47] to address contact loss phenomenon in steady-state forced response. Jumps in the TE frequency response were predicted with accurate correlation with the experiments performed on a dedicated test rig.

Dion et al. [20] performed simulations of contact loss for an idle gear. A gear pair system was excited by fluctuating acceleration of the input shaft, while the output shaft was connected to a rotating inertia. The focus of the paper was on determining acceleration, velocity and angular displacement for the idle gear. After having calculated analytically geometric and elastic parameters and having identified experimentally dissipative parameters, comparison with experiments proved the rotational model to accurately capture all of the kinematic quantities for the impacts.

A rotational model was used by Andersson and Vedmar [48] to evaluate the effects of contact out of the plane of action due to contact onset for a new pair of teeth. The true geometry of the tooth had to be used to avoid orienting the force a-priori along the line of action. Result of the analysis was a quantitative prediction for the contact pressure near the tooth tip during transitions, useful to establish a sufficient tooth tip rounding fillet.

Rotational models have been used in optimisation of tooth profile microgeometry modifications. Lin et al. [49] evaluated, for a spur gear pair connected to a motor and a generator, the differences between optima achieved by using different types of modification trends (linear or parabolic) and different modification lengths on the profile. Faggioni et al. [50] and Bonori et al. [51] used a rotational model to perform the profile microgeometry optimization on the peak to peak dynamic TE value, instead of using the static value.

2.1.2. Two-dimensional models

Rotational models which include profile microgeometry, time-variant mesh stiffness and, in case of contact loss, clearance prove to be useful if gear pairs are not affected by translations in the system or if translational modes of vibration

are decoupled from the rotational modes. However, usually shafts and bearings have radial stiffness values which belong to similar orders of magnitude as gear mesh stiffnesses [52][128][129][130][131]. For this reasons two-dimensional or “planar” models have been introduced. These models “slice” the system in a transverse plane, which is orthogonal to the gear axes of rotation, and model radial deflections of supporting elements by using additional spring-damper elements.

In the study from Ozguven [53], the rotational model adopted in [23] was extended to account for translations of shafts and bearings in the direction of the line of action. It is shown how the dynamic response of the gear pair is substantially affected when the meshing mode is coupled to the translational modes introduced by the supporting structure. In particular, if bearings are compliant, their reaction forces can be substantially different from the meshing forces they support.

Nonlinear response of gears which experience loss of contact is also affected by the coupling between translational and rotational modes of vibration. Examples of such a coupling have been addressed by Walha et al. [54], showing how bearing forces are affected by loss of contact in the gears. Results from Siyu [55] discussed how transverse vibration for the gears, which result in a change for the backlash value, impact on the non-linear behaviour. In particular, dynamic backlash proved to be causing chaotic motion for the gears.

Planar models have also been used to optimize profile microgeometry modifications while capturing the dynamic interaction with the supports deflection. An example of such optimisation can be traced in the work from Parker [13], which addressed the case of a basic multi-mesh gear train (*Figure 2.2*).

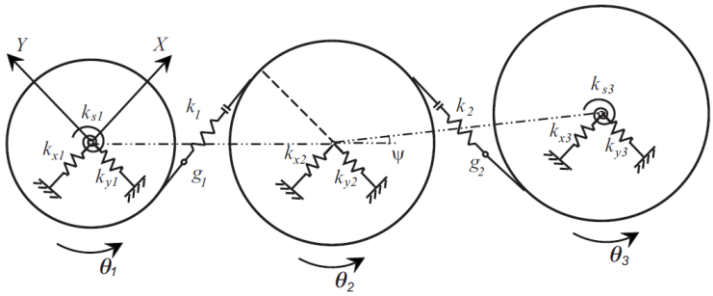

Figure 2.2 – Two-dimensional idler-gear system model used by Parker. Reproduced from [13].

Loss of contact was also included in the model, since the idler gear has no external load applied and can cause loss of contact by travelling through the backlash. Profile microgeometry modifications were shown to be capable of avoiding loss of contact for the system by drastically reducing the internal excitation experienced by the gears. TE and tooth contact forces were predicted and shown to be correlating well with planar FE simulations.

2.1.3. Three-dimensional models

Rotational and planar models do not allow the gears to tilt, namely to rotate out of the plane of rotation. A wide range of phenomena are neglected by this assumption: angular misalignments, axial positioning for the resultant contact force, microgeometry modifications along the face width direction. Effects of these phenomena represent a significant concern not only for the dynamic response (increased excitation, tilting modes of vibration) but also for durability (stress concentration by edge loading).

A first class of three-dimensional models allow tilting of gears without considering the related effects on the contacting teeth. The spring-damper element used in rotational and planar models is simply aligned in a direction which is normal to the tooth surface. This implies, for helical gears, capturing the excitation due to the axial component of the contact force, which generates a bending moment for the gear body out of the plane of rotation. Tilting excitation for spur gears does not come from meshing, but can be induced by the supporting structure. Modes of vibration involving tilting can be captured by this class of models, however effects of misalignment between the meshing teeth and microgeometry modifications in the face width direction are not captured. An example of three-dimensional model with no effects on contact is represented by the study performed by Kahraman [72] and by Kubur et al. [57] on a multi-shaft helical gear system. The study demonstrated the importance of capturing coupling between rotational, transverse and axial motions for helical gears. Good correlation was achieved between simulation and experiments.

More refined models address the distribution of contact pressure in the axial direction. Velex and Mataar [58] introduced a dynamic model to account for three-dimensional contact by thin-slicing the gears in the axial direction and introducing a network of springs between the meshing teeth. Simulations were

performed by Baud and Velex [59] using the same three-dimensional model. Comparison to experimental results for a single helical and spur gear pair proved the importance of considering three-dimensional effects on gear contact. Experimental results also proved that the applicability of the thin-slice method is limited to the case of narrow-faced gears with moderate helix angles. A formulation for overcoming the limitations on the gear face width was proposed by Ajmi and Velex [60] by using Pasternak elastic foundations and address convective effects due to contact shear (*Figure 2.3*).

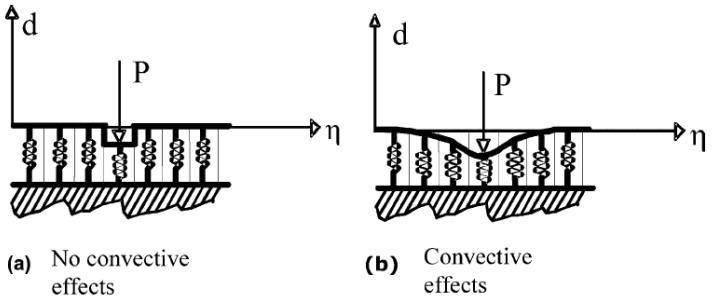

Figure 2.3 – Representation of convective effects due to contact shear. Reproduced from [60].

Recent models by Eritenel and Parker [61][62] discuss how three-dimensional gear contact changes dynamically the contact pattern and introduces partial loss of contact on instantaneous contact lines. A centre of stiffness obtained from the dynamic contact pattern was proposed to locate a single point of application for the contact force and a moment in the contact plane using a lumped-parameter model (*Figure 2.4*).

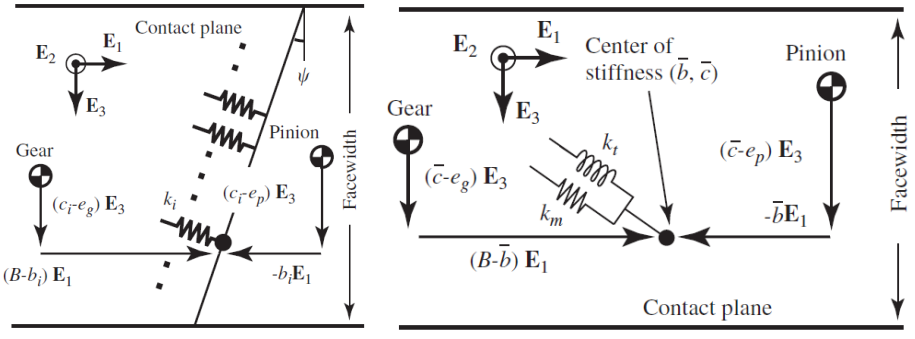

Figure 2.4 – Distributed mesh stiffness (left) and concentrated mesh stiffness (right) for the three-dimensional model proposed by Eritenel and Parker. Reproduced from [62].

2.1.4. Models for planetary gear trains

Models ranging from one- to three-dimensional, similar to the ones discussed in the previous sub-paragraphs, have been applied to planetary gears. However planetary gears deserve a separate discussion due to the specific dynamic behaviour they exhibit. Peculiarity in the dynamic response derives from the mutual coupling between planets which simultaneously mesh on the same sun gear and ring gear. Geometric symmetries in contact forces have been shown to provide crucial information to be exploited to reduce the dynamic response of such gear trains.

Rotational models (*Figure 2.5*) have been used by Lin and Parker [63] to discuss parametric instability building up due to mesh stiffness fluctuation. Instability was shown to be closely related to the relative phase between each sun-planet and ring-planet mesh. In particular, for specific conditions on the mesh phasing, instability could be avoided exploiting the symmetry properties for the related mode of vibration.

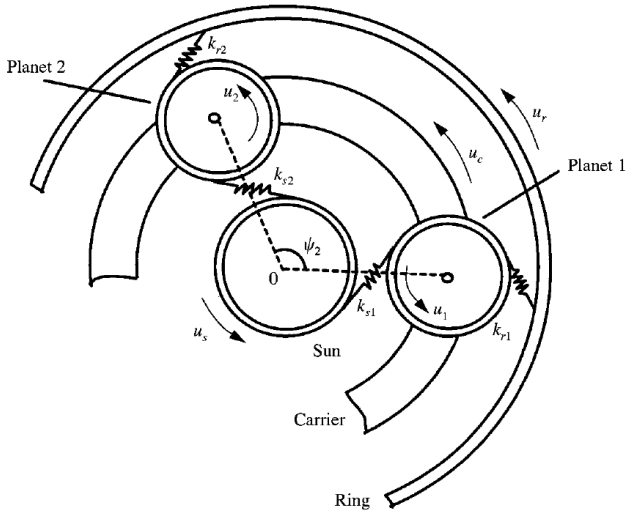

Figure 2.5 – Rotational model for planetary gear sets. Reproduced from [63].

Mesh phasing calculations have been discussed by Parker and Lin [64] using the same model of *Figure 2.5* for a generic planetary gear set.

Al-Shyyab and Kahraman [65] used a rotational model to discuss nonlinear dynamic response due to contact loss in a spur planetary gear set. Jumps in the

frequency response were identified similarly to the ones observed for isolated spur gears.

Another peculiar aspect of a planetary gear set is the quest for achieving even load distribution among the planets. In this direction, relative positioning of planets, sun and ring in a transverse plane plays a crucial role. Clear discussion on the importance of such relative positioning has been provided by Singh [66]. Given the importance of transverse motion, planar models have a long track of application cases for planetary gears. Kahraman [67] provides a comparison between the rotational and the planar modelling approach, showing how the latter are able to include translational modes of vibration. Seager [68] used a planar model to discuss the effectiveness of mesh phasing in suppressing specific tooth frequency excitations (*Figure 2.6*).

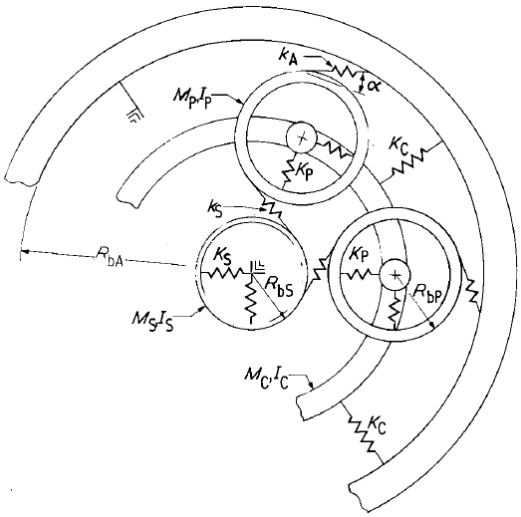

Figure 2.6 – Two-dimensional model for planetary gear sets. Reproduced from [68].

Lin and Parker used a similar model to classify the possible mode shapes for a planetary gear set with equally [69] and unequally [70] spaced planets. The discussion distinguished between rotational, translational and planet modes. The first two involve motion for all the gears of the planetary set, the third only involves planets. Chaari et al. [71] adopted a planar model to assess the effects of eccentricity and profile errors in the gears. They described the eccentricity to generate modulation sidebands and the profile errors to cause an increase in amplitude for the excitation at the mesh frequency.

Three-dimensional models become a prerequisite for addressing helical planetary gear trains. Kahraman [72] showed, using the model illustrated in *Figure 2.7*, how motion out of the transverse plane appears in modes of vibration.

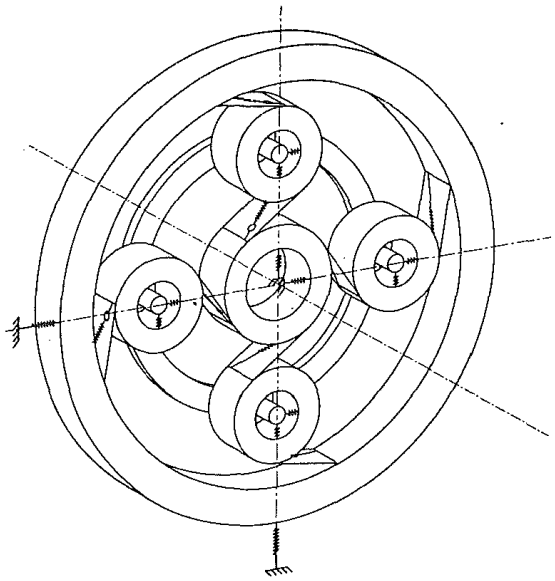

Figure 2.7 – Three-dimensional model for planetary gear sets. Reproduced from [72].

Velex and Flamand [73] simulated with a similar model the dynamic response in terms of tooth loads and sun orbits. Eritenel and Parker [61] extended the planar classification for the possible modes of vibration to the three-dimensional case. Mode families were identified as being rotational-axial, translational-tilting and planet, similarly to the planar case, but now involving motions out of the transverse plane.

2.2. Finite Element models

Finite Element models respond to the need of accurately modelling the complex meshing process. While a-priori assumptions are needed in analytical models to represent tooth global and local deformation behaviour and to represent interactions among simultaneously meshing teeth, FE models do not require such assumptions which unavoidably introduce approximations. On the other hand, an extremely refined mesh and nonlinear solution are required to correctly capture steep gradients in contact stress and strain and to correctly describe tooth

surfaces. As a result, FE models are seldom used for gear dynamics analyses due to unpractical computational time. An original FE formulation allows reducing computational complexity by describing local deformations due to contact analytically. The formulation allows performing planar dynamic FE simulations in a reasonable time, but three-dimensional ones are still unpractical.

2.2.1. Static simulation

As reported in the previous paragraph, estimation of meshing stiffness for a single tooth pair and for the complete mesh represents a complex task. Final goal of such estimation is the calculation of the Static TE for all the gears in mesh, as this is recognised to be related to the internal excitation magnitude. As shown by Conry and Seireg [74] and by Stegemiller and Houser [75], meshing deflections result from a variety of phenomena which involve local contact deformation for the teeth and their global bending and shear deflection; rotation and translations at each tooth base since the gear body is elastic; torsional wind-up of the gear body itself. An additional complication comes from the fact that, already for a single pair of teeth, contact is:

- non-linear with load;
- affected by relative positioning of the teeth (misalignments);
- extremely sensitive to local curvature.

Accurate representation for tooth microgeometry modifications is therefore crucial to correctly capture these contact phenomena. A variety of analytical and empirical tooth behaviour models are available in the literature and are used to feed the models discussed in the previous paragraph. However, a generalisation to model meshing in a variety of tooth proportions and macrogeometry parameters (addendum over dedendum ratio, addendum modification, face width size, helix angle, pressure angle, etc.) introduces approximation.

FE formulations to calculate mesh stiffness and Static TE provide the advantage of considering the real geometry of the teeth in mesh, without relying on a-priori assumptions. This usually yields considerable increase in the results accuracy.

Static FE simulations were used by Andersson and Vedmar [48] in combination with the rotational analytical model to perform the dynamic calculations described in *Paragraph 2.1.1*. Wang and Howard [76] provide a clear example of planar FE calculation aimed at obtaining the Static TE and the mesh stiffness in presence of

profile modifications. From *Figure 2.8*, it can be noted how refined the mesh needs to be to capture contact stress gradients and to describe accurately the profile modification.

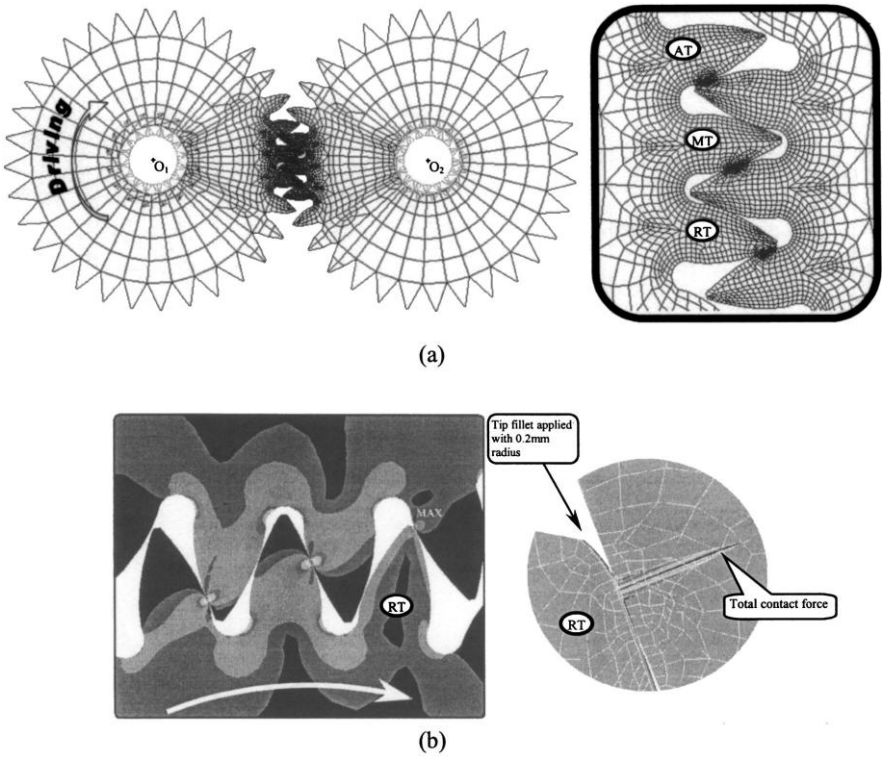

Figure 2.8 – (a) Planar FE mesh for gear contact and (b) contact stress gradients. Reproduced from [76].

Li [77] assessed by means of three-dimensional FE calculations the effects of manufacturing errors, assembly errors and tooth modifications on the meshing. Although very detailed results were obtained, again the FE mesh had to be extremely refined (*Figure 2.9*).

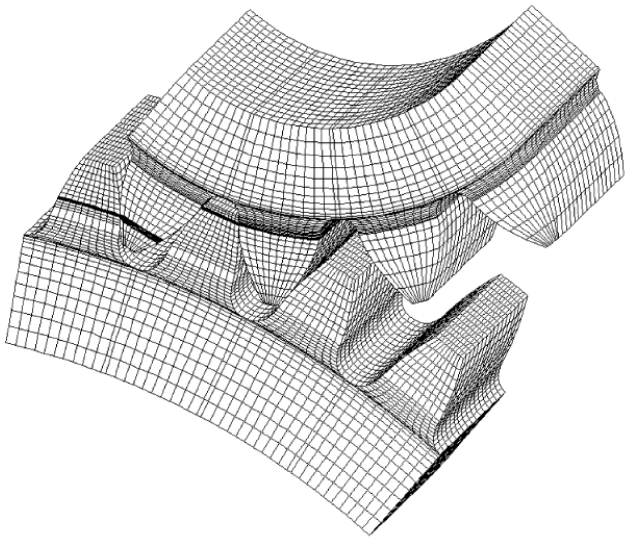

Figure 2.9 – Three-dimensional FE mesh for gear contact. Reproduced from [68].

The price to pay in terms of computational effort is very high, not only because the FE mesh needs to be refined, but also because contact elements are nonlinear. Typical application of static FE simulations is as a benchmark case for comparing analytical models describing tooth behaviour. Examples in this direction can be found in the work by Pedrero et al. [78], Sainsot et al. [79] and Eritenel and Parker [80]. This allows using analytical dynamic models after having verified the mesh stiffness and Static TE trend. This procedure was iterated for each new microgeometry modification assessed by the optimisation algorithm by Faggioni et al. [50] referenced in *Paragraph 2.1.1*.

2.2.2. Dynamic simulation

The computational effort required for solving the gear meshing problem using finite elements represents a major obstacle for running dynamic simulations under instantaneous operating conditions. Dynamic FE simulations in time domain are very limited and only applicable to specific cases.

Impact forces and propagation of elastic waves were simulated by Lin [81]. The simulation was run for the conditions of sudden applied load and initial speed difference. Given the small extent for the impact time, only fixed mesh configurations between the gears were analysed; for the same reason, the FE mesh was limited to the meshing teeth and their surroundings. In sudden load conditions, for higher initial separation between the gears the impact force was

shown to be increasing and the impact duration was shown to be decreasing. In initial speed difference conditions, for higher speed difference the impact force was shown to be increasing and the impact duration was shown to be constant.

The impact problem was also addressed by Ziegler and Eberhard [82][83] by using different modelling approaches. The FE approach yielded a calculation time of 8 days to simulate 13 gear impacts for a total duration of 20 milliseconds.

In the direction of reducing computational time for the FE solution, a hybrid approach was proposed by Abousleiman and Velex [86]. The Authors used three-dimensional FE elements to represent a deformable planetary ring wheel (*Figure 2.10*) and combined them with analytical gear meshing models. Deformation of the ring gear was shown to substantially affect the tooth load distribution. Dynamic simulations were also performed; however the effects arising from ring resonance were not discussed.

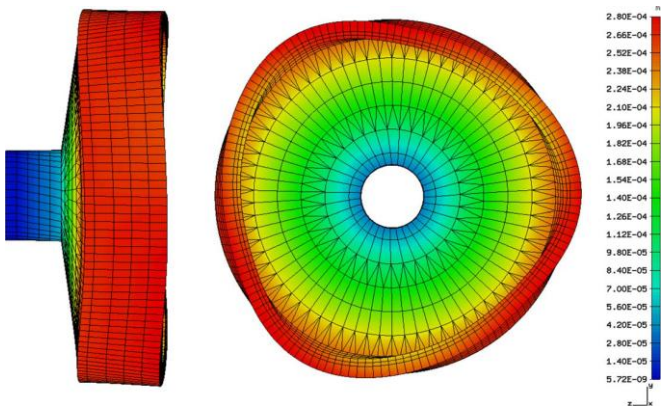

Figure 2.10 – Deformation of a ring gear meshing with three planets Reproduced from [86].

Still in the direction of reducing the computational effort for FE simulations, an original approach was proposed by Vijayakar [87] to eliminate the need of refined mesh on tooth profiles (*Figure 2.11a*). The formulation captures contact analytically by using the Boussinesq formulation for a point load acting on a half-space and the solution is matched with FE nodes at an interface region which is away from contact stress gradients (*Figure 2.11b*).

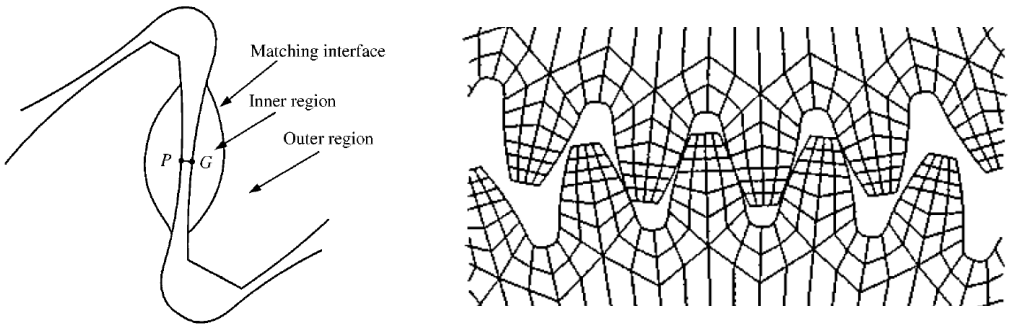

a) *b)*

Figure 2.11 – Hybrid modelling approach by Vijayakar: a) Inner region described by analytical contact solution and outer region described by finite elements; b) Planar FE mesh, to be compared with Figure 2.8. Reproduced from [12].

The tooth surface is descripted analytically to accurately model microgeometry modifications. Planar simulations on a spur gear pair exhibiting contact loss proved to be very accurate when compared to the experiments [11][12]. Planar simulations were also performed to analyse a spur planetary gear set [88] and good agreement was observed comparing the dynamic response to analytical models. The method represents a considerable improvement for FE contact simulations, since the above-mentioned simulations could be ran in time domain with a high number of revolutions for the gears. However similar simulations in three-dimensions are still not possible due to unpractical computational time.

2.3. Multibody models

Multibody models are intrinsically nonlinear, since they are formulated for handling large displacements and rotations between components interacting at a system-level. A typical multibody simulation is based on a model which is built using a “building-blocks” approach: constraints, joints, force elements and standardized subsystems are available in multibody environment to connect the bodies. Bodies represent mechanical components and can be either rigid or flexible. Flexibility can be handled in an efficient way by means of modal reduction techniques [37], allowing an accurate representation of the distributed deformability of the system. For this set of reasons, multibody models offer the greatest potential to capture system-level dynamics for transmissions, without

having to isolate gears. However, gear meshing still needs to be modelled efficiently to the same extent.

2.3.1. Rigid-body models

Rigid multibody gear meshing models are based on the assumption that the gear body is rigid and the full elasticity for the gears is lumped in the meshing process, which is described by using one or more spring-damper elements. A model proposed by Cardona [39] enables to account for the specific orientation of the total contact force for a variety of gear types (*Figure 2.12*).

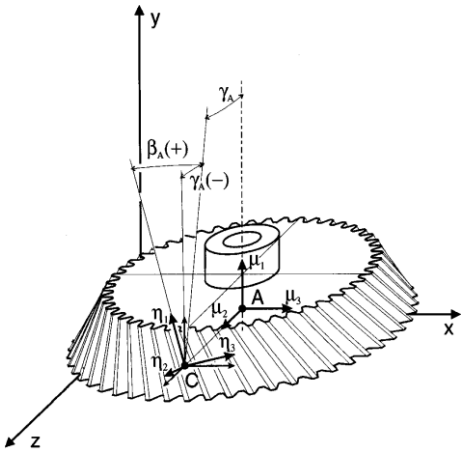

Figure 2.12 – Rigid-body model for total contact force orientation and contact point positioning. Reproduced from [39].

Meshing stiffness is assumed to be constant, therefore the internal source of excitation arising from gear meshing is not captured. Such a modelling approach is very simplified; it allows propagating nominal contact forces in the multibody model and performing a preliminary modal analysis on the full system.

A model accounting for variable number of contacting teeth was proposed by Ebrahimi and Eberhard [90], where each tooth was independently connected to a rigid gear body by means of a tangential spring-damper element (*Figure 2.13*).

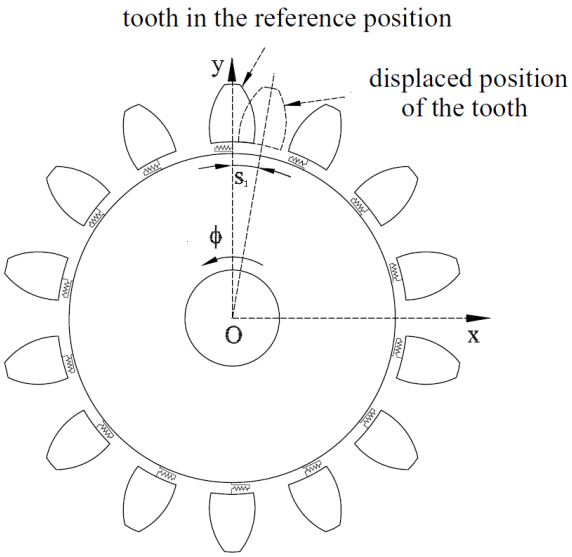

Figure 2.13 –Independently meshing teeth model by Ebrahimi and Eberhard. Reproduced from [90].

A substantial simplification was introduced by assuming constant stiffness for each tooth, although the total mesh stiffness became variable due to the variability of the instantaneous number of meshing tooth pairs. Still such a modelling approach does not accurately represent gear meshing, since contact nonlinearities and tooth microgeometry modifications are not included.

Multibody methodologies for detailed gear contact simulations are partially described in publications by companies developing multibody software like Romax [91], Simpack [92], MSC [93], AVL [94] and LMS [95] which is partnering the present dissertation. Detailed explanations on the methodologies, up to the best of the Author's knowledge, cannot be retrieved in journal publications. Motivations are to be searched on a market level and on a technical challenge level. The fact that detailed system-level simulations for geared transmissions represent a fundamental need for a wide variety of industrial applications connects such a research to marketability and profitability for undisclosed formulations. No exhaustive solution is currently available in the driveline simulation market segment. From a more interesting point of view for the purpose of this dissertation, technical challenges leave ample open margins for scientific research. Examining the available information on commercial formulations it can be noted that many modelling aspects for gear meshing remain unsolved. Romax bases its dynamic solution on a frequency-domain forced response calculation [96]. Gear meshing is modelled with three-dimensional and nonlinear contact

detail only statically and linearization is performed around constant static operating conditions. Simpack [97] accounts for detailed dynamic gear meshing, however the tooth stiffness formulation is either user-defined or based on the ISO 6336 norm approximation. MSC handles detailed gear contact after a simplified dynamic simulation by using external software [98] specialized in static gear contact analysis. AVL also relies on external software [99], which is however embedded in the dynamic simulation by a dynamic link library. LMS [95] calculates dynamic gear meshing by using the approach of Cai, discussed in *Paragraph 2.1.1*, which is limited to the rotational degree of freedom. Degree of validation was discussed to a limited extent in the referenced works and motivates the ongoing investigations.

The multibody methodology proposed in this dissertation can be classified under the category of rigid multibody models aiming to describe detailed three-dimensional nonlinear gear contact dynamics.

2.3.2. Flexible-body models

Flexible multibody models for gear meshing relax the assumption of rigid gear body. Distributed flexibility for the full gear is taken into account, along with its resonance frequencies and modes of vibration. Flexible multibody models represent the most detailed and general modelling approach for capturing system-level gear dynamics. However simulations are currently limited to simple cases due to unpractical computational requirements.

Vinayak and Singh [100] have proposed a multibody formulation which accounts for flexible gear bodies (*Figure 2.14*) by using and FE mesh and for tooth meshing by using the theory of plates. The initially nonlinear time-variant formulation was first reduced to a linearized time-variant and then to a linearized time-invariant formulation to reduce computational time. Good correlation with experiments was obtained for forced response of an isolated gear body including its flexible mode shapes. The discussion showed how gear body flexible modes are strongly coupled with the meshing for thin gears.

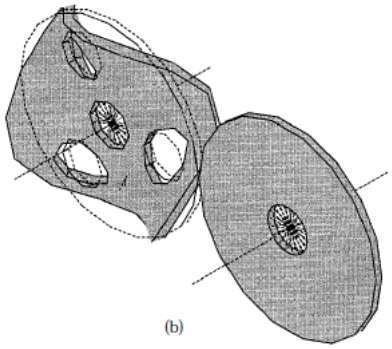

Figure 2.14 – Gear body mode of vibration captured in the model by Vinayak and Singh. Reproduced from [100].

Lundvall et al [101] proposed a planar flexible-body formulation for spur gears including friction. The Authors separated elastic deformations from rigid-body motions and calculated them using a FE mesh. The stiffness matrix related to the FE mesh was re-calculated at each timestep due to contact. The analysis was aimed towards the calculation of the Dynamic TE for different profile microgeometry modifications, with and without friction. Dynamic results provided by the methodology with no a-priori assumptions proved to be in line with analytical three-dimensional models.

Ziegler and Eberhard [82][83] proposed a modal multibody formulation as an alternative to using FE simulations in the study of gear impacts. Results from the FE simulation were taken as a reference and showed a very good comparison to experiments. Results from the modal multibody simulation showed convergence towards the FE results when increasing the number of modes (calculated up to 80 KHz). The Authors provided a comparison between computational requirements needed for FE, modal multibody and rigid multibody simulations (*Table 2.1*). The latter was by far the most computationally efficient technique but it was not able to correctly describe the impact force.

	Model pre-processing time	Integration time 13 impact (20ms)	Disk requirement	Memory requirement
FE	0	~ 8 days	~ 1 GB	~ 1 GB
MB	0	5 seconds	< 100 MB	< 100 MB
Modal MB	28 h	~ 9 minutes	~ 8 GB	~ 500 MB

Table 2.1 – Comparison of the computational effort required for impact simulations performed by Ziegler and Eberhard. [83]

Efforts for reducing computational time of flexible multibody simulations of gears have been made by Heirman et al. [84] and Tamarozzi et al. [85] by introducing the concept of Static Modes Switching. In this modal reduction formulation, the number of modes used to represent gear body flexibility is variable with the active contact points and only include the ones which do actually contribute to dynamic response.

2.4. Fields of application

Since the use of gears is widespread in industry, fields of application for gear dynamics simulations are numerous. The discussion will be limited to the present applications where gears represent a critical component for the operation of the full mechanical power transmission. Criticality is to be intended not only related to mechanical failures, but also to the contribution of the transmission to noise and acoustic comfort. Aside from mechanical failures and noise radiation, a third design topic which benefits from gear dynamics simulations is energy efficiency. Gears represent a non-negligible source of losses, which are mainly due to interactions with the lubricant. Oil churning and windage losses occur between all the wet surfaces; elasto-hydrodynamic lubrication and oil squeeze losses occur between meshing teeth. These topics constitute another wide field of research and since they are not addressed by this dissertation, they will not be examined in the application cases.

Nowadays, for a variety of reasons analysed in the following sub-paragraphs, gears represent a critical component for the automotive, the wind turbine and the aerospace industrial fields. Before stepping into the specifics for these industrial fields, it is worthwhile to outline the general purposes and processing instruments related to mechanical failures and noise radiation.

Mechanical failures can be addressed with different objectives. One objective is addressed by simulations for durability [102][103][104]. These simulations aim at the determination of dynamic (over)loads building up in all the transmission components along with the related stress experienced on the gear teeth. Gear teeth are typically the most failure-prone part of the transmission together with rolling-element bearings. However, while bearings are selected based on their load specifications provided by specialised bearing manufacturers, gears need to be designed on-purpose and accordingly verified. Typical failures for gear teeth

are related to the high levels of peak contact stress and to the stress concentration at the root fillet. A variety of failure modes can be identified (*Figure 2.15*) [105]. Macropitting is one of the most common gear failures and is related to cyclic tooth contact load. The peak shear stress, happening slightly below the tooth surface, causes the nucleation of small cracks. When these cracks propagate until reaching the surface they cause the detachment of small volumes of material and the formation of small craters. Micropitting follows qualitatively the same phenomenology of pitting, however pits are circa one order of magnitude smaller. Micropitting is not a severe failure and can be also classified as wear. It is recently being addressed because of better knowledge of gear loading, better lubricants and increasing use of hardened tooth surfaces allow avoiding macropitting. Scuffing (also known as “scoring”) happens in conditions of poor or ineffective lubrication, when metal-to-metal contact causes adhesive wear scratches on teeth surfaces in the relative sliding direction. Root cracks start from the fillet surface where stress concentration is highest. Bending causes opening normal stress in this region; overloads or fatigue drive the crack through the tooth root.

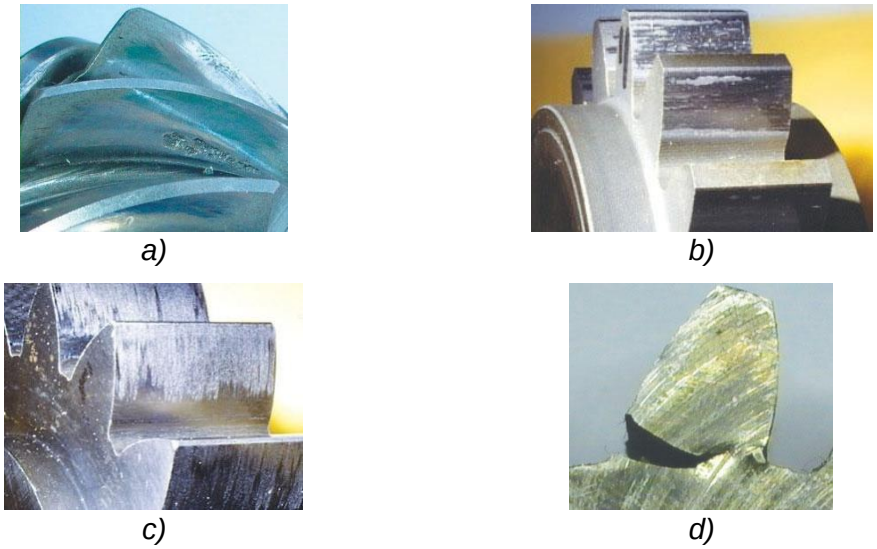

Figure 2.15 – Typical gear failures: a) pitting, b) micropitting, c) scuffing, d) root crack. Reproduced from [105].

Another objective related to mechanical failures is addressed by simulations for diagnostics. A mechanical defect is assumed to be present in the transmission and detection before failure is sought. The ultimate focus is to locate installations,

appropriate instruments and signal processing techniques capable of detecting the defect in the transmission allowing sufficient time for countermeasures. In this direction, the dynamic response and the spectral signature for the transmission are investigated as an important carrier of information. Together with gear simulations, signal processing techniques [106][107][108] represent a major research field to enhance the faulty component of physical quantities measured from the transmission. Industrial applicability in fact requires that the transmission is not dismantled and possibly not diverted from operation. Instantaneous mesh stiffness decrease is a typical change observed in correspondence of cracked teeth [109], which needs to be captured by gear dynamic meshing. Changes in the trend of quantities related to the internal gear excitation (TE, dynamic contact force, tooth microgeometry) have been observed in relation to all the described types of defects. Since gears are typically inaccessible components, the transfer path between the incipient failure and a measurable point is crucial. In view of isolating the part of the signal due to the failure, also accurate system-level response of the transmission constitutes a main simulation objective.

Acoustic comfort simulations aim at calculating the noise pressure level at the ear of a receiver, which is usually annoyed by transmission noise. More sophisticated simulations aim at helping the designers in shaping the sound in specific frequency bands by exploiting psychoacoustics [110]. Noise radiation of a mechanical transmission is usually obtained by calculating first the vibration of the radiating surfaces, usually expressed in terms of velocity, and then applying this result to a Boundary Elements mesh to obtain the sound pressure level at the receiver. Vibro-acoustic simulations are usually avoided, however the coupling between fluid pressure inside the transmission housing and vibration of the housing itself was recently investigated [111]. Two kinds of typical acoustic responses can be observed and they are strictly related to the type of excitation generated by gear meshing. One of them is for gear whine, the other for gear rattle.

In case of gear whine, since the gear excitation is tonal, the analysis of the acoustic response is performed in frequency domain. The gear excitation propagates through the supporting structure and if a meshing frequency, or one of its integer multiples, matches a resonance frequency for the system an amplification for the radiated noise is usually observed. Since mechanical power transmissions typically operate in a range of speeds, spectral analysis is

repeated for samples in the operating speed range. By stacking up spectra at subsequent speeds, three-dimensional diagrams are obtained which are called waterfall plots (*Figure 2.16a*). These diagrams can be flattened on the frequency-speed plane by using a colormap (*Figure 2.16b*).

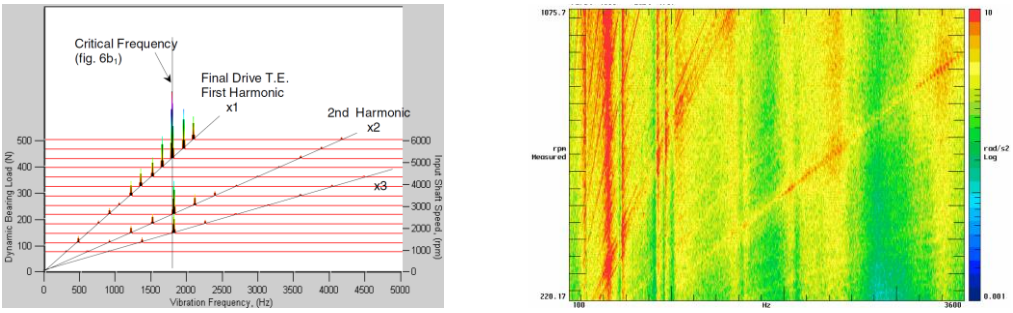

a) *b)*

Figure 2.16 – a) Three-dimensional waterfall plot, b) two-dimensional colormap waterfall plot. Reproduced respectively from [112] and [113].

These plots are particularly useful for distinguishing the internal gear excitation from the resonant acoustic response: gear mesh frequencies are proportional by the number of teeth to the frequency of rotation of the related shaft, therefore linearly depend on the operating speed of the transmission; resonance frequencies for the system typically do not depend on speed. Therefore, in the frequency-speed plane, response dominated by the excitation looks like an oblique line, while response dominated by resonance looks like a vertical line at the resonance frequency.

In case of gear rattle, since the gear excitation is due to impacts, the response is broadband and waterfall plots do not show clear meshing orders (*Figure 2.17*).

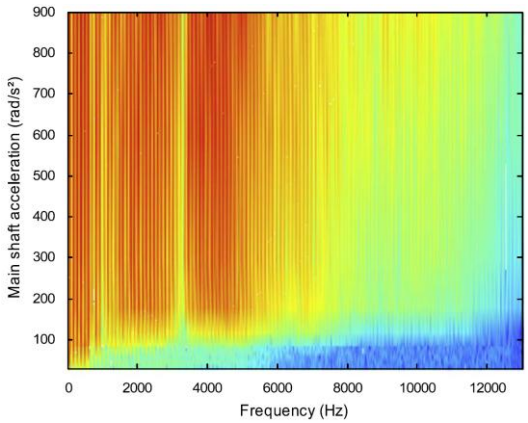

Figure 2.17 – Shaft response due to gear rattle. Reproduced from [114].

2.4.1. Automotive

Transmission dynamics are crucial in the automotive field for the acoustic comfort of vehicle passengers. Both gear whine and gear rattle represent major concerns. Gear whine is particularly important in hybrid and electric vehicles [116]. In electric vehicles and hybrid vehicles in electric mode, noise coming from the internal combustion engine is no longer present. Removal of this source of masking noise makes transmission noise stick out in the interior acoustic signature of the vehicle.

Gear rattle is particularly important in vehicles equipped with diesel engines [117]. The typical torque fluctuations of this engine type facilitate gear loss of contact and repeated impacts, especially at low transmitted torque or when idling. Rattle problems are typically solved by introducing and tuning a dual-mass flywheel (DMF) [118].

Particular care for acoustic comfort, concerning both whine and rattle, is justified for high-end and luxury cars by the price that the customer is proposed to pay.

From a simulation standpoint, different degree of complexity is required for different types of transmissions. Manual transmissions (*Figure 2.18*) involve single gear pairs which engage in a parallel two-stage conventional arrangement. The analysis of manual transmissions does not typically pose particular challenges because of the conventional parallel arrangement of the gear train.

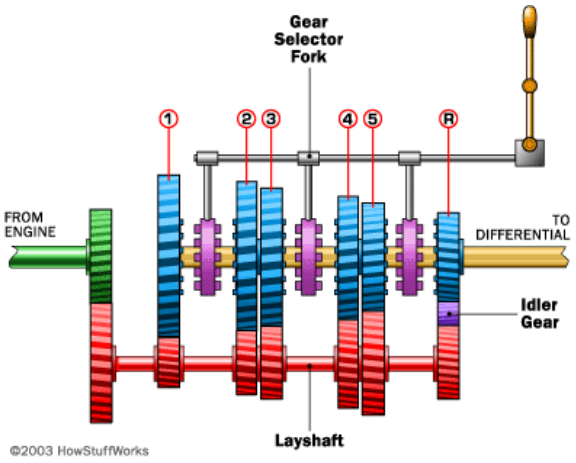

Figure 2.18 – Typical arrangement for a 5-speed manual transmission. Reproduced from [119].

Automatic transmissions (*Figure 2.19*) as well as transmissions for hybrid vehicles (*Figure 2.20*) need planetary gears.

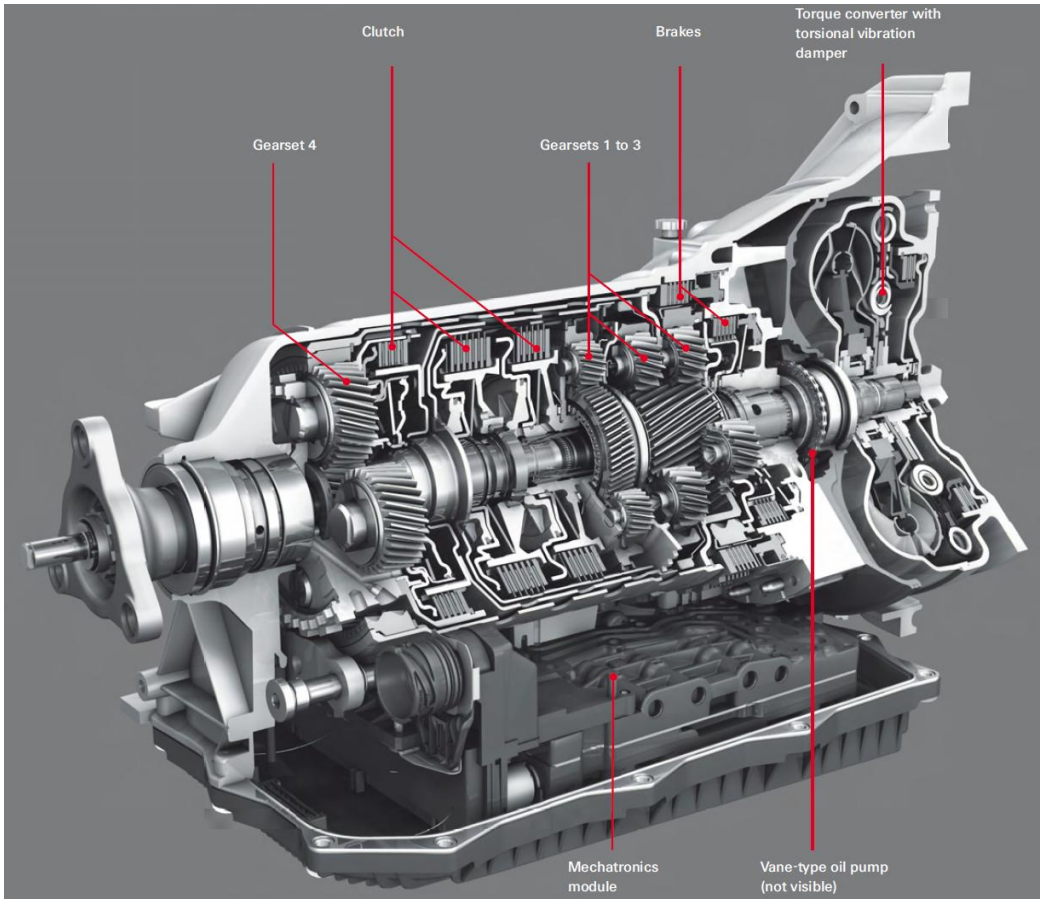

Figure 2.19 – 8-speed automatic transmission ZF 8HP. Reproduced from [121].

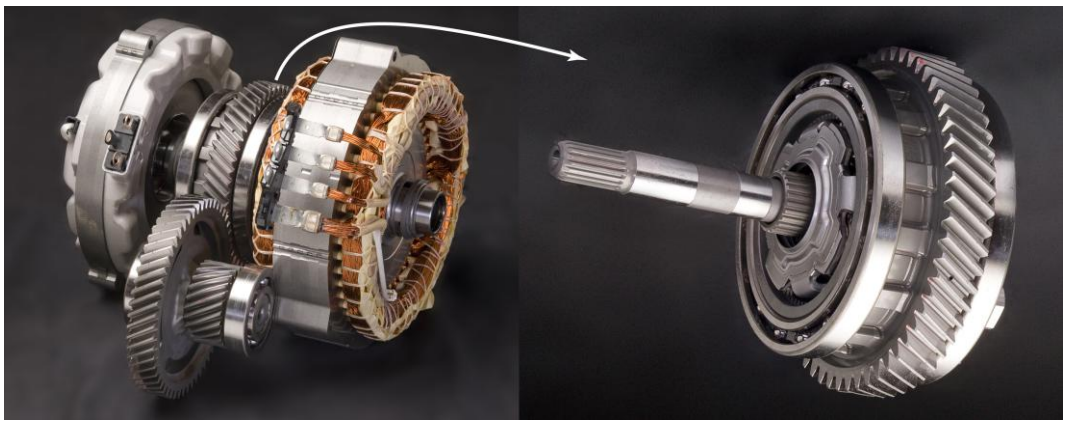

a) *b)*

Figure 2.20 – a) Third-generation Toyota Prius hybrid transmission, b) isolated view of the planetary-gear power split device. Reproduced from [122].

In these cases the dynamic response of gears is tightly coupled with the supporting structure and mutually among the gears. The quest for lighter structures represents a trend which is spread across the whole automotive market and turns for the specific case into more flexible components.

System-level simulation is required to correctly capture this coupling and time-domain integration of the solution is required to capture nonlinearities induced by the coupling. This represents a substantial simulation challenge and no off-the-shelf solution is available on the market.

2.4.2. Wind Turbines

Mechanical failures represent the main concern for wind turbine transmissions, provided that the acoustic emission satisfies the restrictions imposed by regulations [120].

High failure rates for gearboxes, especially localised in bearings [123], are currently being experienced. These failures may lead to lubricant fire, which then spreads to the nacelle and the rotor, causing catastrophic failure of the wind turbine. Even if catastrophic failure is not reached, repairing the transmission or executing frequent maintenance represents a considerable cost for wind turbine operation. To increase reliability and avoid such risks, overloads which are typically caused by the dynamic response or by misalignments need to be accurately assessed. Simulations to perform the assessment are particularly challenging since the most used gear arrangements include a mix of planetary and conventional stages bridging a wide speed gap between the input and the output shafts. For wind turbines up to 3MW rated power [124], a gear arrangement composed by one planetary stage followed by two conventional parallel stages is typically adopted (*Figure 2.21*).

Figure 2.21 – General Electric 1P 2.3 wind turbine transmission, having one planetary stage and two conventional parallel helical stages. Reproduced from [125].

For wind turbines above 3MW rated power [124], a gear arrangement composed by two planetary stages followed by one conventional parallel stage is typically adopted (*Figure 2.22*).

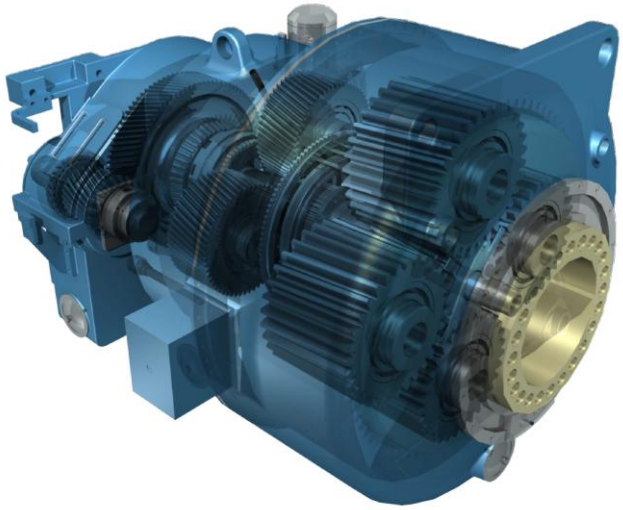

Figure 2.22 – General Electric 2P 2.9 wind turbine transmission, having two planetary stages and one conventional parallel helical stage. Reproduced from [125].

The wind turbine rotor typically turns at a frequency below 1 Hz (60 rpm), while the generator typically turns at circa 25 Hertz (1500 rpm). Therefore the transmission has to provide a very high multiplication ratio, greater than 25:1. Moreover, the flexibility of the supporting structure is found to be affecting the behaviour of both gears and bearings [126]. System-level simulations, including the flexibility of the supporting structure, represent a key tool to quantitatively determine the extent of this structural coupling. Planetary ring gear flexibility and detailed bearing modelling represent additional open challenges for such simulations. Substantial deformation of the ring gear, which is embedded in the transmission housing, has been observed and proved to affect gear meshing [127][4]. Bearing modelling has been proven to neglect important phenomena for transfer path analysis and for residual life estimation. In particular, bearing stiffness needs to account for the coupling induced by loading one constrained degree of freedom and obtaining a response on the other constrained degrees of freedom [128][129][130][131][132].

Gear noise radiation for wind turbines is mainly structure-borne. Blades and the tower, act as “loudspeakers” under the gear excitation [16]. Additional reductions in emitted noise below the regulated acoustic margins represent a competitive advantage on the market and can be achieved by reducing gear excitation and/or by reducing the structural response. Gear excitation can be reduced by carefully designing the tooth microgeometry. This can be done only if loads and misalignment are correctly captured. Since both of them depend on the mutual interaction between the gears and the supporting structure, system-level simulations are crucial for such design process. Reducing the structural response can be achieved if the transfer path followed by the excitation is known. To do so, distributed flexibility of the structure must be included and coupled with the gear meshing process. Again system-level simulations are crucial for achieving the goal.

2.4.3. Aerospace

Transmissions represent critical components for helicopters and aviation jet engines.

In helicopters, transmissions pose main concern for durability and condition monitoring. Acoustics is also important for saving weight by removal of insulating

material. A helicopter main transmission delivers power to the rotor, where blades are connected, operating an extreme reduction ratio. Helicopter turboshaft engine(s) typically turn at circa 30000 rpm, while the rotor at circa 300 rpm. The needed reduction ratio is in the order of 1:100 and requires one or more planetary stages (*Figure 2.23 top*). Input modules and an accessory transmission are used to deliver power to the main transmission for the main and the tail rotor, to start the engine(s), to drive an oil pump for the hydraulic circuit and a fuel pump for the engine(s) [133]. This transmission is typically composed of spur gear trains with idler gears (*Figure 2.23 left*). Spiral bevel gears are used to transmit power between crossed-axis shafts from the accessory transmission to the main transmission and from the main transmission to the tail rotor (*Figure 2.23 centre*).

Figure 2.23 – Cutaway of an Agusta A109 helicopter transmission displayed at Sint Truiden Air Base, Belgium.

Durability and health monitoring is addressed with a number of sensors and signal processing techniques [134][135]. The signal analysis is performed in a more structured Health and Usage Monitoring System (HUMS) which alerts the crew in case of anomalies. It is usually preferred to get as close as possible to

the excitation source by incorporating a number of accelerometers in the transmission housing phase-referenced to a one-per-rev sensor [136].

Acoustics represents a serious concern for the interior of the helicopter. The main transmission is connected to the roof of the cabin, right below the rotor. Transmission noise inside the cabin dominates the low-medium frequency range with meshing frequencies and related sidebands from 0 to 8 kHz (*Figure 2.24*) [137] and can reach 100 dB [16].

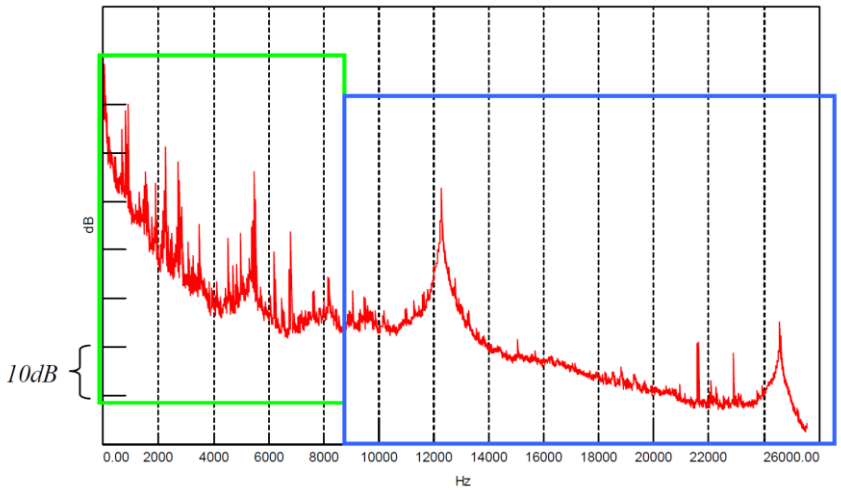

Figure 2.24 – Sound pressure autopower in a helicopter cabin under steady-state operational condition. Reproduced from [137].

Sound-absorbing material is used to limit interior noise with non-negligible increase in weight. Limiting emitted noise therefore represents a way for reducing weight. The market of VIP helicopters targets noise reduction also for improved acoustic comfort for the passengers [138].

In jet engines, the main focus is on transmission health monitoring and durability [139]. Noise emission due to gear excitation is very limited if compared to aerodynamic noise arising from the running engine and the airframe. Transmissions are typically [140] arranged as shown in *Figure 2.25*. An internal gearbox, with spiral bevel gears, is used to extract power from the core of the engine when running or to provide power to start it. A step-aside gearbox is used to reduce the speed and increase the torque for the power extracted by the internal gearbox. Both the internal and the step-aside gearbox use radial drives with spiral bevel gears. The extracted power is transmitted by the step-aside gearbox to the external accessory gearbox by an angled shaft.

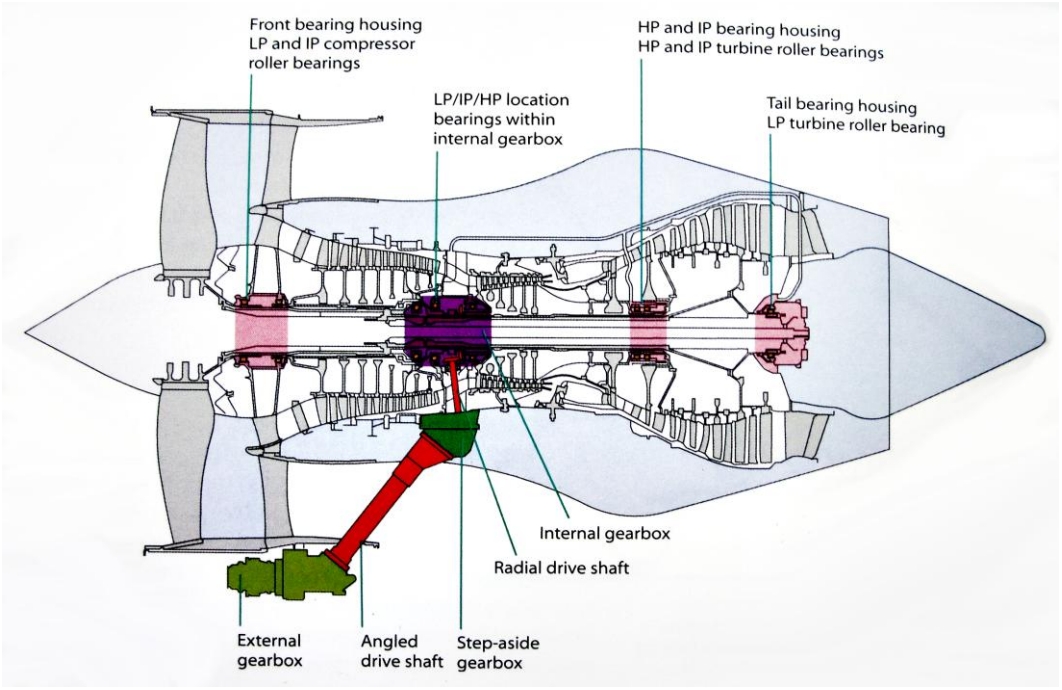

Figure 2.25 – Typical transmissions arrangement in a jet engine. Reproduced from [140].

The accessory gearbox has similar functions as in the case of helicopters and it is also constituted by multiple trains of spur gears. Spur gears allow saving weight by avoiding thrust-absorbing bearings, however they are more prone to loss of contact. Idler gears allow moving along the fan casing to mount the accessories while keeping the frontal area as low as possible.

Both in case of helicopters and jet engines, the coupling between the gears and the supporting structure is enhanced by the need of making lightweight and therefore flexible components. Once again, system-level simulations allow capturing this coupling during the design phase.

Chapter 3.

Theoretical background for the proposed Gear Multibody Element

Up until now, there are no formulations in the literature which allow dynamic simulations with high numbers of revolutions for the gears at an assembly level and where gear contact is modelled with detail in three dimensions. The proposed methodology, developed for internal and external spur and helical gears, allows considering variable mesh stiffness based on the solution of a three-dimensional teeth contact problem under the instantaneous load and three types of relative gear misalignments. Computational efficiency is furthermore increased by calculating mesh stiffness in a pre-processing step and storing the values in multivariate look-up tables which are interpolated during the multibody simulation using the instantaneous operating conditions. The mesh stiffness can be obtained in the pre-processing step using any software tool which allows detailed gear contact simulation. Dynamic contact force is calculated for each gear pair during the multibody simulation and is applied as a resultant along the operating normal to tooth surfaces and the point of application is positioned axially according to contact pressure distribution, allowing to consider shuttling effects. Microgeometry modifications of teeth surfaces are taken into account, including nonlinear load-dependent effects. Friction and losses are not included in the majority of the models mentioned in the state of the art, since their effects on dynamics are limited for the typical case of well lubricated gears. Moreover, friction and damping models based on lubrication physics represent a whole emerging research field [141]. For these reasons, friction and damping are modelled in the proposed methodology using equivalent viscous damping.

3.1. Purposes and structure of the multibody gear element

The proposed element has been developed to provide the following capabilities:

1) Simulate dynamic tooth contact with three-dimensional level of detail, accounting for microgeometric modifications of teeth surfaces;
2) Allow speed-sweep dynamic simulations for spur and helical gear transmissions at the assembly level;
3) Provide scalability such that the user is allowed to enable or disable each of the factors influencing gear meshing independently.

To achieve point 1, equivalent mesh stiffness is calculated for each gear pair using the LDP software (Load Distribution Program) [141], which is specialized for gear contact analysis. This software is based on a three-dimensional static formulation accounting for:

a. Teeth contact stiffness[143];
b. Teeth bending stiffness [144][145];
c. Elastic rotation and deflection at teeth base [146];
d. Gear blank torsional stiffness (assuming an elastic disk);
e. Teeth microgeometric modifications;
f. Position along the mesh cycle;
g. Transmitted load;
h. Gear misalignments.

These factors are taken into account when calculating three-dimensional contact stress distribution and the consequent mesh stiffness due to the actual number of tooth pairs in contact. Points *a* to *e* are constitutive features of each gear, according to material (assumed to be elastic) and tooth surfaces, whereas points *f* to *h* can vary during meshing due to system dynamics. Therefore, the position on the mesh cycle, the transmitted load and the gear misalignments are identified as operating conditions for the gears. They are discussed in the next paragraphs of the dissertation. Quantitative ranges for these operating conditions are estimated and discretised before the dynamic simulation and mesh stiffness is calculated in this pre-processing step for each of these combinations. Mesh stiffness is then stored in a multivariate look-up table, which is interpolated during the multibody simulation by the gear element according to the instantaneous, namely dynamic, operating conditions. A simplified schematic of this process is

illustrated in *Figure 3.1*, where UDF indicates a User-Defined Force element developed for the commercial multibody software LMS Virtual.Lab Motion.

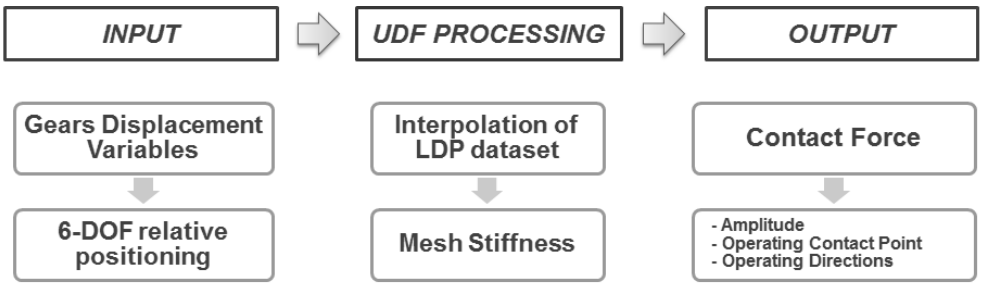

Figure 3.1 – Main processing steps for the referenced gear multibody element.

The algorithm used for multidimensional interpolation [147] is based on the Shepard's method and grants continuity up to the second derivative (C2) across the interpolated domain. All the operating conditions are expressed at the same timestep in terms of 6-DOF relative positioning of the gears (see *Paragraph 4.2* and *4.3*) and are elaborated by the simulation solver (typically implicit BDF with variable timestep) which returns through each gear element the related contact force value, direction and point of application, considering the dynamics of the full multibody model. The execution of the calculation steps is illustrated in the workflow diagram of *Figure 3.2*.

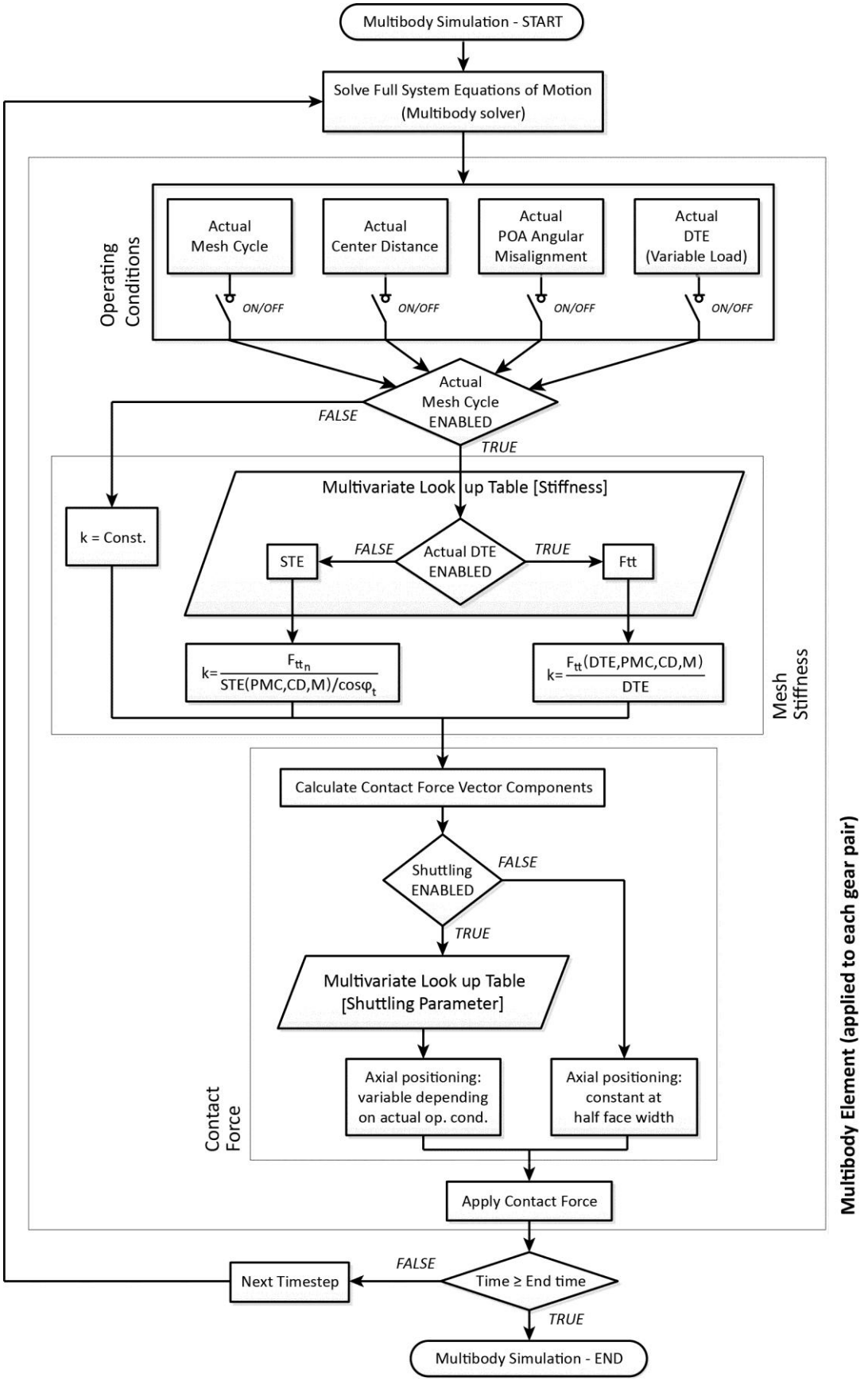

Figure 3.2 – Gear element calculations flow chart.

Computational efficiency is consistently increased for speed-sweep dynamic simulations (point 2) as a consequence of the lumped-parameter approach (where gear mesh stiffness depends on the instantaneous operating conditions) and since gear contact is solved only once before the multibody simulation. Similar static calculations to obtain the mesh stiffness values can be performed using other specialized software for gear contact or non-linear finite element analyses. To provide scalability to the user (point 3), the operating conditions are handled independently from each other by the gear element. In this way their dynamic effects can be enabled or disabled individually, allowing sensitivity analyses to be performed and computational effort to be tuned according to simulation purposes. Enabling or disabling dynamic effects of the operating conditions determines the number of dimensions for the multivariate look-up table, which can degenerate in a single number if the constant mesh stiffness option is selected. Shuttling effects can also be enabled or disabled as they are handled using an additional variable depending on the instantaneous operating conditions besides the mesh stiffness: the position of the contact point in the axial direction. Specifically, when mesh stiffness is set to be variable, the gear element allows selecting between the following dynamic effects on meshing:

1) Position along the mesh cycle
2) Transmitted load
3) Centre distance variations
4) Misalignment in the plane of action
5) Shuttling

Since mesh stiffness is variable, the position on the mesh cycle cannot be disabled, while all the other effects are selectable. An initial value can also be specified for the position on the mesh cycle (mesh phasing). The following paragraphs describe how the above-mentioned effects are implemented in the gear element.

3.2. Relevance of Transmission Error

The TE is not a constant quantity; it varies during the process of teeth meshing and is considered therefore[1] one of the main causes for gear vibration. Several factors concur in the deviation from the case of ideal transmission[2] (*Figure 3.3*).

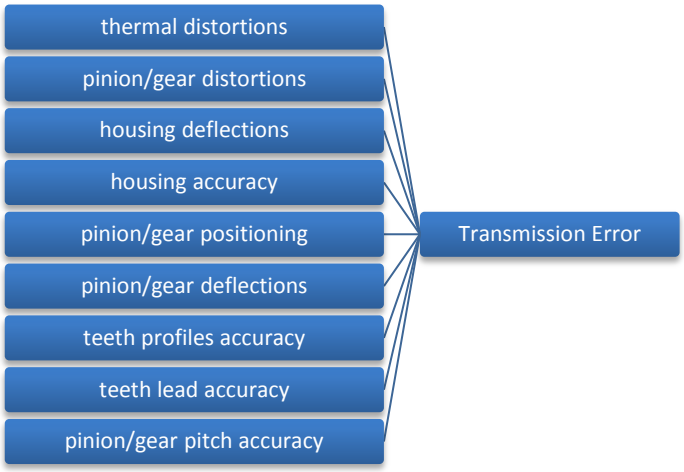

Figure 3.3 – Main concurrent factors affecting TE [16].

From the factors schematized in *Figure 3.3* the TE appears to be caused by imposed displacements (e.g. distortions, manufacturing/assembly errors) and applied loads (which cause deflections). The factors affecting the TE, except distortions, will be discussed in the following paragraphs. Before addressing the discussion, it is worthwhile to mention different quantitative definitions of TE and underline their physical meaning and usefulness.

Definition a) (3.1), *Figure 3.4*: "the Transmission Error is the difference between the angular position that the output shaft of a drive would occupy if the drive were perfect and the actual position of the output" [16].

[1] *A constant TE during meshing would not cause any contact force variation and subsequent vibration.*

[2] *Ideal transmission is synonymous of theoretical transmission, thus perfectly obeying to the kinematic relationship defined between the gears by the gear ratio.*

$$TE = \theta_2{}^* - \theta_2 = \theta_2{}^* - \tau\theta_1 \qquad (3.1)$$

$\theta_i{}^*$: real angular position;

θ_i: ideal angular position;

τ: gear ratio.

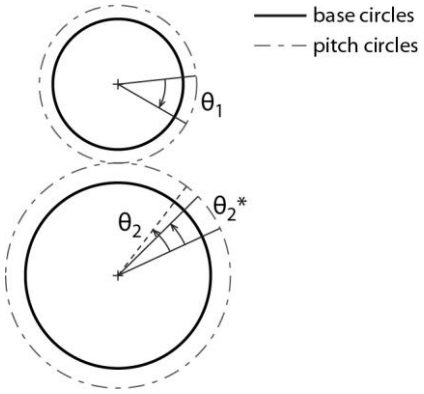

Figure 3.4 – Parameters needed to define the TE in terms of rotations.

It should be noted already that the TE takes into account as an aggregated quantity deviations happening due to all the meshing gear teeth at the given time instant plus both the gear bodies. Moreover, considering the driving gear as the reference does not introduce approximation. This is only needed to establish a reference for calculating a difference in rotations.

Definition b) (3.2), *Figure 3.5*: the Transmission Error is given by the difference between the displacements caused along the Line of Action by the relative rotation between the driving and the driven gear.

$$TE = r_{b1}\theta_1 - r_{b2}\theta_2 \qquad (3.2)$$

θ_i: real angular position;

r_{bi}: base circle radius.

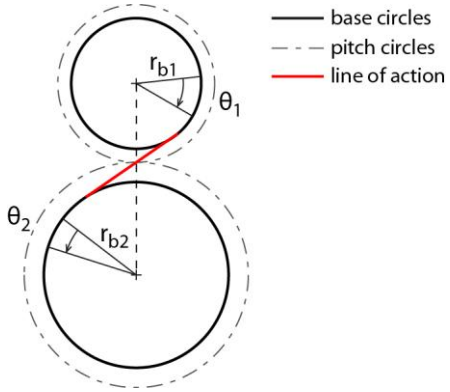

Figure 3.5 – Parameters needed to define the TE as a displacement along the line of action.

This definition becomes more intuitive if referred to the traditional example considering the line of action as a string[1] which unwraps from the base circle of the driving gear to wrap around the base circle of the driven gear. The relative displacement can be thought as either an extension or a contraction of the string.
Definition c) (3.3), *Figure 3.6*: the Transmission Error is given by the difference between the displacements caused in a tangential direction at the operating pitch point by the relative rotation between the driving and the driven gear.

$$TE = r_1\theta_1 - r_2\theta_2 \qquad (3.3)$$

θ_i: real angular position;
r_i: operating pitch circle radius;
C_i: gear centre of rotation;
C_{ij}: operating pitch point.

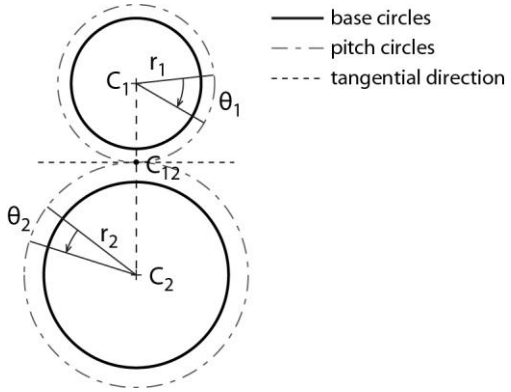

Figure 3.6 – Parameters needed to define the TE as a displacement in a tangential direction.

This definition is similar to the previous case, however the relative displacement is considered in a different direction.
All the three definitions account for contributions to the TE arising from rotations and must be complemented by contributions arising from displacements, as stated in *Paragraph 4.2*.
To recap, the typical TE definitions are defined based on the following parameters:

a) relative rotation of gears;
b) relative displacement along the line of action (a direction which is tangent to the *base* circles);
c) relative displacement along the tangential direction at the operating pitch point, (a direction which is tangent to the *operating pitch* circles)

[1] *As Smith notes "it is a rather peculiar mathematical string that pushes instead of pulling".*

Definition a) is more devoted to the kinematics of the gearing, since it enhances the error in angular position. Definitions b) and c) are more useful for dynamics, because by multiplying the relative displacement and the equivalent mesh stiffness in the contact point, the contact force can be obtained.

To avoid incurring in errors, only one definition is chosen hereby and employed throughout the dissertation: the TE is defined as a relative displacement along the line of action (definition b).

It is moreover important to distinguish between two types of TE: static (STE) and dynamic (DTE). The static TE includes geometric deviations from the ideal case, deflections and contact deformations under the quasi-static assumption. The dynamic TE includes the inertial and damping effects related to a variable contact force alongside of the quasi-static phenomena. The DTE therefore appears to be more relevant for dynamics as it is affected by resonances in the system. Provided this distinction, when only TE is mentioned, both STE and DTE are to be considered as a subject.

3.2.1. Tooth stiffness contribution

The total static deflection of the meshing tooth pairs happens in the direction of the contact force in a transverse plane and can be calculated by means of (*3.4)*, provided that the contact force F and the mesh stiffness K in the configuration θ are known.

$$\delta = \frac{F}{K(\theta)} \qquad (3.4)$$

It is important to acknowledge that the deflection is elastic and changes if loading or stiffness conditions change. Moreover, since the STE has been defined as a relative displacement along the contact force direction in a transverse plane *(3.2)*, the deflection δ represents a direct contribution to the STE. The STE itself can be then decomposed into an elastic component and an imposed displacement (arising for example from manufacturing errors and/or misalignments):

$$STE = \delta + \Delta \qquad (3.5)$$

The above remark motivates why the variable mesh stiffness resulting from all the meshing teeth represents one of the parameters having greatest influence on on the STE.

In a more general consideration, all the supporting flexible bodies contribute to the elastic component of the TE (*Figure 3.7*) as soon as a torque is transmitted (namely the contact force is different from zero).

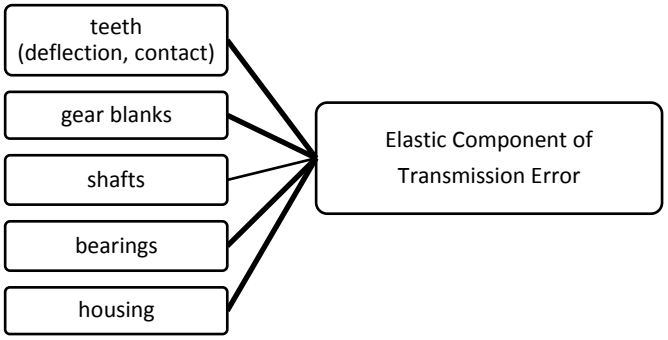

Figure 3.7 – Elastic contributions to Transmission Error.

After a brief description of the different contributions, gear-related elastic contributions will be discussed in this paragraph. Moreover, recalling that a constant deflection during the mesh cycle is not a cause of vibration, the paragraph is focused on the mechanisms which cause a variation of mesh stiffness, hence of TE and contact force.

Bearings have usually a stiffness which is comparable to the gear mesh stiffness. Complex load-dependent nonlinearities play a role in determining their stiffness and cross-coupling happens between loads and deflections in the various degrees of freedom [127][128][129][130][131][132]. A simplified linear assumption for stiffness with a zero-stiffness initial region to represent bearing clearance are illustrated with a qualitative load-displacement curve in (*Figure 3.8*).

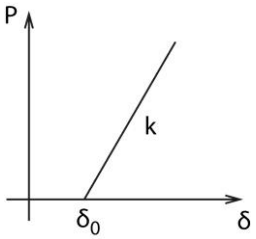

Figure 3.8 – Qualitative load-displacement curve to approximate bearing stiffness.

This modelling approach is sufficient to highlight two important effects determined by bearings. The clearance-type nonlinearity for bearings reverberates on the gears since bearing forces are coupled to gear contact forces. Moreover, the elasticity of bearings introduces misalignments for the gears.

Shaft stiffness is related to their particular geometry. It is not possible therefore to assume any value a-priori. Shafts can also contribute to misalignments due to bending deflection and rotation.

As illustrated in *Figure 3.7* , gear-related contributions to the elastic component of the TE can be split between the gear blank and the meshing teeth. The contribution due to the gear blank becomes dominant on the gear response if the gear is thin-rimmed or thin-webbed [148]. Such a case, although more and more industrially relevant, is currently out of reach for current dynamic simulation techniques. When the gear blank has not undergone lightening modifications, its elastic deformation can be considered as the superposition of a global field due to torsion and bending plus a local field acting at the base of each meshing tooth. The global deformation field depends on the overall load experienced by the gear blank, therefore it represents a constant deformation for the gear and not a source of excitation. The local deformation field depends on the amount of load which is shared by the related tooth. The load sharing on each tooth is variable with the mesh cycle (since teeth enter, handover and leave contact) and strictly depends on the tooth macro and micro geometry as well as relative positioning and loading. Five main mechanisms of tooth bending stiffness variation in the mesh cycle have been identified (*Figure 3.9*) and will be discussed hereafter:

A) partitioning of the contact force alternatively on *n* and *n+1* tooth pairs, where *n* represents the integer part of the contact ratio;
B) variation of the components of compression and bending in the contact force, as a consequence of the varying tilt angle between the contact force and the tooth symmetry axis during the meshing progress;
C) variation of the distance between the contact force point of application and the tooth root (active tooth height);
D) variation of the equivalent stiffness resulting from a pair of meshing teeth;
E) difference in the tooth shape of meshing teeth (e.g. gear having a small number of teeth meshing with a gear having a high number of teeth).

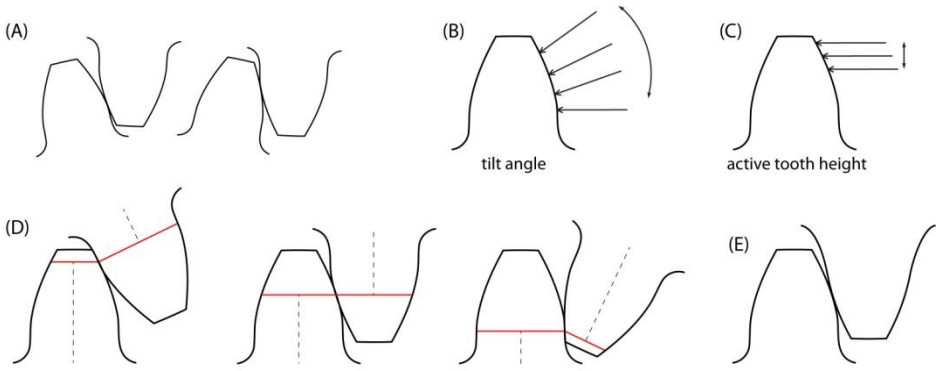

Figure 3.9 – Representation of the main mechanisms which introduce variability in the mesh stiffness during the progress of meshing.

Together with these variation mechanisms for tooth global stiffness, the local contact stiffness effects must be included.

A) *Contact Force Partitioning* – During the meshing process, considering two subsequent tooth pairs, the following pair engages before the leading pair has left contact. This is a direct consequence of achieving a contact ratio always greater than unity to avoid detrimental impacts. The handover between tooth pairs is more gradual for helical gears than for spur gears, generating for the second case a higher mesh stiffness fluctuation (*Figure 3.10*).

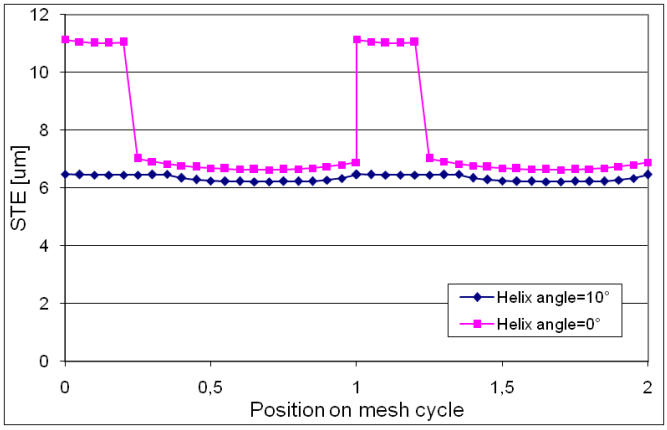

Figure 3.10 – Qualitative elastic component of the STE along two mesh cycles, for a spur and a helical gear pair having the same module and number of teeth.

The smoothness for the STE variation is bound to the different progress of contact lines in the two cases. In case of spur gears, an engagement or disengagement for a tooth pair happens over the full active face width. In case of

helical gears contact starts from a corner, extends progressively on the tooth surface, and terminates in the opposite corner (*Figure 3.11*).

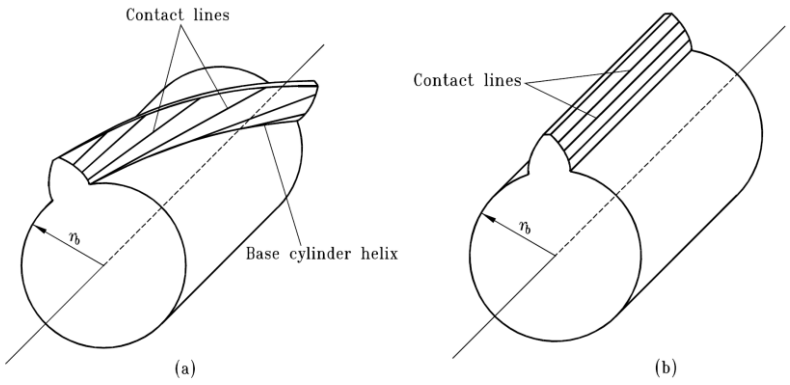

Figure 3.11 – Progress of contact lines for a) helical gears and b) spur gears. [17] p.388

A solution to smooth the mesh stiffness variation due to the tooth pairs handover is to design gears which have an integer contact ratio (*Figure 3.12*), so that simultaneously when a tooth pair is leaving contact, a new tooth pair starts engaging. In reality, such a solution is difficult to achieve due to manufacturing tolerances, trade-offs with tooth strength when selecting the contact ratio and variability of the actual contact ratio under different loads caused by teeth deflections.

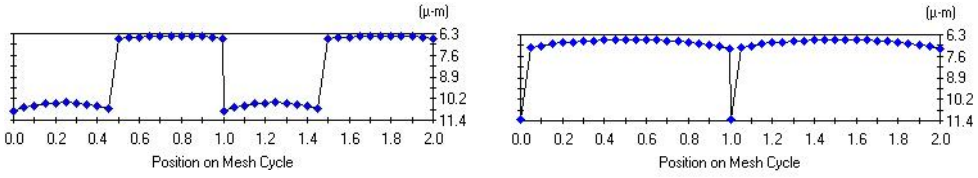

Figure 3.12 – Elastic component for the STE along two mesh cycles for a gear pair having contact ratio of a) 1.5, b) 2.0, given the same module and number of teeth.

The mesh stiffness fluctuation due to tooth pairs handover is usually intense and may cause loss of contact for spur gears which have a contact ratio between 1 and 2. In case of helical gears, the contact ratio does not particularly influence

the trend of the STE thanks to the gradual approach and recess of contact lines [34].

The above-mentioned phenomena can be described quantitatively by calculating the equivalent mesh stiffness from simultaneously meshing tooth pairs (*Figure 3.13*). Contacting teeth are subject to the same load and can be considered as springs in series. Different meshing teeth on each gear are subject to the same rotation and can be therefore considered as springs in parallel.

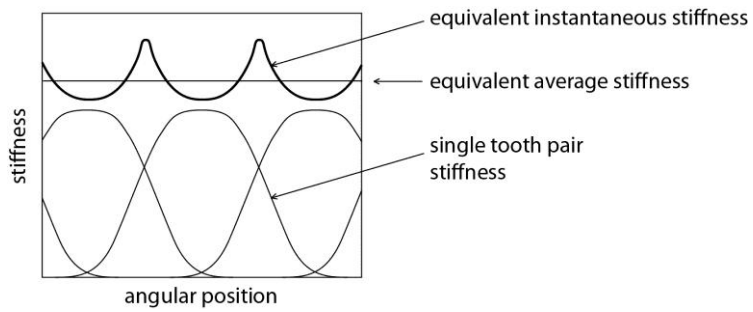

Figure 3.13 – Trend for the equivalent mesh stiffness during meshing, obtained by considering simultaneously engaging tooth pairs.

Considering the frequency domain, the fundamental frequency of the contact force variation caused by teeth handovers will be equal to the frequency of the teeth handovers themselves. During one mesh cycle the number of teeth handovers is always equal to 1. Therefore the fundamental frequency of the contact force will be equal to the meshing frequency. If for example the contact ratio is between 1 and 2, in one mesh cycle there will be contact partly between one pair of teeth and partly between two pairs of teeth. As a rough approximation for a spur gear pair, the mesh stiffness will become 2 times higher when the second tooth pair engages (*Figure 3.14a*). If for example the contact ratio is between 2 and 3, in one mesh cycle there will be contact partly between two and partly between three pairs of teeth. The handover is again equal to one, but the stiffness becomes only 1.5 times higher when the third tooth pair engages (*Figure 3.14b*), leading to a less severe stiffness fluctuation.

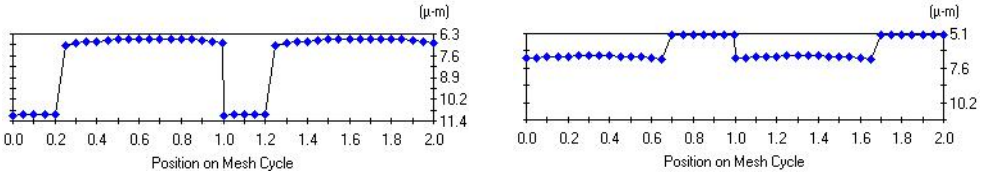

a) b)

Figure 3.14 – Elastic component of the STE along two mesh cycles for a spur gear pair having contact ratio equal to a) 1.77, b) 2.30, given the same module and number of teeth.

B) *Bending over Compression Force magnitude* – The inclination of the line of action with respect to the centre distance remains substantially equal to the pressure angle during the progress of meshing. This property is due to the conjugate action of teeth profiles and implies that, since the gears rotate, the direction of the contact force changes with respect to each tooth symmetry axis. This phenomenon becomes immediately recognisable when considering that the contact force (neglecting friction) is always normal to the tooth surface (*Figure 3.9B*). As a consequence, with respect to the tooth axis, the contact force parallel component (compression) and perpendicular component (bending) (*Figure 3.15*) act in different proportion along a mesh cycle.

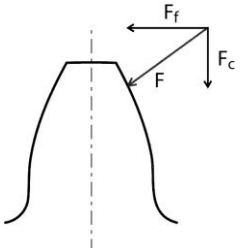

Figure 3.15 – Bending component (F_f) and Compression component (F_c) for the tooth contact force (F).

Therefore also normal and bending stiffness acquire different weights during the mesh cycle, making the tooth deflection variable. The ratio between the two force components along the mesh cycle is determined by the specific geometrical features of the tooth profile.

C) *Active tooth height variation* – Not only, as described in the previous case, the bending and compression force components vary; also the related stiffness components vary along the mesh cycle, since:

a) the active tooth height[1], where the contact force is applied, varies;

b) the tooth geometry encompassed under the active tooth height varies.

For the point a), it is possible to easily verify by approximation how bending stiffness is greatly sensitive to variations of tooth height in comparison to normal stiffness. For that reason in *Figure 3.9C* only the bending stiffness component is reported. Considering the active part of the tooth as a cantilever beam loaded at the extremity, the displacements caused by the two components are:

$$\delta_c = \frac{L}{EA} F_c; \quad \delta_f = \frac{L^3}{EI} F_f \tag{3.6}$$

where L represents the active tooth height, E reporesents the Young's modulus of the material, A represents the average cross section of the tooth and I the geometric moment of inertia of the cross section. Thus, while the normal compliance increases linearly with the active tooth height, the bending component has a considerably higher sensitivity since it varies with the cube of the active tooth height. Such qualitative considerations need Finite Element modelling to be assessed accurately in a quantitative way. This quantification is out of scope for the current discussion, which aims at illustrating the main variability sources of mesh stiffness and motivating the use of TE as a quantity to perform gear calculations in an efficient, yet detailed, way.

D) *Equivalent tooth pair stiffness* – Taking into consideration only one tooth meshing in a pair and following the contact point moving along the profile, it can be noted that when the tooth bending stiffness component increases, the bending portion of contact force decreases. There are, therefore, compensations taking place which could be exploited for reducing mesh stiffness variability. These variability compensations on a single tooth can be evaluated on a case-by-case basis since tooth geometry (and therefore bending stiffness) is also linked to the

[1] *The active tooth height is measured from the root radius of the tooth (root circle). "Active" indicates that this height is loaded by the contact force.*

tooth load evolution during the mesh cycle. This loop makes such optimization problem non-linear. Similar compensations not only happen with focus on a single-tooth, they also happen when considering the mesh stiffness equivalent from the pair of meshing teeth. In this case, while the active tooth height increases along the mesh cycle for one tooth, it decreases for the other (*Figure 3.9D*). If teeth have exactly the same geometry, the single-tooth stiffness increase for one tooth equals the decrease for the other. However teeth in the same pair behave as springs in series, therefore the most compliant tooth dominates the equivalent stiffness of the pair. As a result the compensation will be only partial and will not result in a constant equivalent stiffness. Still from this observation and considering *Figure 3.9D* it is possible to draw qualitatively the trend of the mesh stiffness equivalent to a pair of meshing teeth. At the beginning of meshing one tooth is less stiff because it engages at the tip, while the other is stiffer because it engages at the root. The equivalent mesh stiffness is dominated by the most compliant tooth and therefore it is minimal. When meshing progresses until the teeth reach equal stiffness values a maximum value is achieved for the equivalent mesh stiffness for the pair. A further progress of meshing reverses the condition for the two teeth: the engagement for the first tooth moves towards the root, while for the second tooth moves towards the tip. As a conclusion, the stiffness for a single tooth pair starts from a minimum value, reaches a maximum in proximity of half the length of contact and decreases again towards a minimum value (*Figure 3.16*).

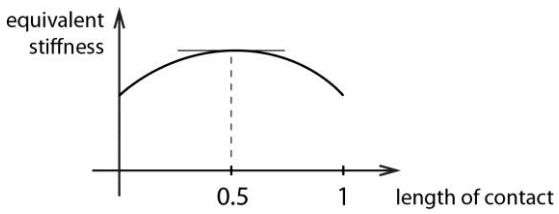

Figure 3.16 – Qualitative trend for the equivalent mesh stiffness of a pair of meshing teeth along the length of contact.

E) *Tooth shape difference* – The equivalent mesh stiffness discussed above presents a symmetric trend only if teeth have exactly the same geometry. This becomes not true already from a macrogeometry point of view if the meshing gears have a different number of teeth (which represents the common case to

achieve a gear ratio different from unity). As shown in *Figure 3.17*, increasing the number of teeth for a gear makes them look closer to the ones of a rack. The teeth of a rack have rectilinear profiles as the radius of curvature of the base radius and of the related involute portion tends to infinity. On the other hand, decreasing the number of teeth leads to more curvilinear involute portions since the base radius decreases and the involute roll angle span increases. Decreasing the number of teeth can also lead to the need of generating a trochoidal tooth profile below the base circle (undercutting), which causes additional decrease of the root tooth thickness. As a general conclusion, the gear with the higher number of teeth has the teeth with the highest stiffness.

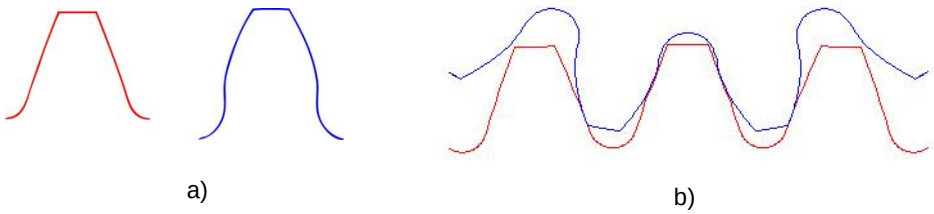

Figure 3.17 – a) Transverse tooth section for a gear with 200 teeth (red line) and a gear with 17 teeth (blue line) having the same module (4 mm, transverse); b) visual verification of meshing.

In this case, the equivalent mesh stiffness (*Figure 3.18*) is lowest when the tooth belonging to the smaller gear engages at the tip. When the tooth belonging to the bigger gear engages at the tip, the corresponding stiffness minimum will be higher if compared to the previous case. The maximum stiffness will no longer be placed in correspondence of half the length of contact and will move towards the higher minimum.

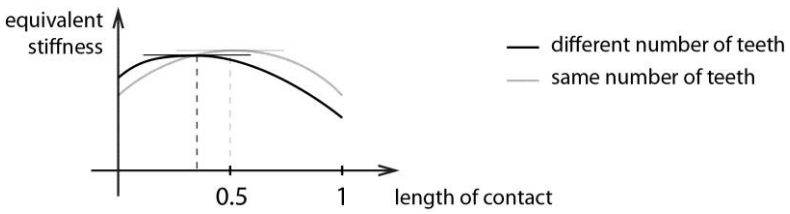

Figure 3.18 – Mesh stiffness trend for a single pair of teeth when gears have different numbers of teeth.

As stated at the beginning of the paragraph, the discussed factors act on the global stiffness of the teeth. Therefore the contact stiffness contribution, which is local to the contact surface between the teeth, must be included aside the above-mentioned factors.

A Hertzian contribution to the deflection in the contact point depends on the load exchanged by all the contacting teeth through a non-linear relationship. The problem is further complicated when considering the effects due to the finite dimensions of the contacting bodies, in contrast to the Hertzian theory. The main effect to be considered in this direction is due to the *buttressing* phenomena: either a stiffening or a softening behaviour can affect the contact stiffness depending on the strain field in the surroundings of the contact area. An example of buttressing can be clearly highlighted at the beginning and the end of meshing for a tooth pair. In these conditions contact occurs for one of the two teeth on a small portion at the tip. Especially for helical gears (*compare in Figure 3.11*) the contact stiffness becomes very low there, since there is no material in the surrounding to restrain lateral expansion (Poisson effect) due to the compression loading. The calculation of deflection and contact strain (and therefore stress) evolution over the mesh cycle constitutes a complex problem, both due to buttressing effects and due to the dependency of the contact area on the contact load. Aspects related to this problem are highlighted in Paragraphs 4.3.5, 5.1 and 6.1.

3.2.2. Misalignment components contribution

For the ideal case in which tooth generation and relative positioning of the gears are both perfect, if bodies are considered to be rigid, contact happens along a common tooth generatrix. Including the spread caused by local deformation, the contact line becomes a contact surface with a rectangular footprint (*Figure 3.19*), according to the Hertzian theory.

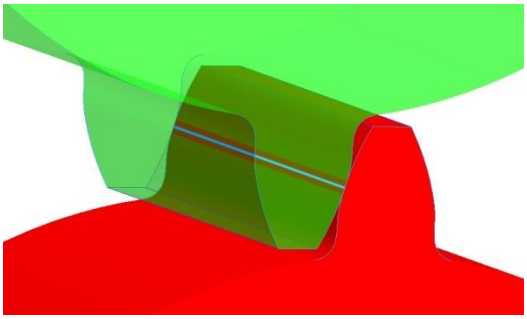

Figure 3.19 – Contact area between two aligned involute spur teeth.

When teeth undergo a misalignment, contact no longer happens along a rectangular contact area but on an elliptical one. This brings consequences on the contact stress distribution and the TE trend.

Misalignment can be due to several causes [149], which are worth to summarize:

a) *Lead slope error*: it is a manufacturing error which can occur when generating the tooth surface. The helix angle (which may be nominally zero, as in spur gears) exhibits a uniform deviation from the nominal value;

b) *Lead wobble*: this error derives from an imperfect parallelism between the gear axis and the rotation axis. It results in a tilting oscillation of each gear periodic with the respective shaft rotation. This wobble can either result from a gear bore which is non-parallel with respect to the teeth faces or from a shaft mounting seat for the related gear which is non-parallel to the shaft rotation axis imposed by the bearings;

c) *Shaft bending deflections*: these deflections can cause relative translations or rotations between the gears, depending on the bending stiffness distribution for the shaft and the axial positioning of each gear on the related shaft. Shaft deflections increase with the applied load, therefore they cause load-dependent misalignments;

d) *Shaft torsional deflections*: rotational displacements induced by shaft torsion are particularly important for helical gears having large face width and low number of teeth, as these displacements generate a variation in the helix angle;

e) *Bearing and housing deflections*: these deflections can be added together since they happen at the shaft supports. Bearing deflections are nonlinear

with load and are coupled to all the degrees of freedom which are prevented by the bearing. Research efforts are being devoted in understanding how bearing stiffness matrices can be calculated to account for load nonlinearities and couplings. Given the lightweight quest for modern structures, housing deflections can be larger than the ones for bearings and if this is the case require measurement or estimation by means of Finite Element models.

f) *Gear blank deflections*: when gears have thin-rims, their body tends to deflect away from the contact region in the overhanging portion of the teeth. This deflection tends to reduce the load carried by the related area.
g) *Spline and bearing clearances*: clearances result in a field of displacements and rotations according to the forces applied on the related gear;
h) *Temperature gradients*: especially for helical gears, the lubricant tends to be pushed across the lead direction while it heats up, thus leading to a differential expansion. The thermal expansion turns into an apparent change in the helix angle and, slightly, in the gear geometry parameters.
i) *Centrifugal forces*: in thin rim gears rotating at high speed, centrifugal forces may cause a differential deflection along the tooth face width.

All the misalignment causes are traditionally taken into account from a static point of view. However, the need for mechanical transmissions which are more reliable, light, energy efficient and quiet, pushes for detailed dynamic understanding. Resonances and the related mode shapes for shafts, housing, bearings and the gears themselves substantially influence the relative positioning of teeth. Assessing dynamic misalignments by means of Finite Element calculations would yield unpractical computational times, since the distributed flexibility of all the involved components needs to be taken into account. A solution to this problem, which however does not account for the distributed flexibility of the gears themselves, is provided by the multibody element proposed in this dissertation. Before going to the dynamic analysis of the misalignments, it is important to identify different components in a convenient reference system and classify them according to the effects on the behaviour of the affected gears. To render the geometrical definition of the misalignment components clearer, it is useful to consider them as if they were applied on unloaded teeth and then include the contact force which presses together the teeth surfaces. This also

clarifies the shape obtained for the contact area and stress distribution. Effects of the centrifugal forces will not be considered here, as they usually represent a rather specific case study. Isolating one gear and considering its teeth unloaded, the displacements descending from the causes discussed above will translate in rigid motions, which can be decomposed according to the six degrees of freedom that a rigid body has in a three-dimensional space. However, the rotation around the free axis needs to be taken out of consideration since this motion is permitted, and therefore accommodated, by the gears. A generic misalignment (*Figure 3.20*) includes five possible components: three relative translations, which will be named “parallel misalignments”, and two relative rotations, which will be named “angular misalignments”.

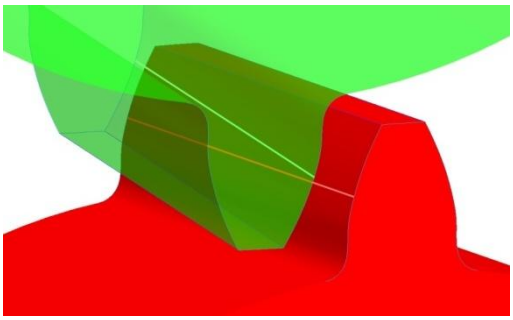

Figure 3.20 – Relative positioning for a tooth pair where all the five components of misalignment are present.

Properly selecting the reference system allows to separate and independently describe the effects caused by each component of misalignment on the TE and the contact stress distribution. The first axis direction is defined along the Line Of Action[1] (LOA), the second axis direction is defined as the orthogonal to the LOA in the transverse plane and named “Offline Line of Action” [149] (OLOA), and the third axis direction is orthogonal to the first two, which is parallel to the axial direction and the gears direction of rotation. Given the reference axes, two planes can be defined which are useful for describing the angular misalignments: the Plane Of Action (POA), which contains the LOA and is parallel to the rotation axis, and the Offline Plane of Action (OPOA), which contains the OLOA and is parallel to the rotation axis. The obtained reference system is illustrated in *Figure*

[1] *The TE has been defined in the same direction, which is oriented along the common normal to the meshing teeth surfaces in a transverse plane.*

3.21. This reference system is aimed at the calculation of a deviation with respect to an aligned configuration, therefore, without loss of generality, one of the two gears can be taken as a reference and the other gear can be considered as misaligned with respect to the reference.

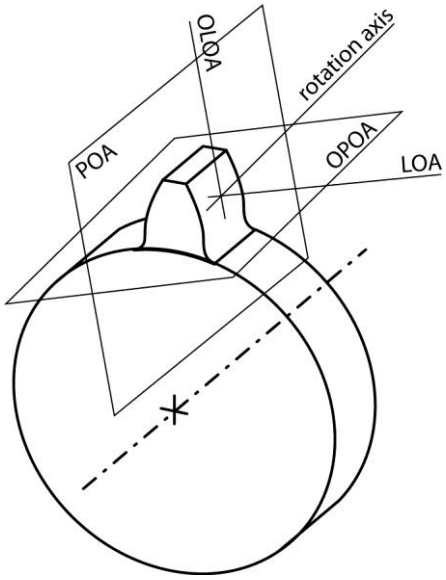

Figure 3.21 – Reference system adopted for defining the misalignment components.

Moreover, instead of defining angular misalignments as rotations around the related axes, it is more convenient to consider the field of translations that they cause in the rotation plane (*Figure 3.22*), which is orthogonal to the axis of rotation.

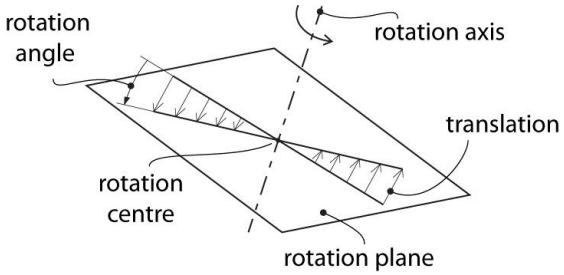

Figure 3.22 – Field of displacement caused by a rigid rotation.

The five components of misalignment can therefore be defined as:

1) Plane of Action Parallel Misalignment;

2) Plane of Action Angular Misalignment;

3) Offline Plane of Action Parallel Misalignment;

4) Offline Plane of Action Angular Misalignment;

5) Axial Parallel Misalignment.

Adopting the conventions described above, the translation and the rotation in the plane of action[1] can be associated to a direct effect on the TE. It is now worth to illustrate each misalignment component, assuming that the teeth surfaces have a perfectly involute shape:

1) Plane of Action Parallel Misalignment, or parallel misalignment in the plane of action (*Figure 3.23*):

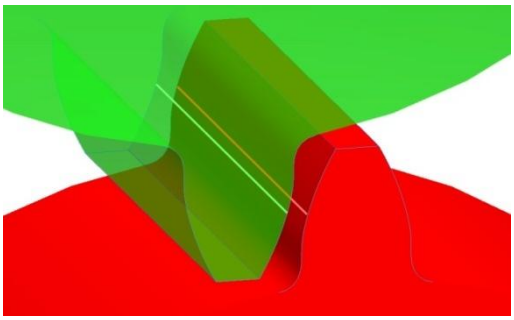

Figure 3.23 – Displacement field illustration for the POA parallel misalignment.

It corresponds to a uniform displacement in the direction of the line of action. *Figure 3.23* shows how this misalignment directly translates in an imposed TE. It is worthwhile to specify that this misalignment component should account for all the displacements in the direction of the line of action which were not accounted for when calculating the TE. If the displacement is trying to separate the gears, as depicted, the contribution to the TE is defined as negative (meaning that the gear that follows is ahead of the gear that drives). If this happens in the opposite direction, the contribution to the TE is defined as positive (meaning that the gear that follows is lagging behind the gear that drives). The latter condition is taken as positive because it is always present and caused by elastic deflections: deflections always result in a delayed positioning for the gear that follows. A constant value for this misalignment does not constitute a source of excitation,

[1] *Defining this misalignment component around the rotation axis, the angular misalignment "in the plane of action" would have been "around the offline line of action".*

since it is accommodated by a constant offset in the rotation of the gears. This misalignment is crucial to determine load sharing in planetary gear sets [66]. Variable values act as a displacement-driven excitation. Since displacement-driven excitations cause contact load fluctuations, the influence of this misalignment type on the mesh stiffness is indirect and due to the load fluctuation.

2) Plane of Action Angular Misalignment, or angular misalignment in the plane of action (*Figure 3.24*).

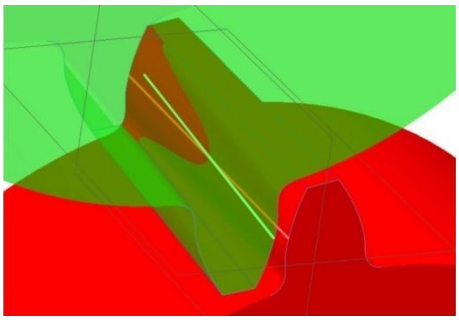

Figure 3.24 – Displacement field illustration for the POA angular misalignment.

Also in this case, the displacement field caused by the rotation becomes directly an imposed TE. For the case depicted in *Figure 3.24*, the rotation has been imposed with respect to the middle of the teeth face width. This shows how the POA angular misalignment tends to separate the teeth on one side and to increase their penetration on the opposite side. In reality this type of misalignment is to be interpreted only as a relative angle between the teeth surfaces: the centre of rotation which appears to be located in the middle of the face width is only due to the geometric interpenetration of the teeth surfaces. In reality, teeth surface cannot interpenetrate and deform under the action of the misalignment. Detailed explanations for quantitative calculations are reported in *Paragraph 4.3.4* and *5.2* along with their effects on the TE and the dynamic loading of teeth. Aim of the current discussion is to highlight how the contact stress distribution will tend to increase where the misalignment tries to increase the penetration and will tend to decrease on the opposite side, where the misalignment tries to separate the teeth. Higher contact stresses induce higher local deformation and hence higher tooth deflection. Therefore, the POA angular misalignment directly affects mesh stiffness and makes it decrease. An

alternative way to explain how mesh stiffness decreases is to consider that the POA angular misalignment reduces contact for unloaded teeth from a line to a point; then when the surfaces are pressed against each-other, contact area will spread and active face width will increase along the axial direction. The extent of the active face width will depend on the magnitude of the misalignment and of the applied load. This enhances the load-dependent nonlinearity of the mesh stiffness. POA angular misalignments usually experienced by industrial gears can lead to active face width which is lower than the nominal value, meaning that a portion of the teeth can become unloaded and will cause severe increase of contact stress towards the opposite tooth side and eventually edge loading. POA angular misalignment therefore represents a major concern in gear reliability, such that a calculation factor ($K_{H\beta}$) is included in the design norm ISO 6336.

3) Offline Plane of Action Parallel Misalignment, or parallel misalignment in the offline plane of action (*Figure 3.25*).

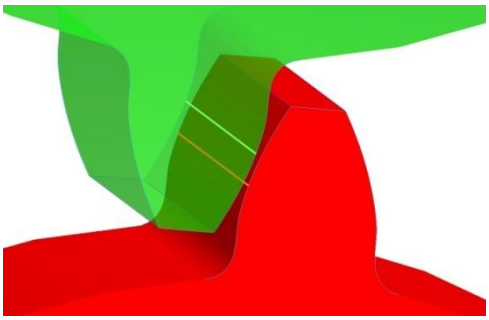

Figure 3.25 – Displacement field illustration for the OPOA parallel misalignment.

With reference to *Figure 3.25*, the translation caused by a parallel misalignment in the OPOA acts in a normal direction to the POA, therefore it brings no direct effects on the TE. This misalignment is practically equivalent to a change in centre distance, it affects therefore the average mesh stiffness as it changes the active tooth height and the variability of the mesh stiffness as it changes the transverse contact ratio. Increasing values cause an increase in the active tooth height (lower mesh stiffness) and a decrease in the transverse contact ratio (shorter period for maximum number of teeth in contact). The OPOA parallel misalignment also affects backlash, which increases with the misalignment.

4) Offline Plane of Action Angular Misalignment, or angular misalignment in the offline plane of action (*Figure 3.26*).

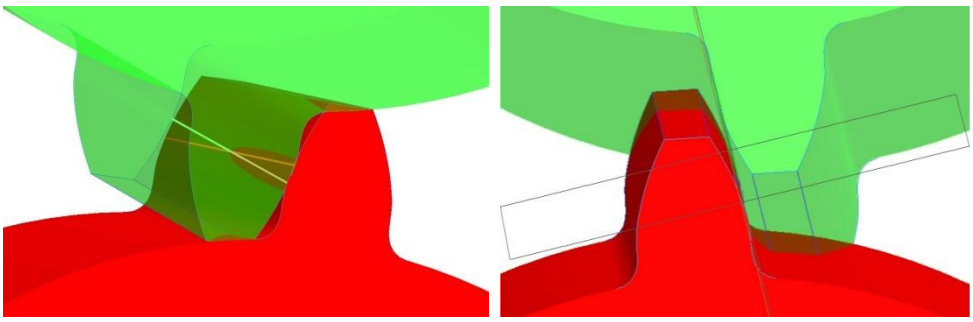

Figure 3.26 – Displacement field illustration for the POA parallel misalignment.

Also the angular misalignment in the OPOA has no direct effects on the TE, because the related field of displacement (*Figure 3.26*) acts in a direction which is normal to the POA. It affects the backlash, increasing it where teeth are made apart and decreasing on the opposite side where teeth are brought closer. No significant variation of the mesh stiffness is caused by the OPOA angular misalignment [149]: although it yields an elliptical contact area caused by the non-parallelism of the teeth generatrices, the major semi-axis of the ellipse remains significantly wider than the teeth face width. The shape of the contact area is therefore lightly affected, unless gears have very large face width.

5) Axial Parallel Misalignment (*Figure 3.27*).

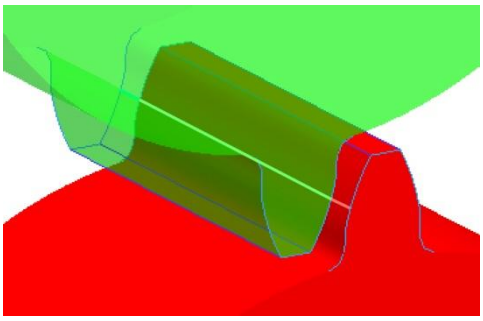

Figure 3.27 – Displacement field illustration for the Axial Parallel Misalignment.

The translation due to Axial Parallel Misalignment (*Figure 3.27*) has no direct effects on the TE if gears are spur, since it is tangent to teeth surfaces and causes sliding. If gears are helical, axial translation is coupled with gear rotation and also affects the backlash. A constant Axial Parallel Misalignment is

accommodated by the gears and does not represent a source of excitation. However if this happens in planetary gear sets, load sharing among planets can be altered. A variable Axial Parallel Misalignment for helical gears can represent an additional source of excitation. Axial Parallel Misalignment can reduce the mesh stiffness if it reduces the active face width. This effect is usually very limited since this misalignment is considerably smaller than the gear face width.

3.2.3. Tooth microgeometry contribution

The term “tooth microgeometry” refers to deviations of the tooth surface from a perfect and correctly aligned involute. These deviations can be caused either by deliberate modifications applied on the surface or by manufacturing errors. These errors make microgeometry modifications differ from tooth to tooth. Tooth microgeometry can therefore be specifically defined for each tooth. Manufacturing errors and their variability will not be addressed in this dissertation and constitute a specific research field. The basic theory explained by Smith [16] will be complemented with definitions and own observations from the dissertation Author, which will turn to be instrumental during the continuation of the reading.
Deviations from the perfectly generated and aligned involute are defined by a magnitude which represents the normal distance from the ideal surface and are expressed with respect to two positioning coordinates (*Figure 3.28*):

1) The position along the tooth profile in a transverse plane (*profile errors, profile modifications*), measured by the roll angle on the base circle;
2) The position along the lead of the tooth (*lead errors, lead modifications*), measured by the distance from one face of the gear along the face width.

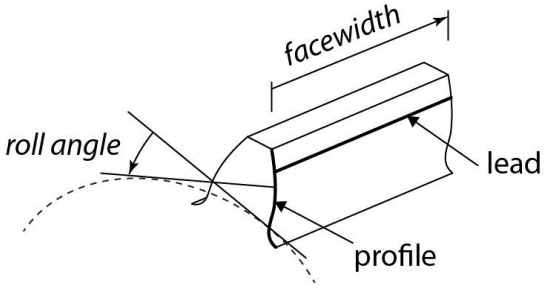

Figure 3.28 – Coordinates to describe tooth microgeometry.

The design and the execution of microgeometry modifications differ between gear manufacturers and are usually covered by industrial secret. From a general point of view it is however straightforward to understand the usefulness and the substantial impact of modifications along each of the two coordinates.

Profile modifications are useful to smoothen the handovers between tooth pairs approaching and leaving contact. Let us consider the case of a driving gear which is pushing the driven gear. The elastic deflection between the teeth causes a slight decrease in the pitch encompassed between a contacting tooth and the tooth immediately before. Under the hypothesis of perfectly involute, aligned and spaced profiles, the incoming tooth pair would start contact under an interference condition which is exactly equal to the already-engaging-teeth deflection and which would cause impacts. Hence aiming towards an involute profile is not recommended in the region of the teeth where contact begins or terminates. A profile modification is suited to compensate for this phenomenon, removing material (from a few to a few tens of microns) towards the extremes of the teeth (*Figure 3.29*). When material is removed towards the tip, the modification is called “tip relief”; when towards the root, “root relief”; when a combination of the two, “profile relief”.

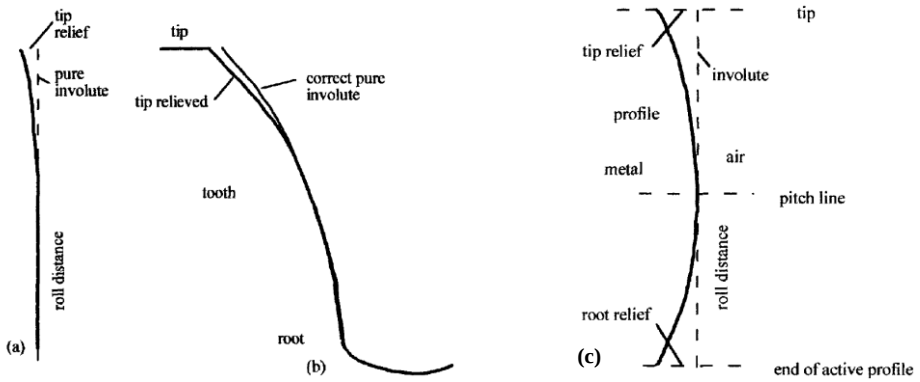

Figure 3.29 – (a) Profile microgeometry modification towards the tip of the tooth (tip relief) as a function of the roll angle; (b) effect on tooth geometry; (c) Profile microgeometry modification both at the tip and at the root (profile relief). [16] p.15

A parabolic profile relief takes the name of “profile crowning” or “profile barrelling” *(Figure 3.30)*.

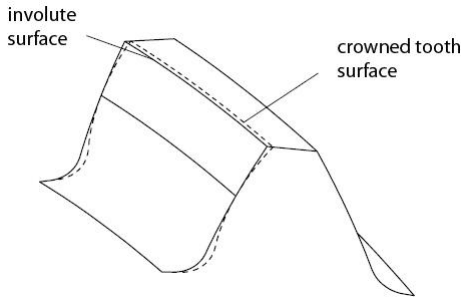

Figure 3.30 – Three-dimensional view of a tooth surface having a profile crowning modification (dashed) against a pure involute (continuous). [17] p.406

The effectiveness of profile modifications in smoothing contact handovers result from their capability of directly affecting the TE, since profile modifications are equivalent to imposed displacements in the POA for teeth where they are applied. Under no-load conditions, involute profiles which are perfectly generated, aligned and spaced will yield zero STE. Modified profiles under the same conditions will yield for a single tooth pair the profile modification trend in the STE (*Figure 3.31*).

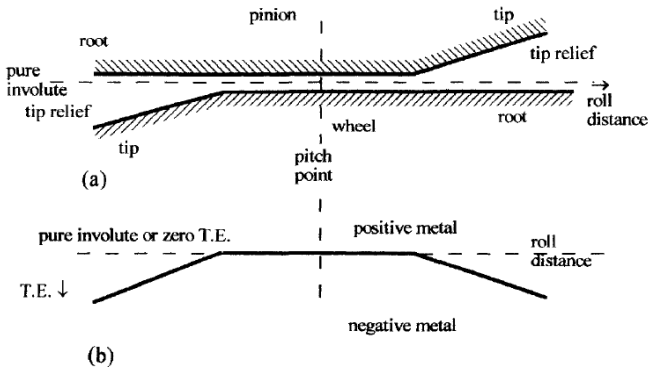

Figure 3.31 – a) schematized meshing teeth having tip relief modifications; b) no-load STE for the modified tooth pair. [16] p.20

Since more than one tooth pair will engage simultaneously, in reality the STE under no-load conditions can be calculated considering along the mesh cycle that the tooth pair which has the least material removal will be in contact (*Figure 3.32*).

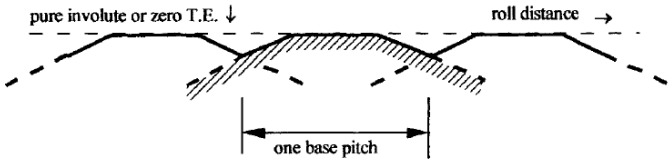

Figure 3.32 – STE during meshing of tooth pairs having tip relief modifications. [16] p.21

When gears transmit torque, it is necessary to add the elastic deflection of the teeth to the profile modifications. This deflection can eventually overcome the profile modification amount, bringing into contact tooth pairs which were not contacting under no-load conditions. Following this consideration, profile modifications can alter the load-dependent nonlinearity of the STE. In 1958, Harris [14] analysed the STE of a gear pair having profile modifications on the teeth at different loads. The diagrams he introduced are in use to assess the optimal load associated to a given microgeometry modification and are called "Harris maps" (*Figure 3.33*). They will be discussed hereafter keeping the approach of Smith [16], which has some additional simplifications with respect to the approach of Harris. Both of them are approximate but describe well the mechanisms behind the load-dependent nonlinearity of mesh deflections in combination with profile modifications. A gear pair having contact ratio between one and two is discussed.

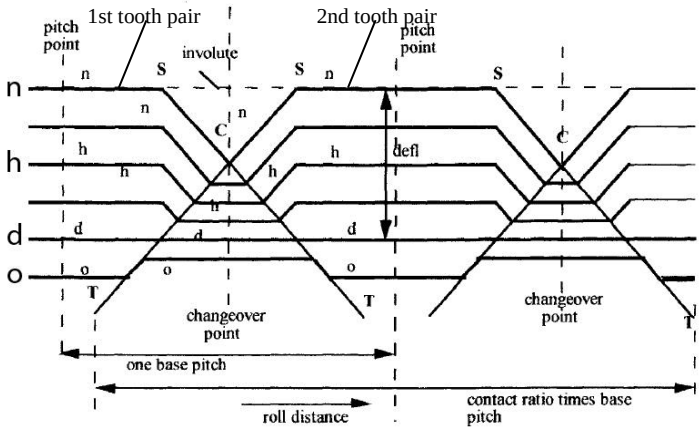

Figure 3.33 – Harris map for STE analysis (along the ordinate axis) for different loads and in presence of profile modifications. [16] p.22

The curve *n* in *Figure 3.33* represents the no-load case illustrated in *Figure 3.32* and the segments indicate the amount of material subtracted by the profile

modification to each tooth *pair*. The dashed horizontal line is related to the case of involute profiles. When load is increased, the curves move towards the bottom of the figure indicating higher deflections. To approximate the combined deflection behaviour of the contacting tooth pairs, Smith assumed constant mesh stiffness for each tooth pair throughout the mesh cycle. Since the total contact force is constant and is distributed over the contacting teeth, the deflection of a single tooth pair is double than that of two tooth pairs.

Under these assumptions, following curve *h*, the STE keeps constant in the first segment in the part of profile which has not been modified. As soon as the segment $\overline{ST}$ for the first tooth pair is intercepted, the modified profile part for the contacting pair is reached and the amount of modification adds up to the STE. Then the segment $\overline{ST}$ for the second tooth pair is intercepted and therefore the second tooth pair engages. The two overlapping $\overline{ST}$ segments compensate, since while the profile modification for the first tooth pair increases as meshing progresses, the profile modification for the second tooth pair decreases at the same rate as meshing progresses. As a result, the deflection remains constant until the profile modification becomes higher than the deflection for the first tooth pair. This implies that the first tooth pair leaves contact and therefore the second tooth pair takes over. The modification for the second tooth pair decreases towards the involute, therefore the deflection decreases with the same trend. When the modification terminates for the second tooth pair, the deflection keeps constant until the same cycle starts repeating with the next approaching tooth pair. This behaviour is typical of an amount of profile modification which is above-optimal: the profile modification is higher than required to compensate for the mesh deflection.

Under the assumptions of Smith, the profile modification is optimal when it matches the mesh deflection at contact onset for a new tooth pair. This case can be observed in curve *d*. The mesh deflection is initially constant since contact is progressing for the first tooth pair along the involute. When the $\overline{ST}$ segment for the second tooth pair is intercepted, the mesh deflection is exactly equal to the amount of modification, therefore the mesh deflection does not vary. At the same time, the $\overline{ST}$ segment for the first tooth pair starts and when contact progresses the two $\overline{ST}$ segments (increasing for the first pair and decreasing for the second pair) compensate, yielding constant deflection. This implies that the handover between the teeth is perfectly smooth and the deflection curve is perfectly

constant, thus generating no vibration. The handover completes when the $\overline{ST}$ segment for the second pair reaches the involute: the first tooth pair leaves contact and the second tooth pair continues alone on the involute surface.

If load is further increased, the applied profile modification becomes sub-optimal: the profile modification is smaller than the one required to compensate for the mesh deflection. This case can be observed in curve *o*. The mesh deflection is initially constant as contact progresses along the involute for the first tooth pair. Since the deflection is too high, the $\overline{ST}$ segment governing the profile modification for the second tooth pair is intercepted before the one of the first pair starts. This means that part of the contact load is transferred to the second tooth pair according to the modification law and this stiffens the meshing, leading to a lower mesh deflection. As soon as the $\overline{ST}$ segment for the first tooth pair is intercepted, the two profile modifications compensate and the mesh deflection keeps constant. When the profile modification terminates for the second tooth pair, the first tooth pair will not leave contact since the mesh deflection would be still higher than its profile modification. As a result, the remaining part of the contact load carried by the first tooth pair is transferred to the second according to the profile modification trend. The mesh deflection increases until it becomes higher than the profile modification for the first tooth pair and therefore contact continues only on the second tooth pair.

Lead modifications are useful to compensate for angular misalignments in the plane of action, avoiding that dangerous edge-contact conditions could be reached. Let us consider the case of perfectly involute, aligned and spaced teeth. Assuming the case of rigid teeth, contact happens on a line along the two overlapping tooth generatrices (*Figure 3.34a*). When a POA angular misalignment is introduced, the two surfaces become tilted and contact happens on a point towards one of the two edges (*Figure 3.34b*).

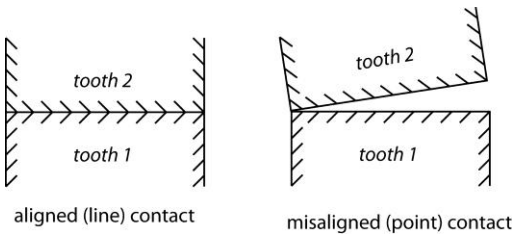

Figure 3.34 – Schematic tooth sections showing aligned line contact and misaligned point contact under the assumption of perfect and rigid teeth.

Right to avoid that even a slight misalignment can substantially displace the contact stress distribution and cause severe edge overloading, the tooth surface is rounded removing material along the lead. This modification is usually parabolic along the tooth face width and takes the name of *lead crowning* (*Figure 3.35*).

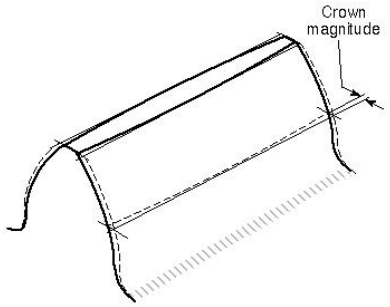

Figure 3.35 – Three-dimensional view of the surface of a spur tooth having lead crowning (continuous) against a pure involute (dashed). [ANSI/AGMA 1012-G05]

As a by-product of this modification, in aligned conditions, the maximum contact stress is higher than in the un-modified case. This happens because the curvature of the surface is increased by the lead modification. A compromise between decreasing the sensitivity to POA angular misalignment and increasing the maximum contact stress has to be solved. When the amount of lead crowning modification is chosen and applied, within the design range, a misalignment causes only a shift of the contact stress distribution in the direction of the misalignment. The stress distribution itself is not changed by the misalignment and overloading effects are avoided. *Paragraph 5.2* shows how POA angular misalignments which are outside the design range affect contact stress distribution.

Chapter 4.

Formulation for the proposed Gear Multibody Element

4.1. Static gear contact analysis using the Ohio State University Load Distribution Program (LDP)

Based on the observations highlighted in *Paragraph 3.2*, the TE is a consequence of the following factors:

1) Tooth deflection (global);
2) Contact deflection (local);
3) Torsional deflection of the gear bodies;
4) Supporting structure deflections;
5) Bearing deflections and clearances;
6) Manufacturing Errors and Microgeometry Modifications;
7) Misalignments;
8) Thermal distortions.

The LDP software [141] allows to calculate the Static TE accounting for the factors highlighted above except thermal distortions. The latter will be left out of the simulation, since no capability is currently available also in the multibody simulation environment to simulate heat flow.

LDP manages contact deflections (local) and microgeometry modifications by dividing the gears into slices (*Figure 4.1*), while it manages tooth deflections (global) using a plate model. A static problem is solved to determine the contact stress distribution along the contacting teeth surfaces, contact forces on each contacting tooth pair and the STE. The simulation is run for a single gear pair and requires as an input the macro- and micro-geometry of the gears, the misalignments and the applied resisting torque.

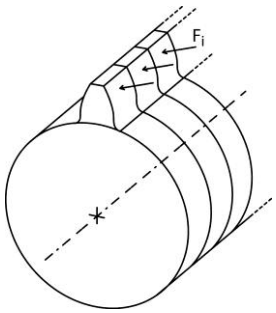

Figure 4.1 – Discretisation for distribution of the contact force.

How each of the listed factors is taken into account by LDP will be discussed hereafter.

Tooth global deflection is calculated based on the plate model by Yakubek [144], later modified by Yau [145] to include the effects of shear. A tooth is considered as a stubby cantilever beam (*Figure 4.2a*) loaded at its extremity. The clamping at the base of the beam is assumed to be compliant [75][146], since the tooth is mounted on the elastic foundation of the gear body. A rotation accounts for bending moment applied on the tooth base and a translation accounts for the shear (*Figure 4.2b*).

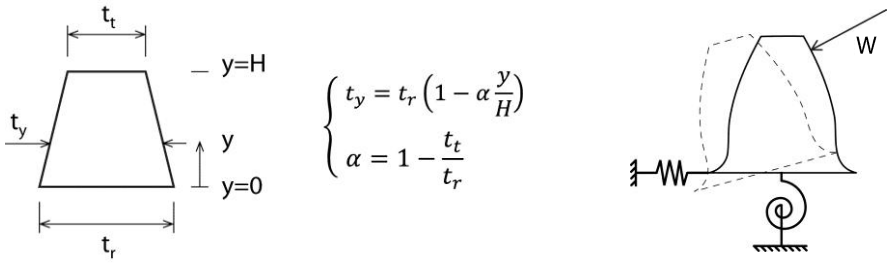

Figure 4.2 – a) Geometry of the transverse section for the beam; b) compliant clamping constraint.

Local contact deflections are calculated based on the analytical contact model developed by Weber [143] to extend the theory of Hertz to the case of gears. The expression for the contact deflection is [150]:

$$\delta_H = \frac{2W}{\pi F_a}\left\{\frac{1-{\nu_1}^2}{E_1}\left[ln\left(\frac{2h_1}{b}\right)-\frac{\nu_1}{2(1-\nu_1)}\right]+\frac{1-{\nu_2}^2}{E_2}\left[ln\left(\frac{2h_2}{b}\right)-\frac{\nu_2}{2(1-\nu_2)}\right]\right\} \quad (4.1)$$

where:

W = force acting on the considered line of contact;

F_a = length of the contact line across the face;

ν = Poisson coefficient;

E = Young's modulus;

h = distance from the contact point to the tooth centreline;

b = half of Hertzian contact length, which can be calculated as follows:

$$b = \sqrt{\frac{4W}{\pi F_a}\left(\frac{1-{\nu_1}^2}{E_1}+\frac{1-{\nu_2}^2}{E_2}\right)\frac{r_1 r_2}{r_1+r_2}} \quad (4.2)$$

Where r is the radius of curvature for each surface at the contact point.

The value b represents the length of the major semi-axis for the contact ellipse; it depends on the applied force W and influences the contact stiffness. Due to the dependency on the load, an initial guess for the share of contact load taken by each meshing tooth pair is made by LDP. For the initial guess the load is equally split between the teeth, the contact stiffness is then calculated and used to re-calculate the load distribution. The new load distribution can then be used to re-calculate the contact stiffness and iterate the loop to refine the calculation.

Torsional deflection of the gear bodies is estimated considering the path followed by lines of force induced by the applied torque: each gear is assumed to be clamped on the opposite side where the torque is being applied by the shaft. The approximation is justified from the fact that (apart from friction in the supporting bearing) the torque goes to zero on the side where the shaft is unloaded. The clamping therefore allows obtaining at this location zero torsional *deformation on the gear body*. As a consequence, the misalignment effect due to the torsional deformation of the gear bodies is included in the calculation. The loading scheme for a gear body is illustrated in *Figure 4.3*. The contact pressure distribution is concentrated for the calculation in the resultant contact force Q, which is applied at a distance ξ with respect to the input face of the input gear. The gear body is assumed to be a solid cylinder with a radius equal to the one of the operating pitch circle.

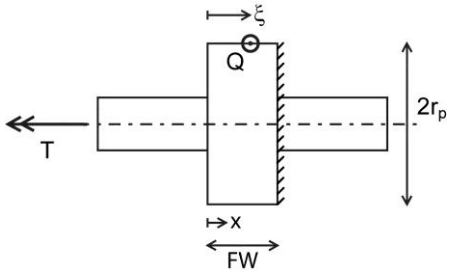

Figure 4.3 – Loading and constraining scheme
to calculate torsional deformation of a gear body.

Solving the problem under the assumption of de Saint-Venant, the torsional deflection on the tooth along the axial coordinate x for the input gear is linear for $\xi \leq x \leq FW$ and it is constant for $0 \leq x \leq \xi$. The deflection can be calculated as:

$$\delta_T = \begin{cases} \frac{Q{r_p}^2}{GJ}(FW - \xi), & 0 \leq x \leq \xi \leq FW \\ \frac{Q{r_p}^2}{GJ}(FW - x), & 0 \leq \xi \leq x \leq FW \end{cases} \tag{4.3}$$

When the torsional deformation has to be calculated for the output gear, since the axial coordinate x is already set based on the input gear, two cases are possible: the output torque may be applied either on the same side or on the opposite side as the input gear. In the case of same side *(4.3)* still holds, in the case of opposite side, the equations become:

$$\delta_T = \begin{cases} \frac{Q{r_p}^2}{GJ}x, & 0 \leq x \leq \xi \leq FW \\ \frac{Q{r_p}^2}{GJ}\xi, & 0 \leq \xi \leq x \leq FW \end{cases} \tag{4.4}$$

Supporting structure deflections can be partially accounted for in LDP. Housing and carrier geometry (if the gears belong to a planetary stage) cannot be modelled. However shaft deflections and rotations can be taken into account at two levels of detail: a simplified and a complex. The simplified modelling approach considers each shaft as a cylindrical beam supported at the extremities using the analytical formulation from theory of elasticity. The complex approach uses an external Finite Element module where the shaft geometry and the constraints can be specified. For the purposes stated in this dissertation work,

LDP is used only to isolate the contribution from the gear contact. Structural components are taken into account during the multibody dynamics simulation. Therefore it is important to exclude the structural contributions from the gear contact calculation.

Bearing deflections and clearances can be also partially accounted for in LDP. Bearing deflection can be considered making the shaft constraints compliant. In the simplified shaft modelling, linear stiffness for bearing forces can be introduced, but the coupling with moments and the rotational stiffness are not captured. In the complex shaft modelling a 6x6 fully populated matrix can be input by the user. Clearance cannot be included. Again, all these effects not due to gear meshing need to be excluded from the gear contact calculation since they are taken into account directly into the multibody simulation.

Manufacturing errors and tooth microgeometry modifications are embedded in the same section for tooth surface description. If the shape of the tooth surface is varying from tooth to tooth, a surface shape can be defined for each tooth with the possibility of specifying the three-dimensional shape by means of a sampled topology matrix. If the shape of the tooth surface is consistent between the teeth, the typical microgeometry modifications and manufacturing errors can be specified along the profile and the lead by adding linear and parabolic trends (*Figure 4.4*).

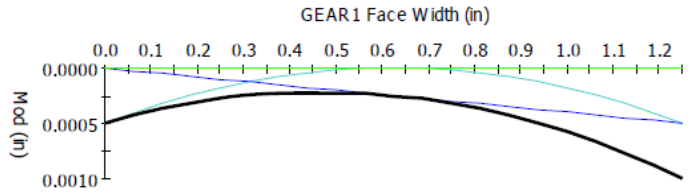

Figure 4.4 – Example of tooth microgeometry modification in LDP.

Misalignment is included in LDP with all the possible components except the angular OPOA misalignment, due to the reason stated in *Paragraph 3.2.2*.

Angular and parallel misalignments in the POA are summed together in a linear relationship (*Figure 4.5*):

$$\delta_{POA} = E_0 + SLOPE \cdot x \qquad (4.5)$$

where:

δ_{POA} = combined misalignment displacement field in the POA;

E_0 = offset coefficient due to parallel misalignment;

$SLOPE$ = angular coefficient due to angular misalignment;

x = position of the axial direction to span the face width.

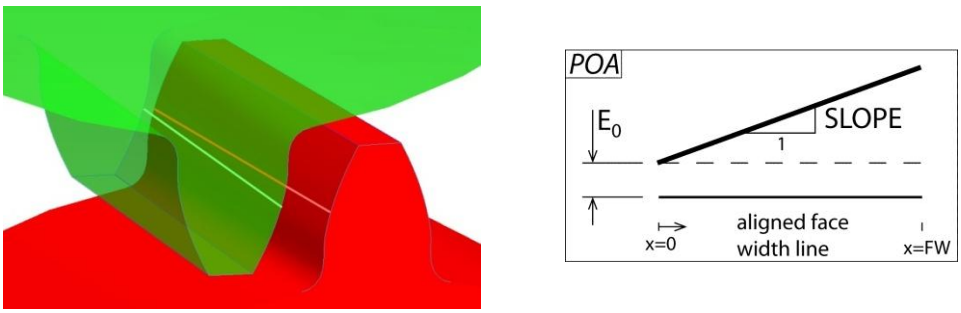

a) *b)*

Figure 4.5 – a) Combined misalignment displacement field in the POA; b) Linear relationship to describe the POA misalignment displacement field (4.5).

The parallel misalignment is accounted for in the offset coefficient as it causes a uniform translation of the tooth face parallel to the axial direction. The angular misalignment is accounted for in the angular coefficient given by the tangent of the relative of angle of rotation.

Parallel misalignment in the OPOA is accounted for imposing a variation on the nominal centre distance.

Parallel misalignment in the axial direction is accounted for by imposing an axial offset between the gear faces (*Figure 4.6*).

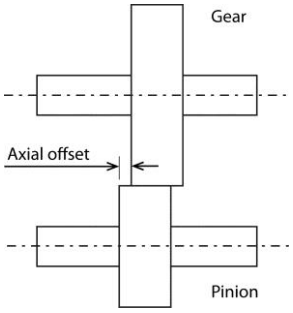

Figure 4.6 – Axial offset between gear faces.

The following scheme (*Figure 4.7*) summarizes how and by which quantitative parameters misalignments are accounted for in LDP.

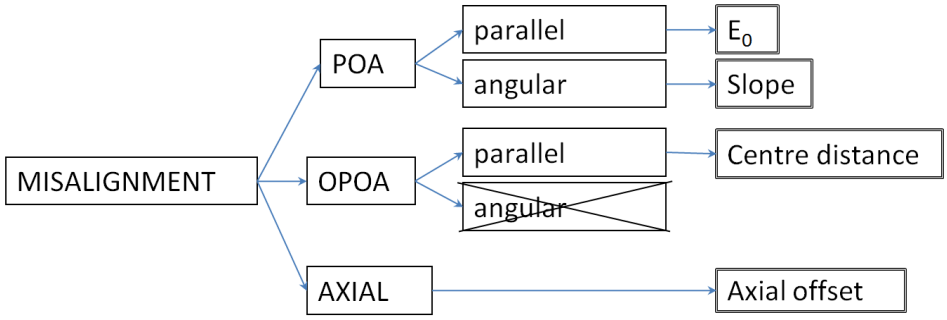

Figure 4.7 – Misalignment components in LDP and related quantitative parameters.

4.2. Dynamic contact force calculations based on Transmission Error

The TE is used by the gear element to calculate the equivalent mesh stiffness and apply contact force accounting for the effects mentioned in the previous paragraph. In *Paragraph 3.2* the importance of TE for dynamic simulations has been discussed. TE incorporates information about deviations from the ideal case due to load-dependent and geometric contributions. Load-dependent contributions are typically due to deflections occurring on teeth (contact and bending), gear blanks, shafts, bearings and other structural elements. Teeth contact and microgeometric modifications introduce key nonlinearities on the load dependency. Geometric contributions instead can be obtained measuring TE under no-load conditions. These contributions are related to the topology of meshing teeth surfaces, gear misalignments due to assembly errors and distortions of the gears. TE can be defined between two gears as a relative displacement or, equivalently, as a relative rotation; the first definition is the most convenient for our spring-damper approach and is also the one used in the LDP software. Under this definition, TE directly translates into the displacement of the spring-damper element, while the time derivative of the TE represents the velocity. During the multibody simulation, for each gear element, TE is calculated comparing in terms of position and orientation two coordinate frames connected to the gear bodies with a reference coordinate frame. *Figure 4.8* shows the

arrangement for the reference systems in case of external gears, the same configuration holds when gears are internal. Each gear coordinate frame has its origin at the intersection between the gear axis of rotation and the plane containing the gear face, where gear faces are chosen on the same side. *Z* axes lie on the axes of rotation of the gears and *x* axes point towards each other along the line joining the two origins. The two gears can be numbered arbitrarily and the reference frame overlaps with that of gear 1. This reference frame is fixed to the gear carrier, which can be fixed to the ground (conventional gear stage) or rotating (epicyclic gear stage). All the coordinate frames are chosen having no gear misalignment in the initial conditions.

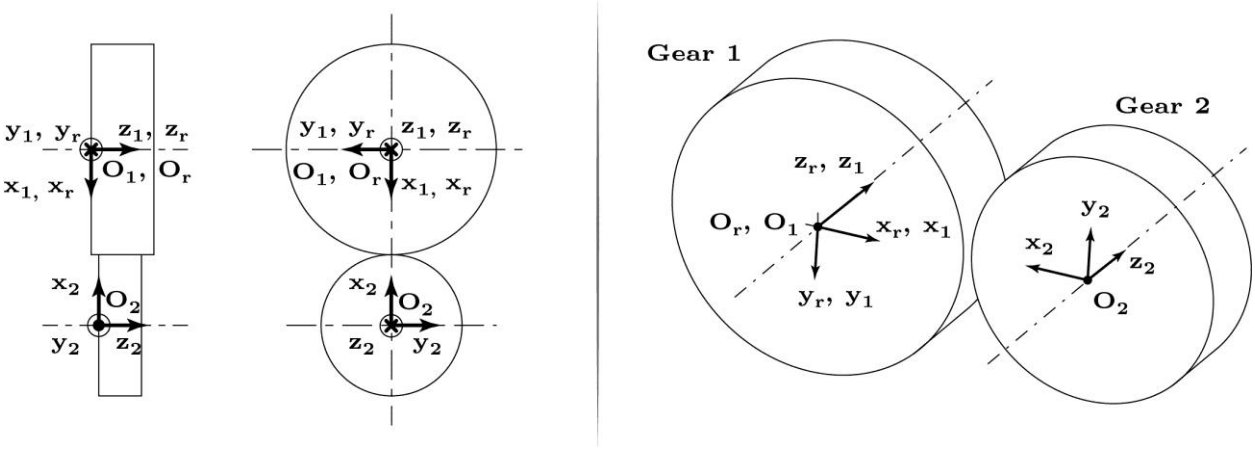

Figure 4.8 – Coordinate systems for TE calculation at initial conditions.

The Dynamic TE is calculated at each timestep in the reference transverse plane at the pitch circles, therefore it is expressed as a relative displacement in the normal direction. Calculations are performed first in the reference frame (tangential direction) and then scaled on the Line of Action of the gears (normal direction). This relative displacement accounts for the following two contributions (*Figure 4.9*):

$$DTE = DTE_r + DTE_t \tag{4.6}$$

where DTE_r is due to relative rotation of the gears and is given by:

$$DTE_r = \theta_1 r_{po1} + e\theta_2 r_{po2} \tag{4.7}$$

$$r_{pi} = \frac{z_i}{ez_1 + z_2} |\boldsymbol{CD} * \boldsymbol{x_r}| \qquad (4.8)$$

and DTE_r is due to relative translation in the tangential direction and is given by:

$$DTE_t = -e\, \boldsymbol{CD} * \boldsymbol{y_r} \qquad (4.9)$$

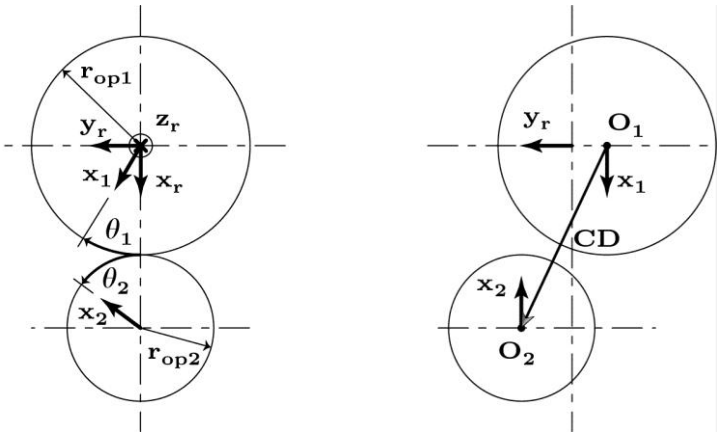

(a) *(b)*

Figure 4.9 – Rotational (a) and translational (b) components of TE.

Angles θ_i in *(4.7)* are calculated between the actual *x* axes of the gear frames and the reference *x* axis, positive in the direction of the reference *z* axis, in the reference transverse plane ($x_r y_r$) as shown in *Figure 4.10*. The variable *e* in *(4.7)* is used to account for internal or external gears. Variable *e* is equal to 1 for external gears, since angles have opposite sign and *(4.7)* converts into a difference. Variable *e* is equal to -1 for internal gears, since gear 2 rotates in the same direction of gear 1. The variable *e* is also used in *(4.8)* since centre distance is given by the sum of the operating pitch radii for external gears, while by the difference for internal gears. The operating pitch radii, r_{poi}, are calculated projecting the actual centre distance $\boldsymbol{CD}$ on the reference *x* axis and splitting it keeping constant the gear ratio. The relative translation in the tangential direction is calculated projecting the centre distance on the reference *y* axis *(4.9)*. The minus sign appears since the centre distance is defined as pointing from O_1 to O_2.

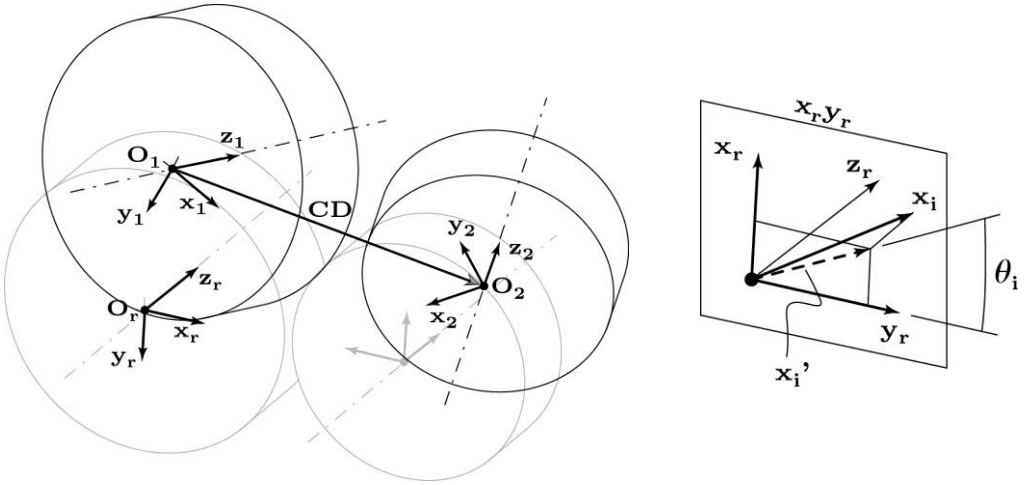

Figure 4.10 – Gear angle calculation scheme for displaced gear frames.

Relative velocity is also calculated identifying rotational and translational components, according to:

$$\frac{dDTE}{dt} = \frac{dDTE_r}{dt} + \frac{dDTE_t}{dt} \tag{4.10}$$

$$\frac{dDTE_r}{dt} = \omega_1 r_{op1} + e\omega_2 r_{op2} \tag{4.11}$$

$$\frac{dDTE_t}{dt} = -e\, \boldsymbol{v_{21}} * \boldsymbol{y_r} \tag{4.12}$$

where ω_i in *(4.11)* is the angular velocity of gear *i* in the reference transverse plane and $\boldsymbol{v_{21}}$ in *(4.12)* is the relative velocity of gear 2 with respect to gear 1.

A key difference has to be highlighted between static and dynamic TE (respectively STE and DTE). The STE is calculated through LDP, contains information about the stiffness and the topology of teeth surfaces and it is stored in the look-up tables; the DTE is calculated during the multibody simulation and includes the dynamic effects of inertia, damping and elasticity due to the complete assembly. The multibody software solves the full system of equations of motion, where each gear element is included in the form of:

$$\begin{cases} F_{tt}\boldsymbol{T} = \boldsymbol{F} \\ F_{tt} = F_{tt_k} + F_{tt_c} \\ F_{tt_k} = k\ DTE \\ F_{tt_c} = c\dfrac{dDTE}{dt} \end{cases} \qquad (4.13)$$

where $\boldsymbol{F}$ is the normal contact force vector, which is obtained applying the transformation vector $\boldsymbol{T}$ to the magnitude of the tangential contact force F_{tt} (*Figure 4.11*), F_{tt_k} is the elastic component of the spring-damper element and F_{tt_c} is the damping component, *k* is the equivalent mesh stiffness and *c* is the viscous damping coefficient. The damping coefficient *c* must be defined by the user. If mesh stiffness is set to be constant, *k* is also defined by the user; whereas in the variable case it becomes a function of the instantaneous operating conditions. Effects of operating conditions on the mesh stiffness are discussed in the next section of the dissertation. Since DTE and its time derivative are calculated on the pitch circle, in a transverse plane, the related contact force is aligned in the tangential direction ($\boldsymbol{F_{tt}}$). However normal contact force, $\boldsymbol{F}$, oriented in the direction normal to teeth surfaces at the actual contact point, is applied to the gear bodies. The normal contact force represents the resultant force of the meshing teeth and is found by calculating its radial, $\boldsymbol{F_r}$, tangential, $\boldsymbol{F_{tt}}$, and axial, $\boldsymbol{F_a}$, components (*Figure 4.11*), respectively aligned along the *x*, *y* and *z* reference axes. These components are mutually related by the normal pressure angle ϕ_n and the helix angle β (*Figure 4.11*), as expressed by the transformation vector $\boldsymbol{T}$ *(4.14)*.

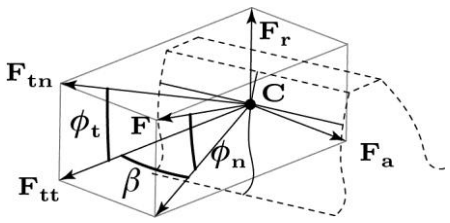

Figure 4.11 – Contact force components and tooth angles.

$$\boldsymbol{T} = \begin{Bmatrix} tan\phi_n / cos\beta \\ 1 \\ -e\ tan\beta \end{Bmatrix} \tag{4.14}$$

The operating contact point is finally calculated to apply the normal contact force to the gear bodies. In the reference transverse plane this point is always located as the operating pitch point, while its axial coordinate is calculated differently whether shuttling effects are enabled or disabled. When disabled, the contact point is located in the middle of the active face width. When enabled, the axial coordinate accounts for contact pressure distribution. The three components of the contact point when shuttling is disabled are given, with respect to the reference frame *(Figure 4.12)*, by:

$$\boldsymbol{C} = \boldsymbol{q_1} + [\boldsymbol{s}] * \boldsymbol{CD} + \boldsymbol{O_z} \tag{4.15}$$

$$[\boldsymbol{s}] = \begin{bmatrix} \dfrac{z_1}{ez_1 + z_2} & 0 & 0 \\ 0 & \dfrac{z_1}{ez_1 + z_2} & 0 \\ 0 & 0 & 1 \end{bmatrix} \tag{4.16}$$

$$\boldsymbol{O_z} = \begin{Bmatrix} 0 \\ 0 \\ {}^1/_2 \min(FW_1, FW_2) \end{Bmatrix} \tag{4.17}$$

where $\boldsymbol{q_1}$ is the displacement vector of the origin of gear 1, $[\boldsymbol{s}]$ *(4.16)* is matrix scaling of the *x* and *y* components of the centre distance vector to find the operating pitch point in the transverse plane, and $\boldsymbol{O_z}$ *(4.17)* is a vector applying an offset along the reference *z* axis equal to the minimum between the two face widths FW_i.

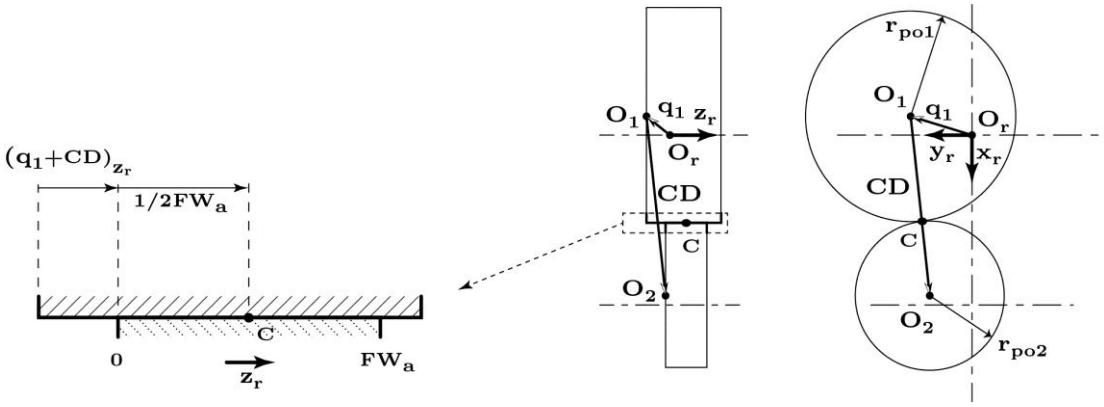

Figure 4.12 – Contact point location.

4.3. Modelling of dynamic operating conditions

The static effects of operating conditions are considered in the mesh stiffness when generating the look-up tables through LDP. Dynamic effects, instead, are considered when operating conditions vary during the multibody simulation and mesh stiffness is set at each timestep depending on their actual value. Actual values of position on the mesh cycle, gear misalignments and transmitted load are identified as operating conditions.

4.3.1. Position along the mesh cycle

The current formulation of the gear element is based on the assumption that all the teeth have the same surface topology and are equally spaced. Under this assumption, the mesh stiffness variation is cyclic with spatial period of a tooth pitch, for a given set of operating conditions. Considering a gear pair, position on the mesh cycle can be calculated by normalizing the rotation angle of one gear, taken as a reference, with respect to the angular pitch of the same gear. The obtained value is included between 0 and 1. The above procedure is executed in the gear element using the angle of gear 1 according to:

$$PMC = \frac{1}{\theta_{p1}}\left[|\theta_1 + \theta_{1s}| - floor\left(\frac{|\theta_1 + \theta_{1s}|}{\theta_{p1}}\right)\theta_{p1}\right] \qquad (4.18)$$

where θ_1 is the actual angle, θ_{1p} is the angular pitch and θ_{1s} is the initial angular position. Considering a gear train, the initial angular position for one of the gears can be selected arbitrarily as it does not affect the dynamic response of the transmission. Once this value is set, it is possible to calculate the initial value for all the other gears of the train adding the mesh phasing to the arbitrary value [64]. This parameter is crucial for the dynamic response of planetary gear sets (*Paragraph 2.1.4*).

4.3.2. Misalignments

Misalignments can be defined for a gear pair in terms of relative position and orientation of the gears. Since rotation around the axes is allowed and gear bodies are assumed to be rigid, misalignment can affect the other 5 degrees of freedom. Three translational or parallel misalignments and two rotational or angular misalignments can be identified. Directions discussed by Houser et al. [149] are used to define the axis system shown in *Figure 3.21* and described hereafter. The three orthogonal directions are chosen as the Line Of Action (LOA) in the direction of the normal contact force in the transverse plane as well as tangent to the base circles of the gears, the Offline Line Of Action (OLOA) orthogonal to the LOA still in the transverse plane and the axis of rotation direction and finally the axis of rotation. Since the TE is calculated in LDP along the LOA and this direction is normal to mating teeth surfaces, this axis system is particularly convenient as it allows understanding how fields of displacement caused by parallel and angular misalignments affect TE and mesh stiffness. As explained in *Paragraph 3.2.2*, parallel misalignments can be defined along the LOA, the OLOA and the gear axes of rotation (axial offset). Effects of each misalignment (*Paragraph 3.2.2*), reported hereafter, were analysed through the LDP software (*Paragraph 4.1*). Parallel misalignment along the LOA (*Figure 4.13a*) and angular misalignment in the POA (*Figure 4.13b*) act along the normal direction to teeth surfaces and can easily change contact patterns, therefore they significantly affect mesh stiffness. Also parallel misalignment along the OLOA (*Figure 4.13c*) significantly affects mesh stiffness since it mainly causes a change in centre distance. Angular misalignment in the OPOA (*Figure 4.13d*) is found to have limited influence on contact stress distribution according to Hertzian contact theory [149]. Axial offset (*Figure 4.13e*) affects mesh stiffness by changing the

active face width of the gear pair. Since deviations are small compared to the total face width, effects on mesh stiffness are limited. Both will be neglected in the proposed element and only misalignments in the POA and OPOA parallel misalignments will be accounted for.

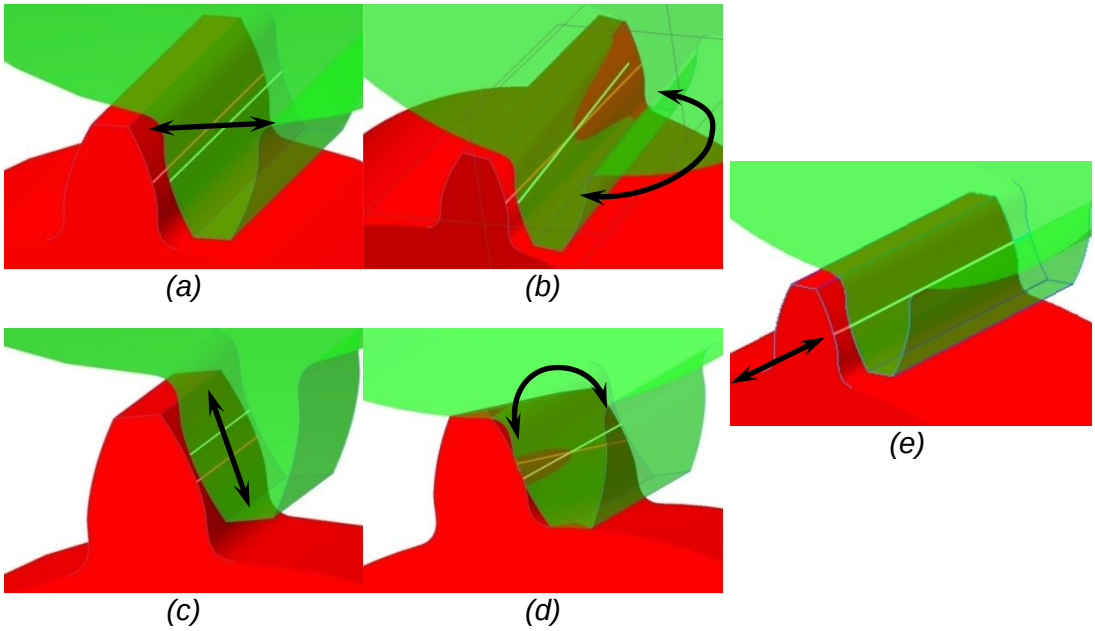

Figure 4.13 – Misalignment components.
(a) POA parallel, (b) POA angular, (c) OPOA parallel,
(d) OPOA angular, (e) Axial offset.

4.3.3. Centre distance variations

When dynamic effects of centre distance are disabled, mesh stiffness is calculated using the nominal value; when they are enabled the actual centre distance is used to interpolate the look-up tables. In this case, effects on mesh stiffness due to changes in contact ratio and active tooth height are included together with alterations on the effects of profile modifications, since teeth profiles become displaced relatively to each other. The actual centre distance is calculated projecting the vector connecting the origins of the gear frames on the reference transverse plane *(Figure 4.10)*, according to:

$$CD_{xy_r} = \sqrt{(\boldsymbol{CD} * \boldsymbol{x_r})^2 + (\boldsymbol{CD} * \boldsymbol{y_r})^2} \qquad (4.19)$$

This value is also used to calculate the actual operating transverse and normal pressure angles (*Figure 4.11*), respectively ϕ_t and ϕ_n:

$$\phi_t = \operatorname{acos}\frac{r_{b1}}{r_{po1}} \tag{4.20}$$

$$\phi_n = \operatorname{atan}(tan\phi_t \, cos\beta) \tag{4.21}$$

where r_{b1} is the base radius of gear 1.

4.3.4. Misalignments in the plane of action

Misalignments in the plane of action are calculated with respect to the reference frame. To identify the plane of action two directions are needed: the direction for the line of action and the one for the axis of rotation of the gears. The former must be calculated in relation to the contacting tooth flanks; the latter is already available in the reference frame. The LOA direction (unit vector) is calculated in the reference frame, rotating the *x* axis around the *z* axis of a quantity complementary to the transverse pressure angle:

$$\boldsymbol{LOA_r} = \begin{Bmatrix} \cos\left(\pi/2 - \phi_t\right) \\ sign(DTE)\sin\left(\pi/2 - \phi_t\right) \\ 0 \end{Bmatrix} \tag{4.22}$$

Contacting tooth flanks are identified by the sign of the DTE, which is also used for the rotation around the reference *z* axis (*Figure 9*).

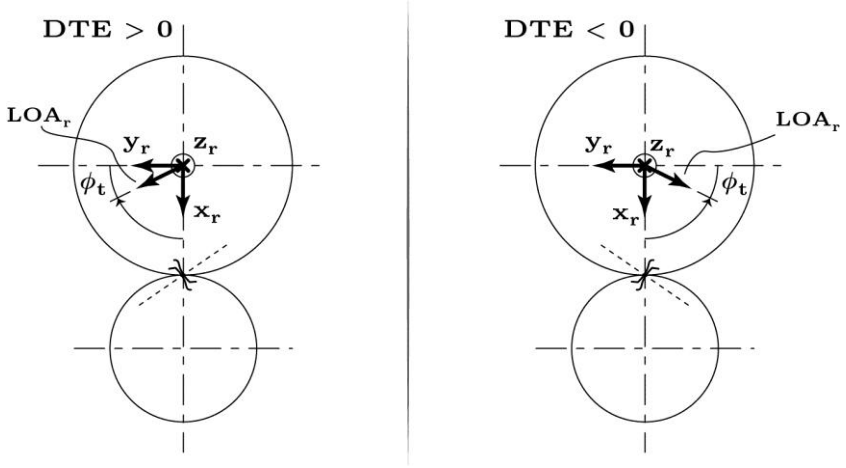

Figure 4.14 – Location of the LOA direction according to Transmission Error sign.

Once the line of action is found, misalignments in the POA can be calculated. LOA parallel misalignment directly translates into a TE therefore it can be seen as a displacement excitation. This misalignment component is due to the relative displacement of the gears along the LOA and is already considered, scaled along the transverse direction, in *(4.9)*. POA angular misalignment is calculated through the following procedure:

1) Each axis of rotation is projected on the POA in the reference frame;
2) Angles between the projected axes and the reference axis are calculated in the reference POA;
3) Misalignment is obtained by the difference of the rotations (since same rotation in the same direction implies aligned gears).

The axis $\boldsymbol{OLOA_r}$ defines the positive rotation for the misalignment angle α_i as shown in *Figure 4.15*.

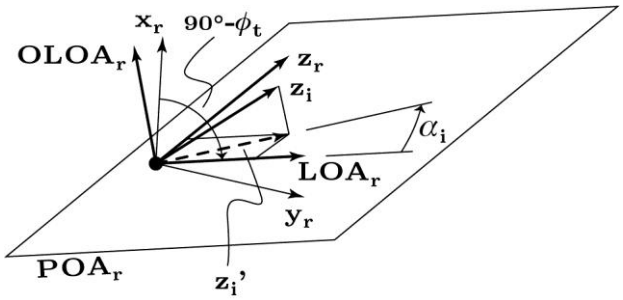

Figure 4.15 – POA angular misalignment calculation scheme.

POA angular misalignment is finally expressed in terms of slope coefficient, to enter the look-up tables, as:

$$M = \tan(\alpha_1 - \alpha_2) \tag{4.23}$$

POA angular misalignment causes increased separation, if negative, or extra penetration, if positive, of teeth surfaces towards one side of the active face width *(Figure 4.16)*.

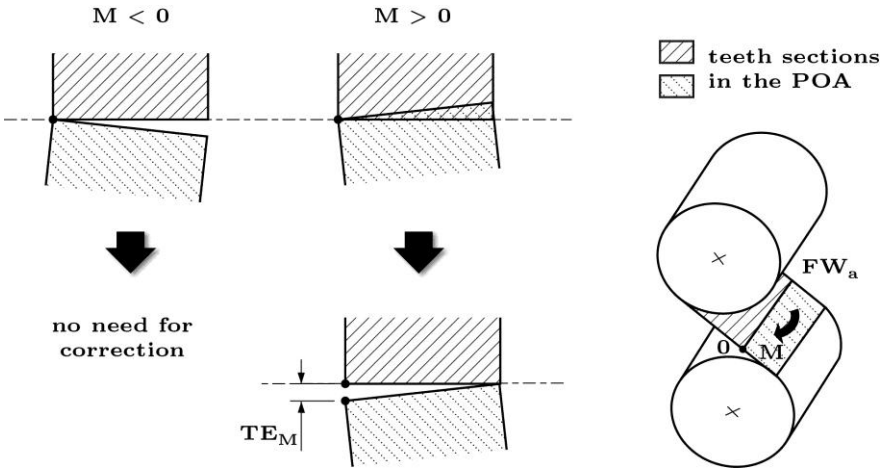

Figure 4.16 – Separation (M<0) and extra penetration (M>0) caused by POA angular misalignment.

Since DTE and its time derivative are calculated in the reference transverse plane, which is positioned on one gear face, the other gear face remains to be considered. If extra penetration is caused on the opposite side, an additional contribution to DTE *(4.6)* and its time derivative *(4.10)* must be added according to *(4.24)* and *(4.25)*; if instead separation is increased, there is no need for correction. *(4.24)* is scaled by the cosine of the transverse pressure angle, since DTE is calculated on the pitch circles in the tangential direction while the plane of action is tangent to the base circles. *(4.25)* is already expressed in the tangential direction since the relative angular velocity vector $\boldsymbol{\omega_{12}}$ is projected on the reference *x* axis.

$$DTE_M = \frac{1}{\cos(\phi_t)}[M \cdot \min(FW_1, FW_2)] \tag{4.24}$$

$$\frac{dDTE_M}{dt} = \boldsymbol{\omega_{12}} * \boldsymbol{x_r} \cdot \min(FW_1, FW_2) \tag{4.25}$$

4.3.5. Transmitted load

Transmitted load can be considered equivalently in terms of contact force or torque. For the purpose of calculating the actual equivalent mesh stiffness, transmitted load can be assumed by the proposed gear element as being constant or variable. Nonlinear load-dependent effects on mesh stiffness are taken into account only in the second case.

4.3.5.1. Constant load

Transmitted load is considered equal to the nominal value under the assumption of constant load. Since this load is known a priori during the multibody simulation and STE is interpolated for the actual operating conditions, stiffness can be calculated dividing force by displacement both in the tangential direction:

$$k(PMC, CD, M) = \frac{F_{tt_n}}{STE(PMC, CD, M)/\cos\phi_t} \tag{4.26}$$

where the STE calculated by LDP along the line of action is converted on the pitch circle using the cosine of the transverse pressure angle ϕ_t and the nominal tangent contact force in the transverse plane F_{tt_n} is given by:

$$F_{tt_n} = \frac{T_{1_n}}{r_{op1}} = \frac{T_{2_n}}{r_{op2}} \tag{4.27}$$

where T_{i_n} is the nominal torque applied to gear *i* and r_{opi} is the operating pitch radius of the same gear. Hence, under the assumption of constant transmitted load, multivariate look-up tables contain values of STE as a function of the

operating conditions expressed in terms of position on the mesh cycle and/or misalignment in the plane of action and/or centre distance variation. It is important to highlight that the transmitted load is assumed to be constant only when calculating the actual equivalent mesh stiffness, while in the multibody simulation load can be variable due to system dynamics.

4.3.5.2. Variable load

Under the assumption of variable load, it is no longer possible to apply *(4.26)*, since at the actual timestep transmitted load is an unknown of the problem and its value must also be used to calculate mesh stiffness. This circular dependency can be avoided using the actual DTE as an indicator of the actual transmitted load. The DTE is related by mesh stiffness to the elastic component of the dynamic transmitted load *(4.13)*. This elastic component is the only component of the transmitted load used by LDP to calculate STE. Therefore, if look-up tables are generated for a variety of applied loads, F_{tt_k} can be calculated entering the tables with the actual DTE value. In particular, look-up tables are generated for a discrete range of applied static torques to the gear 1 as well as for discrete ranges of operating conditions. Let us consider, for two-dimensional graphing purposes, only the position on the mesh cycle among the operating conditions. The procedure is immediately extendable to the n-dimensional case, because the other operating conditions are also known at the actual timestep and can be used as independent variables for the interpolation. Entering the look-up tables at the actual position on the mesh cycle, it is possible to interpolate the static torque value which causes the actual DTE (*Figure 4.17*).

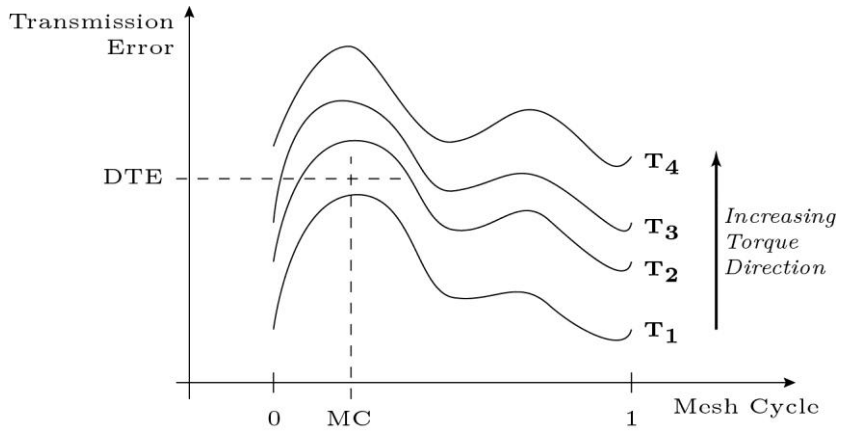

Figure 4.17 – Torque extraction based on DTE and position on the mesh cycle.

Once the static torque value is known, it is then possible to extract mesh stiffness again by dividing force and displacement in the tangential direction:

$$k(DTE, PMC, CD, M) = \frac{F_{tt}(DTE, PMC, CD, M)}{DTE} \tag{4.28}$$

where transverse tangential contact force F_{tt} is obtained dividing the interpolated torque T_1 by the operating pitch radius of gear 1 r_{po1}:

$$F_{tt} = \frac{T_1(DTE, PMC, CD, M)}{r_{po1}} \tag{4.29}$$

Due to the above considerations, in the variable load case, look-up tables must contain torque values as a function of all the operating conditions expressed in terms of displacement variables. However torque is set in a discrete range to calculate STE through LDP, therefore the former is originally an independent variable while the latter is dependent. To make the applied torque a dependent variable and the STE the independent variable the load-displacement discrete function must be inverted. Homogeneous elastic material properties ensure that this function is invertible, since increasing applied torque always causes increasing STE for a given set of operating conditions. For a given position along the mesh cycle, which is a function of the instantaneous angular position of the driving gear, there is a one-to-one correspondence between the instantaneous DTE and the instantaneous contact force (higher DTE for a higher contact force,

here the damping contribution is not accounted for). Namely, given a PMC and the actual DTE, the actual contact force can be calculated as a function of the two variables *(4.30)*.

$$F_{contact} = f(PMC, DTE) \qquad (4.30)$$

This two-variables function is described by a dataset of STE values calculated through LDP considering different working conditions. In particular, the dataset is constituted by a set of STE curves calculated for a range of contact forces (resulting from a range of applied torques). In this way, given a PMC, the STE is available as a function of the applied force (*Figure 4.18*). The instantaneous DTE is used in place of the STE to enter the dataset, together with the instantaneous PMC, during the multibody simulation, so that the instantaneous contact force can be calculated. This operation will be mentioned as “extraction”. The properties of the extracted contact force are discussed in the next paragraph. Keeping the focus on the mathematical aspects of the procedure, the one-to-one correspondence between applied contact force and STE is shown for a sample calculation in *Figure 4.19*. The one-to-one correspondence still holds after applying a misalignment and microgeometric modifications (lead and profile), as it can be verified in *Paragraph 6.1*.

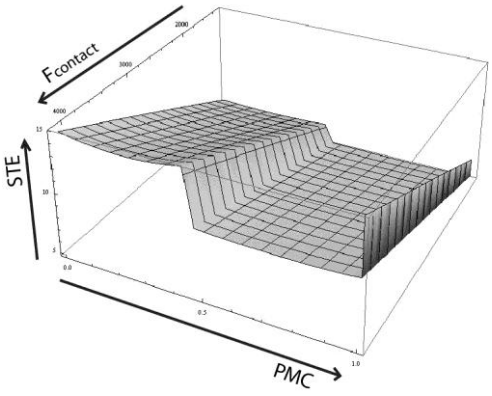

Figure 4.18: STE calculated through LDP as a function of PMC and the applied contact force.

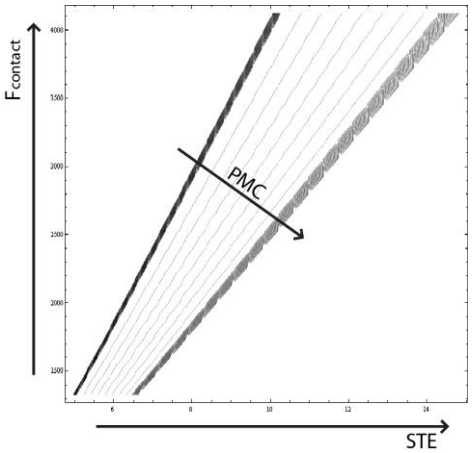

Figure 4.19: Applied force as a function of STE. (Sections of the left figure surface in the $STE - F_{contact}$ plane)

It has to be noted that LDP calculates the STE in a discrete number of PMC and applied torque values, therefore the dataset is discrete and requires interpolation (*Figure 4.20*).

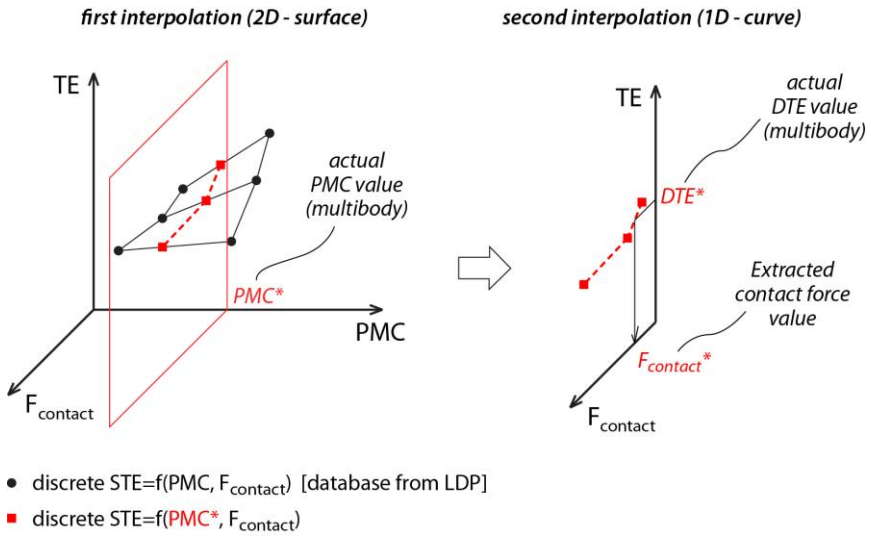

Figure 4.20: Interpolation steps for contact force extraction.

Smooth interpolation (C1 continuity) is needed to avoid inducing stability problems for the multibody solver, therefore a simple linear interpolation cannot be used. Cubic spline interpolation ensures the C1 continuity but produces overshoots if rapid variations in STE values occur. To avoid this problem, Akima interpolating schemes [151] were adopted for two independent variables. An important consideration is needed about the properties of the extracted contact force. The dynamic TE is used to enter a static TE dataset (*Figure 4.21*).

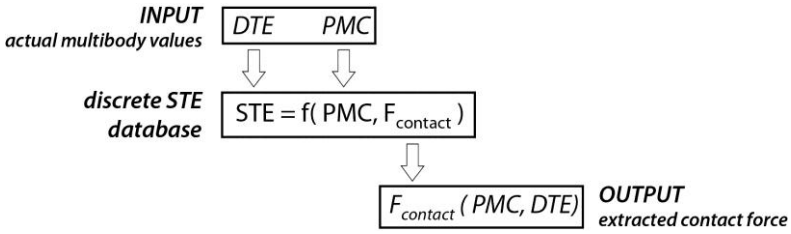

Figure 4.21: Contact force extraction procedure.

This implies that the extracted contact force is equal to the static part of the dynamic contact force. From a mathematical point of view, the DTE time

derivative which appears in (4.13) goes to zero. The extracted force is therefore used only to calculate the static stiffness of the mesh. Dynamic effects are then included by the multibody solver which solves the equations of motion accounting for the chosen value of linear viscous damping and the inertias in the system. To verify the variable torque extraction technique, a constant torque is applied to the driven gear shaft and the obtained results are compared with the ones obtained using the constant torque technique. The results, shown in the next graphs, match each other while the variable torque technique relaxes the a-priori assumption of a constant torque. This proves that the extracted static contact force is actually the static component of the dynamic contact force and is a consistent method to excite the system. The simulated DTE obtained using the variable torque technique (contact force extraction) perfectly traces the one from the constant torque technique (*Figure 4.22*).

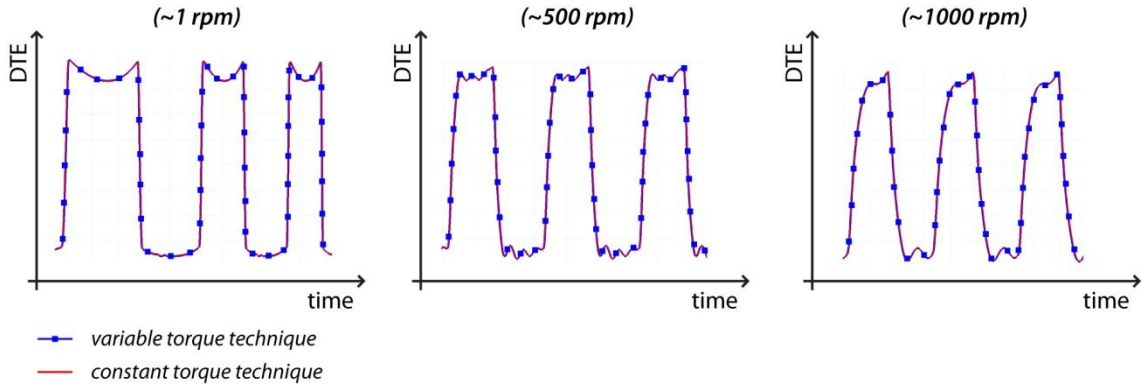

Figure 4.22: DTE with constant and variable torque techniques for different regimes.

Also the *dynamic* contact forces overlap for the two techniques (*Figure 4.23*). The extracted *static* contact force shows impulses at tooth pair handovers due to system response delay (peaks in *Figure 4.23*). In particular, the impulse forces are higher than the nominal contact force when the second tooth pair comes into contact, since the mesh stiffness increases suddenly while the DTE is still high because of system response delay. The opposite happens when the second tooth pair leaves contact, since the mesh stiffness suddenly decreases while the DTE is still low.

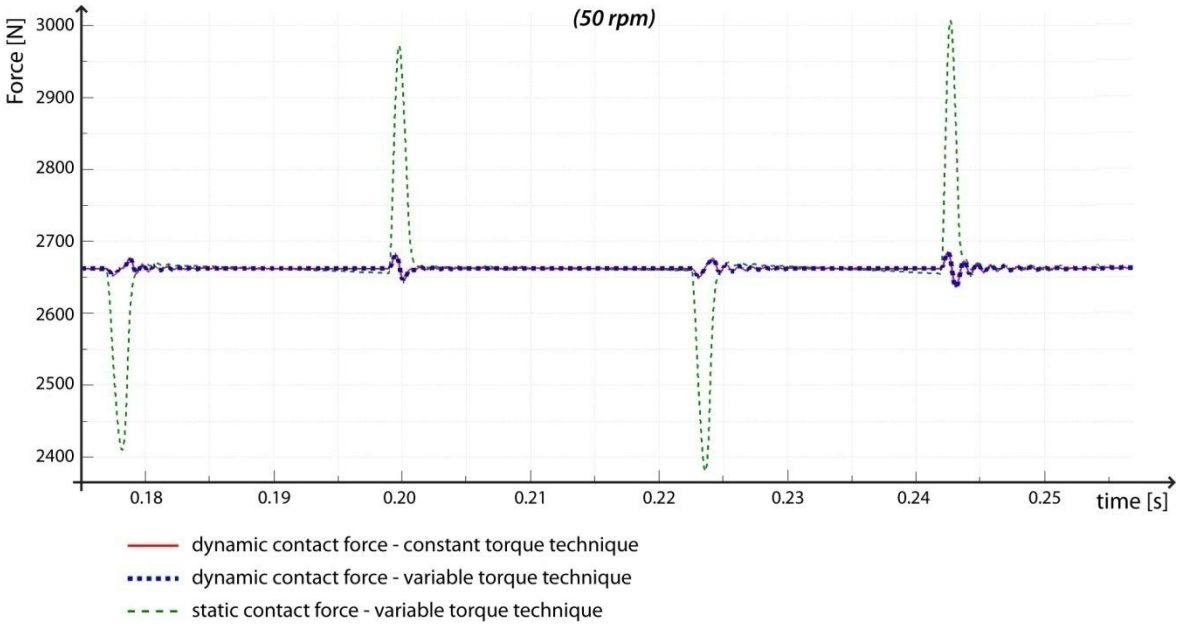

Figure 4.23: Dynamic contact force with constant (smooth line) and variable (marked line) torque techniques; static contact force with variable torque technique (dashed line).

4.4. Shuttling phenomena

Shuttling is a fluctuation in the axial position of the resultant contact force point of application. This fluctuation leads to oscillations on bearing forces and dynamic moments in the plane of action. Shuttling happens intrinsically for helical gears, due to the traveling contact lines from one corner of the tooth surface to the opposite, or can be due to shifts in contact stress distribution caused by gear misalignment. Two kinds of shuttling models are proposed. The first model considers the path of contact lines in helical gears and the misalignment effects using shuttling parameters which result from static contact calculations, stored in multivariate look-up tables. The second model does not consider the path followed by contact lines in helical gears and is based on the interpolation of the axial position according to the angular misalignment magnitude and direction. Two thresholds for angular misalignment magnitude causing a contact force close to each of the gear faces are calculated by means of static simulations. Misalignments leading to point-edge contact are not considered since it is practically unlikely to have gears with such a severe misalignment. Interpolation is performed during the dynamic simulation for misalignments between the maximum thresholds to obtain shuttling parameters between the extremes.

4.4.1. Contact-based model

Shuttling is taken into account considering the contact pressure distribution calculations in LDP. For each operating condition, LDP is able to decompose the contact force resultant according to static equivalence. In particular, taking a pivot point on one edge of the active face width, LDP returns a force value calculated at the opposite edge which causes the same moment of the resultant contact force (*Figure 4.24*).

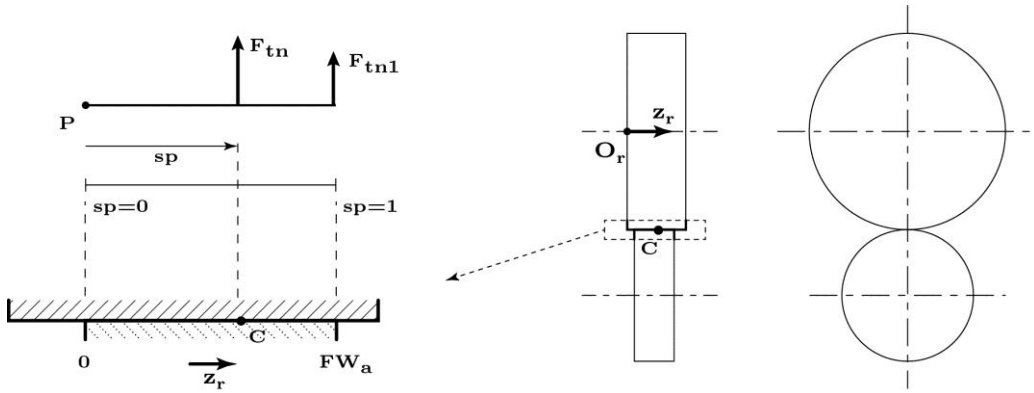

Figure 4.24 – Contact point axial positioning with shuttling.

This force value can be used to calculate the axial position of the contact force resultant normalized on the active face width according to:

$$sp = \frac{F_{tn1}}{F_{tn}} \tag{4.31}$$

This parameter is stored in a second look-up table, calculated for the same discrete range of operating conditions used for the mesh stiffness, and interpolated during the multibody simulation. *Eq. (4.17)* is therefore modified as follows to account for shuttling:

$$\boldsymbol{O_z} = \begin{Bmatrix} 0 \\ 0 \\ \min(FW_1, FW_2) \cdot sp(DTE, PMC, CD, M) \end{Bmatrix} \tag{4.32}$$

4.4.2. Angular POA Misalignment-based model

Without the need of generating and interpolating extra multivariate look-up tables, shuttling is taken into account in a fast, but simplified way, considering two extreme misaligned conditions and a centred condition. Linear interpolation is used in between to obtain the axial position of the contact point. When gears are aligned, assuming symmetric lead modifications, the contact load distribution is centred on the face width and the shuttling parameter is 0.5 (*Figure 4.25a*). As the POA angular misalignment α is increased, significant edge loading is reached (*Figure 4.25b*). Having a shuttling parameter exactly equal to 0 or 1 would mean having all the contact load distribution concentrated on one single point, which is practically remote. Therefore threshold values can be defined by the user (e.g. 0.1 and 0.9). The misalignment value for which the edge loading condition happens is recorded and the same procedure is repeated towards the other face (*Figure 4.25c*).

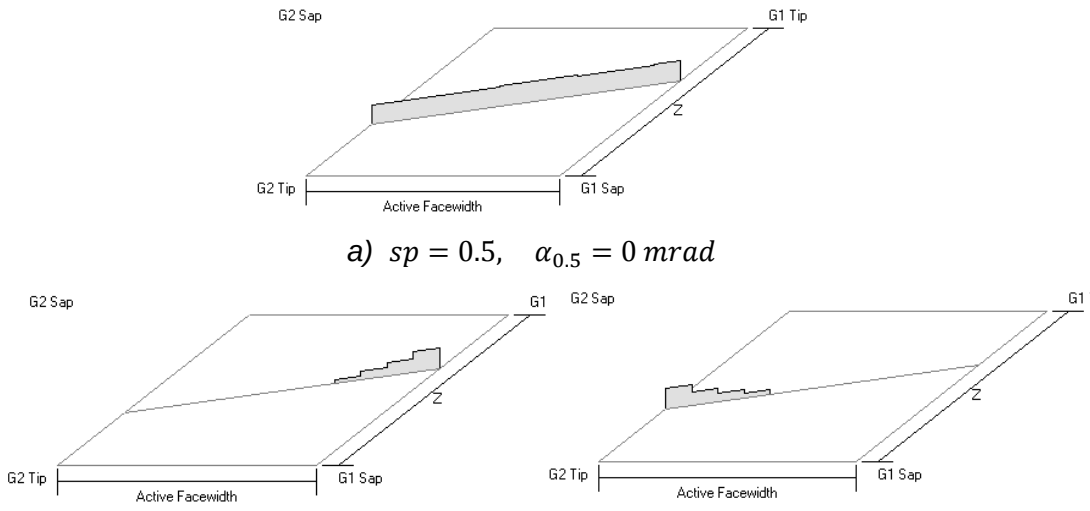

a) $sp = 0.5, \quad \alpha_{0.5} = 0\ mrad$

b) $sp = 0.9, \quad \alpha_{0.9} = -2.5\ mrad$

c) $sp = 0.1, \quad \alpha_{0.1} = +2.5\ mrad$

Figure 4.25 – Contact load distributions for misalignment threshold reaching shuttling parameters of:
a) 0.5 (centred distribution), b) 0.9 and c) 0.1 (edge contact).

Having recorded the misalignment thresholds, corresponding to shuttling parameters of 0.1, 0.5 and 0.9, intermediate configurations are interpolated linearly according to:

$$\begin{cases} \alpha > \alpha_{0.1} & \rightarrow sp = 0.1 \\ \alpha_{0.1} \geq \alpha \geq \alpha_{0.5} & \rightarrow sp = 0.4\dfrac{\alpha - \alpha_{0.1}}{\alpha_{0.5} - \alpha_{0.1}} + 0.1 \\ \alpha_{0.5} \geq \alpha \geq \alpha_{0.9} & \rightarrow sp = 0.4\dfrac{\alpha - \alpha_{0.5}}{\alpha_{0.9} - \alpha_{0.5}} + 0.5 \\ \alpha < \alpha_{0.9} & \rightarrow sp = 0.9 \end{cases} \quad (4.33)$$

4.5. Backlash

Backlash is defined by the user as arc length (circular backlash) on the theoretical pitch circles, therefore it can be directly compared to the actual DTE. At the beginning of the simulation, gears are assumed to be centred in the backlash, therefore half the backlash value is subtracted from actual DTE to define the elastic component of the DTE:

$$DTE_{el} = DTE - sign(DTE) \cdot \frac{1}{2} b \quad (4.34)$$

When backlash is enabled, DTE_{el} is used in *(4.13)* to calculate the contact force and to enter the look-up tables in case of variable load approach (*Paragraph 4.3.5*). Contact force is applied if DTE is greater in absolute value than half the backlash, if lower, contact force is set to zero. Back-face contact is allowed since DTE can assume positive or negative values.

Chapter 5.

Advances for gearbox simulation and analysis

5.1. Tooth microgeometry modifications

Although all the considerations hold and have been generalized for helical gear pairs (*Chapters 4* and *6*), a pair of spur gears has been chosen as reference model to demonstrate the microgeometry effects. There are two main reasons for this choice: first spur gears show higher and clearer TE fluctuations than helical gears, second spur gears are useful to clearly visualize misalignment effects in 3D drawings. The sample spur gear pair is shown in *Figure 5.1* and its specifications are reported in *Table 5.1*. The gears are constrained using rigid revolute joints leaving one degree of freedom (DOF) per gear, the axial rotation.

Parameter name	Value
Driving gear tooth number	20
Driven gear tooth number	20
Helix angle	0°
Pressure angle	20°
Module	4 mm
Face width	25 mm
Centre line	80 mm
Contact ratio	1.557

Table 5.1 – Gears specifications.

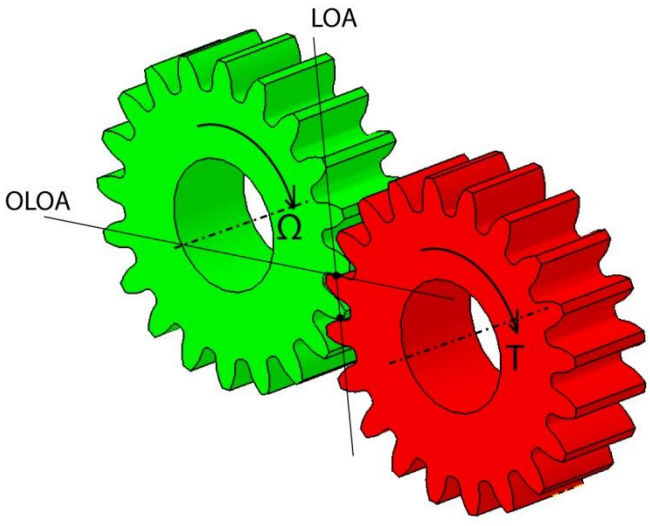

Figure 5.1 – Three-dimensional view of the gear pair.

The STE dataset was generated for a discrete range of torques and misalignments. Torque spans a range of ±40 Nm around the nominal value of 100Nm, from 60 to 140 Nm with 9 equally spaced samples. Angular misalignment in the plane of action, typically in the order of magnitude of milliradians, is expressed in terms of slope coefficient and spans the range from -0.01 to 0.01 with 11 samples. As discussed in *Paragraph 3.2.3*, microgeometry modifications along profile and lead of the gear face bring substantial improvements when optimizing both vibration and contact stress patterns. The ability to capture the effects of these modifications is crucial for accurate simulations. The proposed method is able to take microgeometry modifications into account intrinsically in the STE dataset generation step. Both profile and lead modifications are applied to the example gear pair. Lead modifications allow reducing sensitivity to misalignment. A lead crowning modification of 9 µm is applied to the example gear pair to minimize peak contact stress within a misalignment range of ±0.001 slope. More details for lead modification and the effects of misalignment are provided in *Chapter 3*. Profile modifications are applied to minimize peak to peak value of the STE at the nominal torque value of *100 Nm*. Under the action of this torque value, the deflection value calculated with LDP just before the second tooth pair comes into contact is equal to 6.8 µm. In first approximation, the optimal profile modification at the nominal torque value can be obtained removing from the tip of the meshing teeth (for both the pinion and the gear) an amount of material roughly equal to this maximum deflection. A linear modification is applied to reach a zero value at the highest point of single tooth contact (HPSTC), as illustrated in *Figure 5.2*.

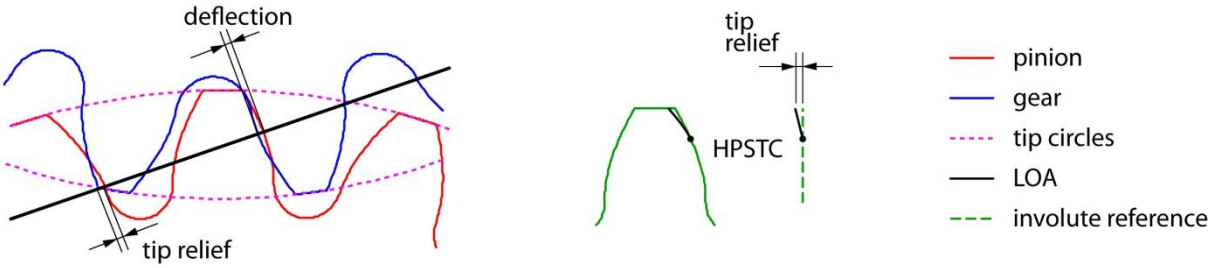

Figure 5.2 - Linear tip relief modification applied to the pinion and the gear teeth.

The applied tip relief is equal to 7 μm and minimizes the peak to peak value of the static TE for the nominal torque value of 100 Nm as shown in *Figure 5.3*.

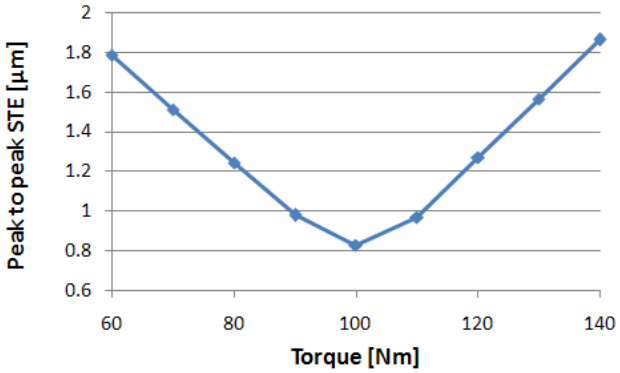

Figure 5.3 – Peak to peak value of the STE between ±40% excursion on the nominal torque value.

The Harris map plot shown in *Figure 5.4* illustrates the non-linear variation of the STE with torque, in the range used for the STE dataset generation. The non-linearity is due to the interaction between the deflection and the applied profile modification, which is changing the load sharing between meshing teeth pairs during the mesh cycle.

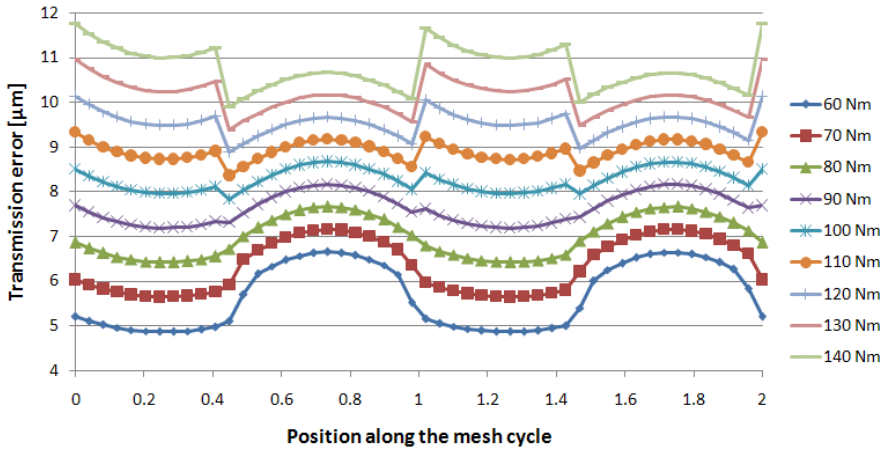

Figure 5.4 – STE variation along the mesh cycle for different torques in the range 60-140 Nm (Harris map plot).

The same chart can be obtained by flattening on a plane different sections of the multidimensional STE dataset at given torque values, as is shown in *Figure 5.5* and *Figure 5.6*.

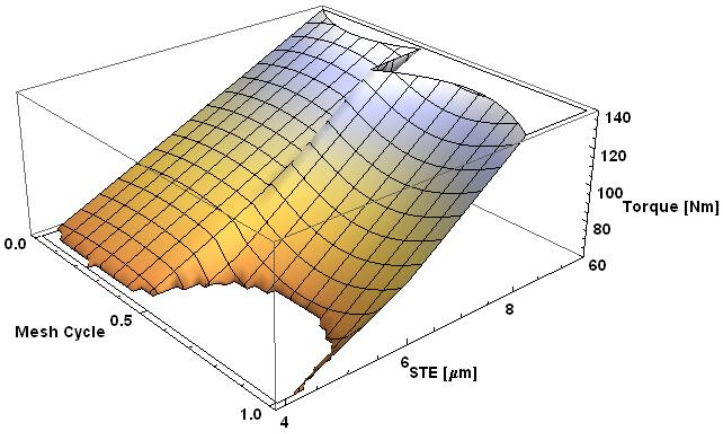

Figure 5.5 – The surface STE(PMC,VT), subspace of the STE dataset.

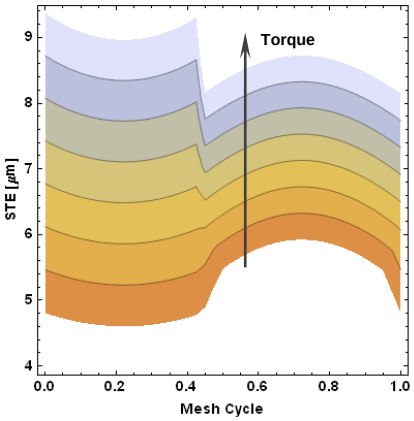

Figure 5.6 – Contour plot.

The proposed method contains the information needed to account for torque variation effects on the mesh stiffness. On the contrary, the time-varying mesh stiffness approach yields a linear increase in the TE average and peak to peak, and it is not able to account for the non-linear behaviour described by the Harris map plot.

5.2. Misalignments

The goal of this paragraph is to highlight the sensitivity of gear static TE and stress distribution with respect to the misalignment components. Gear contact simulations are therefore performed in LDP.

Errors affect the relative positioning of the meshing teeth. These errors affect the peak to peak TE in different extent. As discussed in *Paragraph 3.2.2*, they originate from assembly errors, tooth generation deviations and structural deflections. To discuss misalignments, tooth generation deviations will be excluded from the current discussion: such deviations are assumed to be consistent from tooth to tooth (no manufacturing variability) and therefore can be included in the description of the tooth microgeometry. Assembly errors in parallel

gears are mainly located at the bearings with deviations from the ideal positions, clearances and deflections which affect the shafts orientation and therefore the teeth relative positioning. Deflections may also substantially arise from deformable supporting structure, such as shafts, housing and carrier(s) in case of planetary stages. Assembly errors and deflections therefore are the factors to focus on to discuss sensitivity to misalignments. Although an axial displacement can result in a reduction of the active face width, good positioning accuracies are also normally achieved in the axial direction, resulting in axial displacements which are by far smaller than the active face width they affect. For that reason axial displacement will not be considered in the present analysis. A uniform displacement along the LOA coincides with a constant additional TE, which does not alter the peak to peak TE value. For that reason LOA displacement will not be considered in the present analysis. A rotation in the POA alters the load distribution along the face width of the teeth, thus affecting the mesh stiffness and so the peak to peak TE. A uniform displacement along the OLOA can be considered as a centre line variation which affects the contact ratio and so the peak to peak TE. A rotation in the OPOA is found to be ineffective on the contact area [149] and the tooth load distribution [77], so it is ineffective also on the TE.

On the basis of the above considerations, the effects of rotations in the POA, commonly called (angular) misalignment, and variations in centre line will be assessed hereafter by means of LDP analyses. This is useful to decide if both the assembly errors have to be included in the dynamic analysis or one of the two is predominant. Two gear pairs without microgeometric modifications, belonging to an automotive and a wind turbine gearbox, have been considered (*Table 5.2*).

Parameter name	**Automotive**	**Wind turbine**
Driving gear tooth number	39	40
Driven gear tooth number	40	80
Helix angle	26°	0°
Pressure angle	20°	20°
Module	3 mm	4 mm
Face width	25 mm	80 mm
Centre line	134.5 mm	240 mm
Nominal contact force	6000 N	13300 N

Table 5.2 – Automotive and Wind turbine gear pairs specifications.

Realistic values of the centre line variation are estimated in a range of *±0.2%* of the whole centre line, as confirmed by the values used in [77].
Since misalignment is a rotation in the POA, it can be defined in terms of a rotation angle, the slope associated to this angle, or the displacement caused by the rotation at a tooth face (*Figure 5.7*).

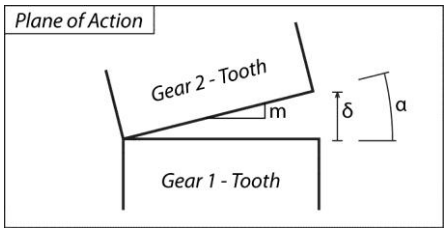

Figure 5.7 – Schematic representation of misalignment and definitions in terms of angle (α), displacement (δ) and slope (m).

Misalignment is affected by parameters such as shaft deflections, bearing positioning and clearances which cannot be assumed a priori. However the 1328 ISO Standard for Gear Quality provides the allowed ranges for slope errors along the lead direction. The slope error value has been used to estimate the range of misalignments for the considered gear pairs. Assuming a medium/precise gear quality (ISO 7), the allowed slope deviation is found to be for both gear pairs equal to *20 µm* in terms of displacement. This value has been doubled because the slope deviation can be the maximum and add up for both the meshing teeth. The contribution due to shafts and bearings is then assumed to have the same magnitude of the slope deviation, so that the final misalignment is estimated to be in a range from *0* to *60 µm* in terms of displacement.
The peak to peak STE percentage variation has been evaluated for centre line variations and misalignments within the defined ranges (*Figure 5.8*).

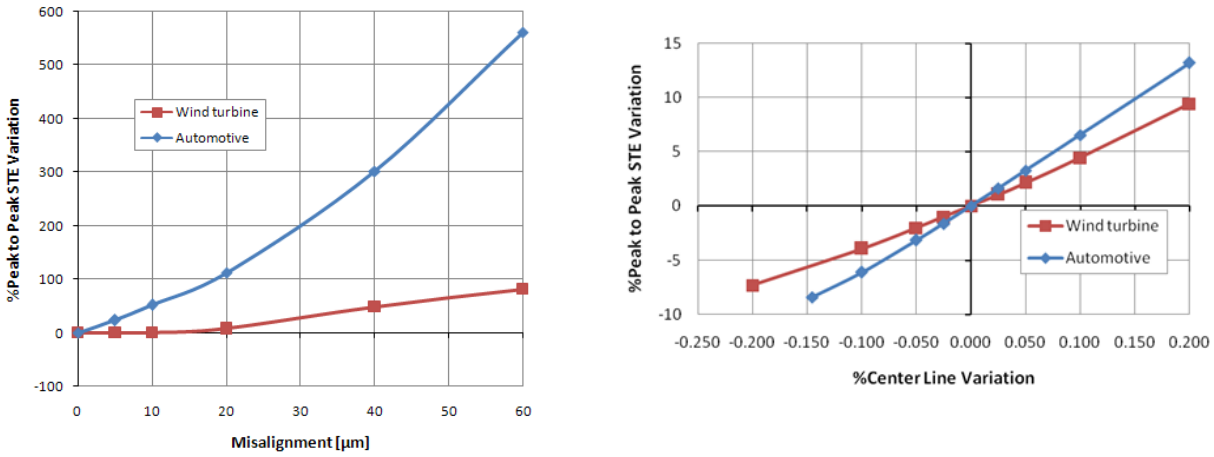

Figure 5.8 – Effects on peak to peak STE value due to misalignment and centre line variation.

The peak to peak STE value increases for both the gear pairs if misalignment or centreline is increased. The maximum increase of the peak to peak STE caused by the misalignment is about *100%* for the wind turbine gear pair and *600%* for the automotive gearbox gear pair. Considering the centre line variation, the maximum increase is below 15% for both gear pairs. The gear pair from the automotive gearbox, which is helical, shows a higher sensitivity to both misalignment and centre line variation. Considering the maximum values, the misalignment can be considered as dominant with respect to the centre line variation. Although, at low misalignment values, the centre line variation effects prevail on misalignment, especially for the wind turbine gear pair. It has also to be pointed out that the sensitivity to misalignment is increased by the absence of lead modifications, which are usually adopted when misalignments are significant as in this case. Based on these considerations it is worthwhile to extend the technique to take into account both the dynamic misalignment and the centre line variations. In fact, when lead microgeometry modification is applied, the following simulations show how the average value is altered but STE variability undergoes a limited effect. Effects on contact stress distribution when gears have no lead modification are shown in *Figure 5.9* for the aligned and the misaligned case, when misalignment slope is equal to ±0.001 (equivalent to 1 milliradian or 0.057 degrees). For the aligned case stress distribution is uniform along the teeth face width with a maximum contact stress of 786 MPa, while in the misaligned case stress distribution is moved to one face of the gears and the peak contact stress becomes 1375MPa with a 75% increase compared to the aligned case. A lead

crowning modification of 9 µm is applied to the teeth *Figure 5.10*, which minimizes the stress increase due to applied misalignment of ±0.001 slope. The peak contact stress in the misaligned case is reduced to 1056 MPa (+34%), however also the peak stress in the aligned case has now increased to 988 MPa (+26%) as shown in *Figure 5.11*.

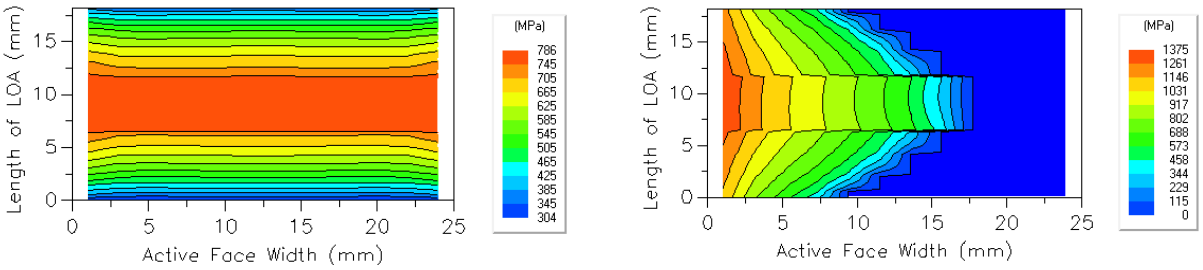

a) *b)*

Figure 5.9 – Contour plots of contact stress distribution along the teeth face width and the length of Line of Action. Gears without lead modifications.
a) aligned, b) misaligned with 0.001 slope.

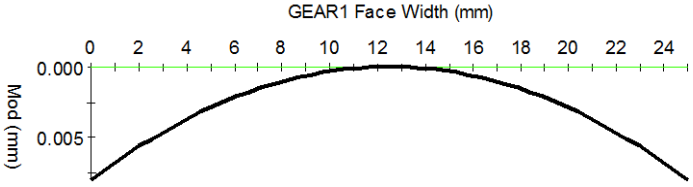

Figure 5.10 – Total lead crowning modification applied to the teeth.

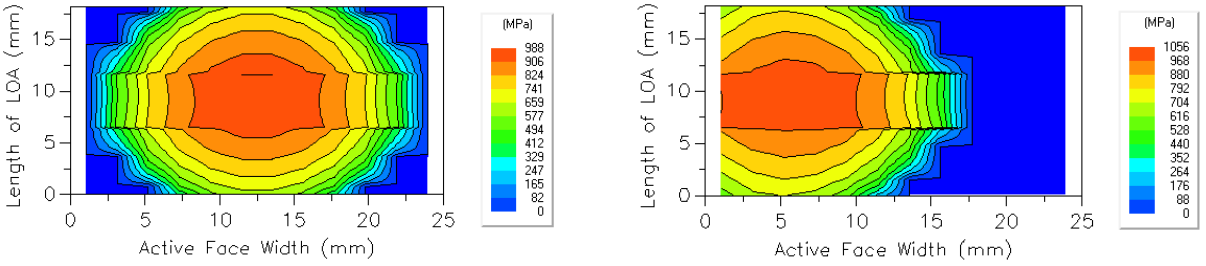

a) *b)*

Figure 5.11 – Contour plots of contact stress distribution along the teeth face width and the length of Line of Action. Gears with lead modifications.
a) aligned, b) misaligned with 0.001 slope.

STE curves relative to the aligned and misaligned case, with and without lead crowning are shown in *Figure 5.12*.

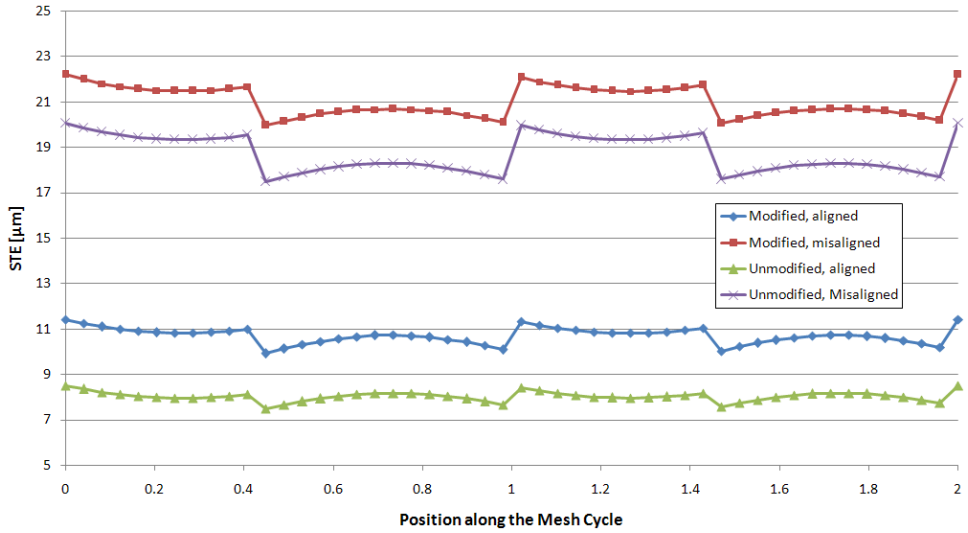

Figure 5.12 – STE curves with or without lead crowning and aligned or misaligned.

The curves for the aligned and the misaligned cases show how angular misalignment increases the average and the peak to peak value of the STE. Higher average value of the STE implies reduced average mesh stiffness. Contact patterns provide an explanation for these effects: in *Figure 5.9b* and *Figure 5.11b* misalignment reduces contact area to nearly half the face width in average; the peak to peak variation instead is due to the different extent of contact area when a single tooth pair is in contact (0 to 6 mm and 12 to 18mm in length of LOA) and two tooth pairs (6 to 12 mm in length of LOA). Comparing the curves for modified and unmodified lead shows how a further reduction in average mesh stiffness is introduced by lead crowning. When taken into account in the multibody simulation, these variations of the average mesh stiffness enable to model the shift in natural frequencies for modes which are coupled with teeth deflections. Three considerations about misalignment can be highlighted from this example:

- sensitivity can be reduced but up to a certain extent due to trade-off with stress increase;
- effects on the equivalent mesh stiffness are a decrease in the average value and an increase in the peak to peak value;
- the contact area is moved towards one edge.

Chapter 6.

Application to case studies

6.1. Single helical gear pair

Simulations for an example helical gear pair (*Figure 6.1*) are performed to show how the effects discussed in the previous paragraphs are captured in the multibody simulation. The gears specifications are reported in *Table 6.1*, teeth have standard size. Gears are constrained using rigid revolute joints. One gear is driven in velocity, while a resisting torque with a nominal value of *100 Nm* is applied to the other gear, causing a nominal normal contact force of *2726 N*. Viscous damping has been added to smooth the DTE curves, equal to 10^5 Ns/m.

Parameter name	Value
Driving gear tooth number	20
Driven gear tooth number	20
Helix angle	13°
Normal pressure angle	20°
Normal module	4 mm
Face width	25 mm
Centre distance	82.104 mm
Transverse contact ratio	1. 540
Overlap ratio	0.448
Total contact ratio	1.988

Table 6.1 – Gears specifications.

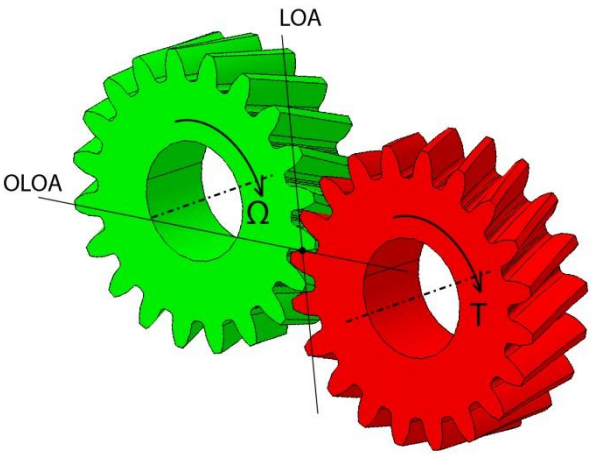

Figure 6.1 – 3D view of the gear pair.

Few cases were tested:

1) Gears without microgeometric modifications
    a. Run-up from 0 to 3000 rpm;
2) Gears having microgeometric modifications
    a. Variable resisting torque;
    b. Applied POA angular misalignment (positive and negative);

Case 1a simulation is performed under the assumption of constant applied load to calculate mesh stiffness and actually applying a constant resisting torque equal to the nominal value. Mesh stiffness is considered variable and depending only on the position on the mesh cycle; periodicity originates from the assumption of equally spaced teeth. The DTE for several speed values (*Figure 6.2*) show overlapping with the STE curve at low speed and increasing delay due to inertia and damping effects when speed increases. The single gear pair transfer function (*Figure 6.3*), obtained by the linearized model described by Ozguven et al. [23], explains filtering effects at high frequency causing subsequent DTE harmonics to be cut. This effect is clearly visible at a speed of 3000 rpm, where the DTE frequency content is dominated by the fundamental mesh frequency and assumes a more harmonic trend in time (*Table 6.2*).

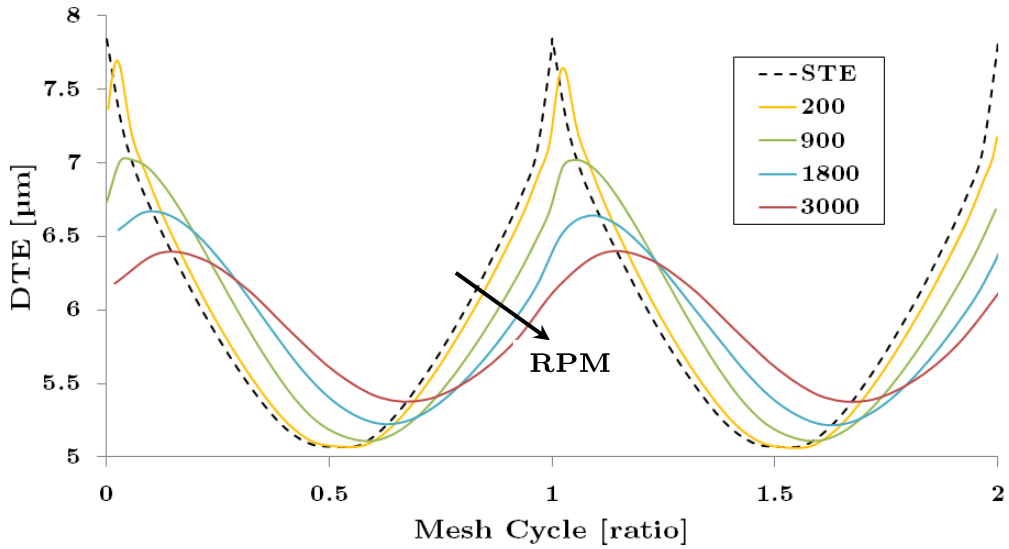

Figure 6.2 – Comparison between STE and DTE for different values of angular speed.

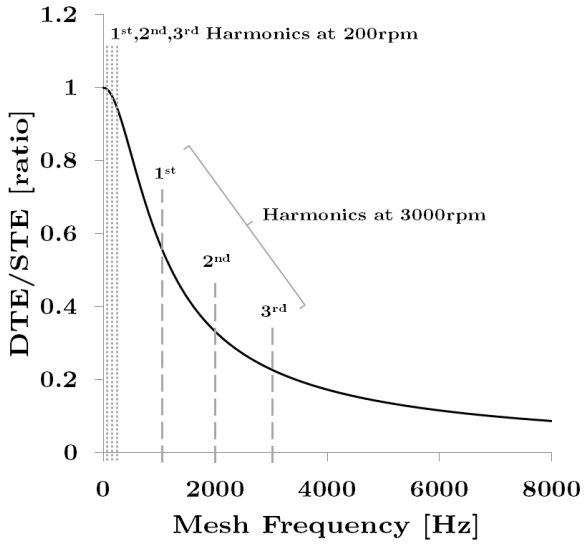

Figure 6.3 – Frequency response function for the analysed gear pair and first three harmonics frequencies highlighted for 200rpm and 3000rpm.

	200 rpm		***3000rpm***	
Harmonic Number	*Mesh Frequency [Hz]*	*Gain [ratio]*	*Mesh Frequency [Hz]*	*Gain [ratio]*
1	66	**0.99**	1000	**0.57**
2	133	**0.98**	2000	**0.33**
3	200	**0.96**	3000	**0.23**
4	266	**0.93**	4000	**0.17**
5	333	**0.90**	5000	**0.14**

Table 6.2 – Comparison between STE and DTE harmonics for lowest and highest analysed angular speeds.

When the contact force, e.g. the normal component, is considered within a mesh cycle, oscillations around the nominal value appear where sharp changes in the mesh stiffness happen. Tooth transition occurs when the mesh cycle ratio reaches 1, this is where the STE reaches a peak as shown in *Figure 6.2*: the highest STE is reached (lowest mesh stiffness) for a brief period, since the gear pair has a total contact ratio slightly below 2 (*Table 6.1*). *Figure 6.4* shows how contact force oscillations increase with angular speed due to damping effects and start with an unload since mesh stiffness initially drops (TE in *Figure 6.2* first increases) and continue with an overload since mesh stiffness raises back.

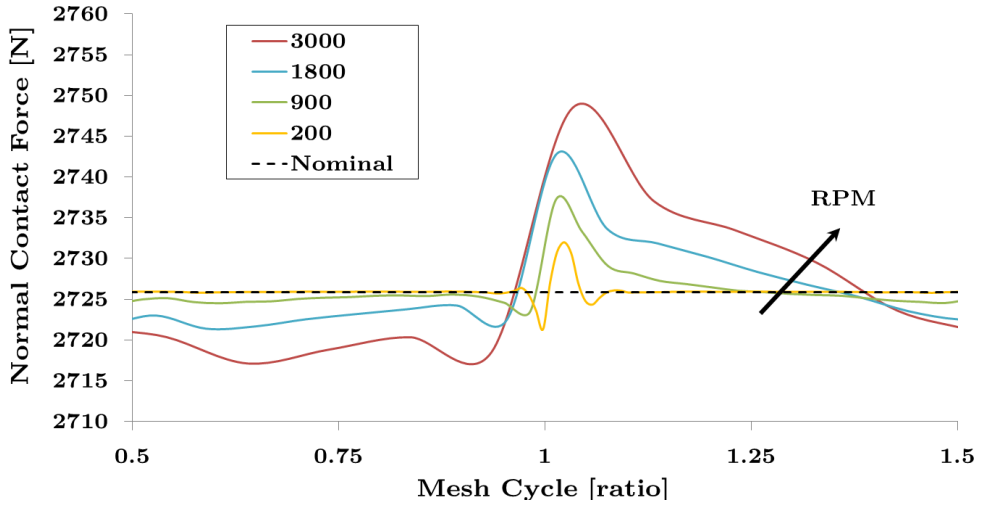

Figure 6.4 – Comparison between Dynamic and Nominal Normal Contact force for different values of angular speed.

Case 2a is showing the substantial differences introduced by the variable load approach when microgeometric modifications are applied to teeth surfaces. In particular, a linear tip relief of 7 µm starting from the theoretical pitch point and a parabolic lead crowning of 4.5 µm were applied to teeth surfaces of each gear (*Figure 6.5*). The profile modification minimizes STE peak-to-peak value (0.2 µm versus 2 µm in the non-modified case) at the nominal torque. The lead modification minimizes the peak contact stress difference between the cases of aligned and misaligned (3 mrad) gears.

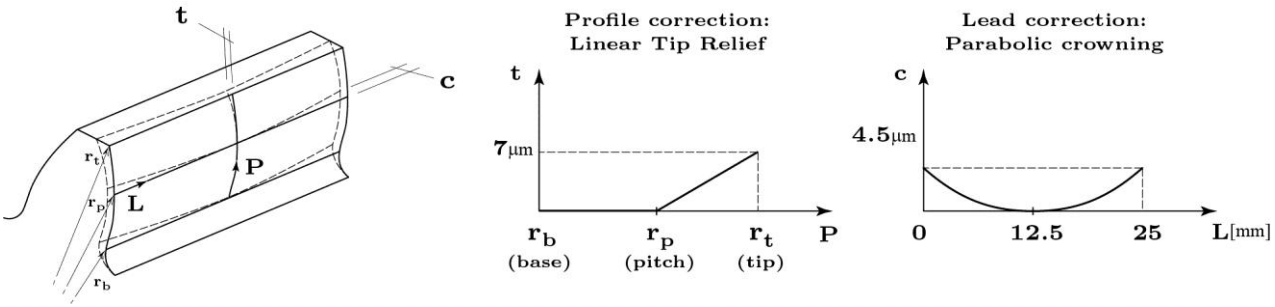

Figure 6.5 – Teeth microgeometry modifications along lead (L) and profile (P).

Angular speed for the gears was kept sufficiently low (50 rpm) to clearly show the TE trend due to profile modification without dynamic effects. Applied torque is varied from 70 to 130 Nm. As shown in *Figure 6.6*, variable and constant load approaches agree where the applied torque value is equal to the nominal one.

For the constant load approach, the DTE cycles are simply scaled by load with respect to the nominal case. Therefore DTE variability is proportional to the applied load, leading to lower excitation when load is lower than the nominal value and vice-versa. When considering the curve with variable load effects, it is possible to see a substantial change in shape for the DTE curve cycles. Cycles show increasing peak-to-peak values away from the nominal torque value, where profile modification is no longer optimal.

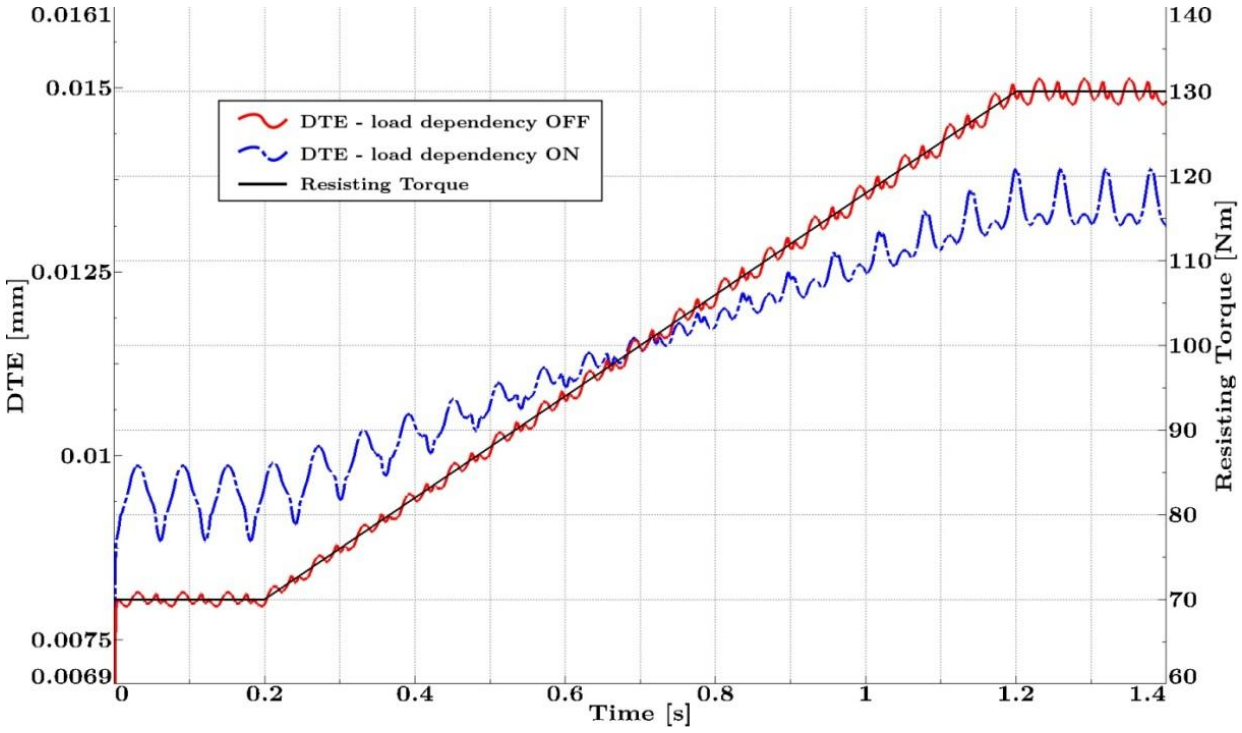

Figure 6.6 – DTE comparison between variable and constant load approach, gradually varying resisting torque.

When load dependency is activated, non-linearity occurs not only in the peak to peak STE value, but also in the average value over a mesh cycle. In this case TE is higher (lower mesh stiffness) for low loads and lower (higher mesh stiffness) for high loads. This phenomenon is due to contact mechanics and is strongly related to teeth microgeometry corrections. Contact patterns for the analysed gear pair are shown in *Figure 6.7*. For loads lower than the optimal, the contact area is smaller and therefore the contact stiffness contribution to the total stiffness decreases. On the contrary, for loads higher than the optimal, the contact area is more extended and the contact stiffness contribution increases.

When load dependency is deactivated (linear case), the contact stiffness contribution remains constant with respect to load as well as the number of teeth in contact along the mesh cycle.

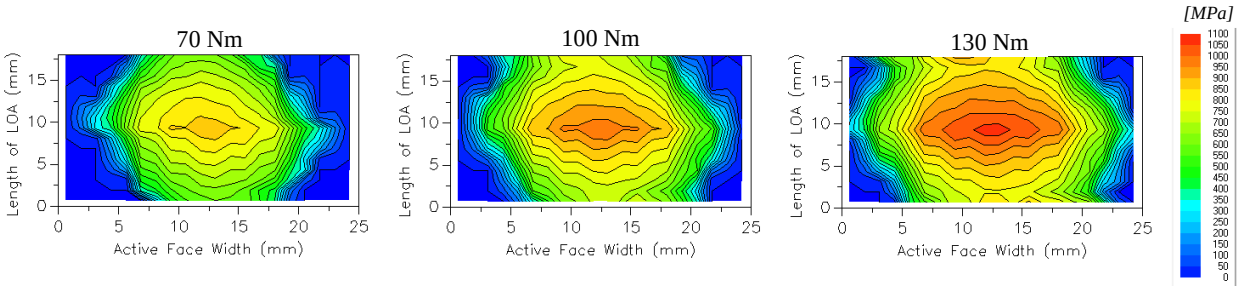

Figure 6.7 – Contact patterns for the analysed gear pair, aligned, at 70, 100 and 130 Nm applied torque.

Case 2b in *Figure 6.8* shows the effects of misalignment on the DTE. Resisting torque is kept constant at the nominal value. Misalignment is increased linearly from 0 to -0.003 radians, causing DTE peak-to-peak and average value to rise. Mesh stiffness decreases due to misalignment, either positive or negative, because the active face width reduces (unless specific lead modifications are applied to compensate for misalignment).

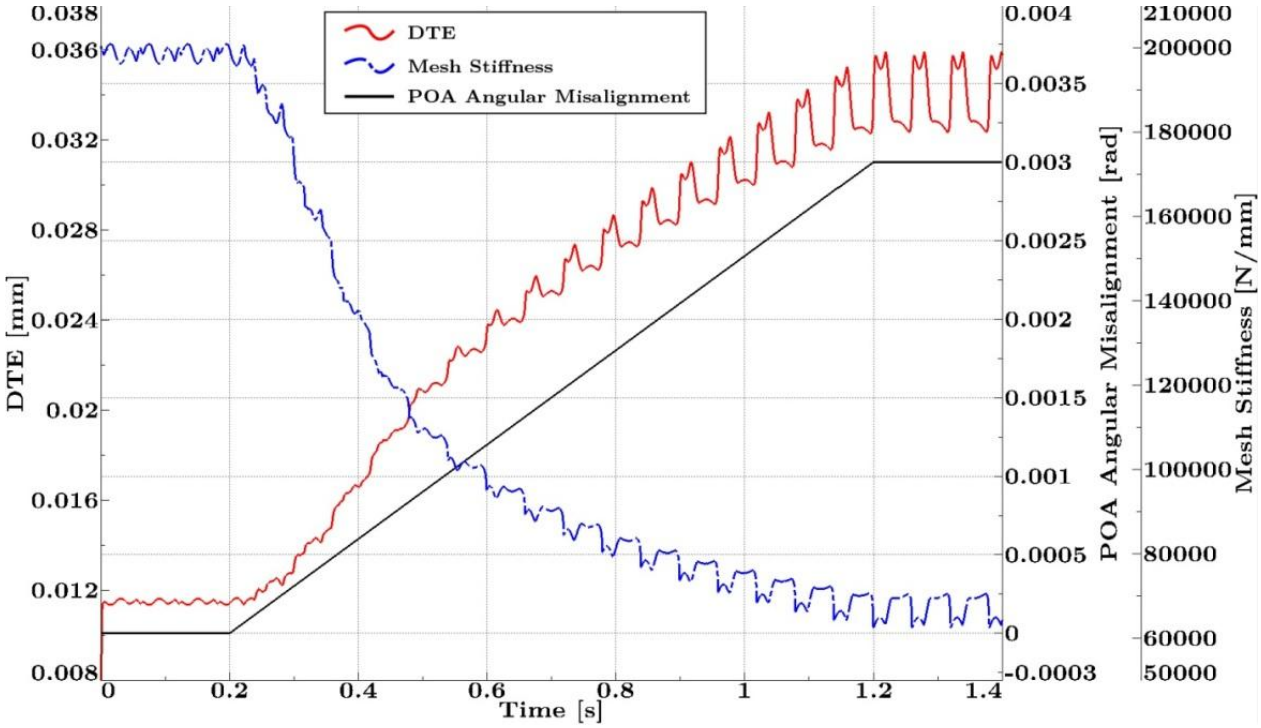

Figure 6.8 – Effects of POA angular misalignment (plotted in absolute value) on DTE.

Misalignment is also causing a shift for the axial coordinate of the contact point. As shown in *Figure 6.9*, the axial coordinate is oscillating due to shuttling effects according to LDP calculations, around half the face width in the aligned case. When misalignment is applied, the average value of the axial coordinate shifts to circa 10 mm.

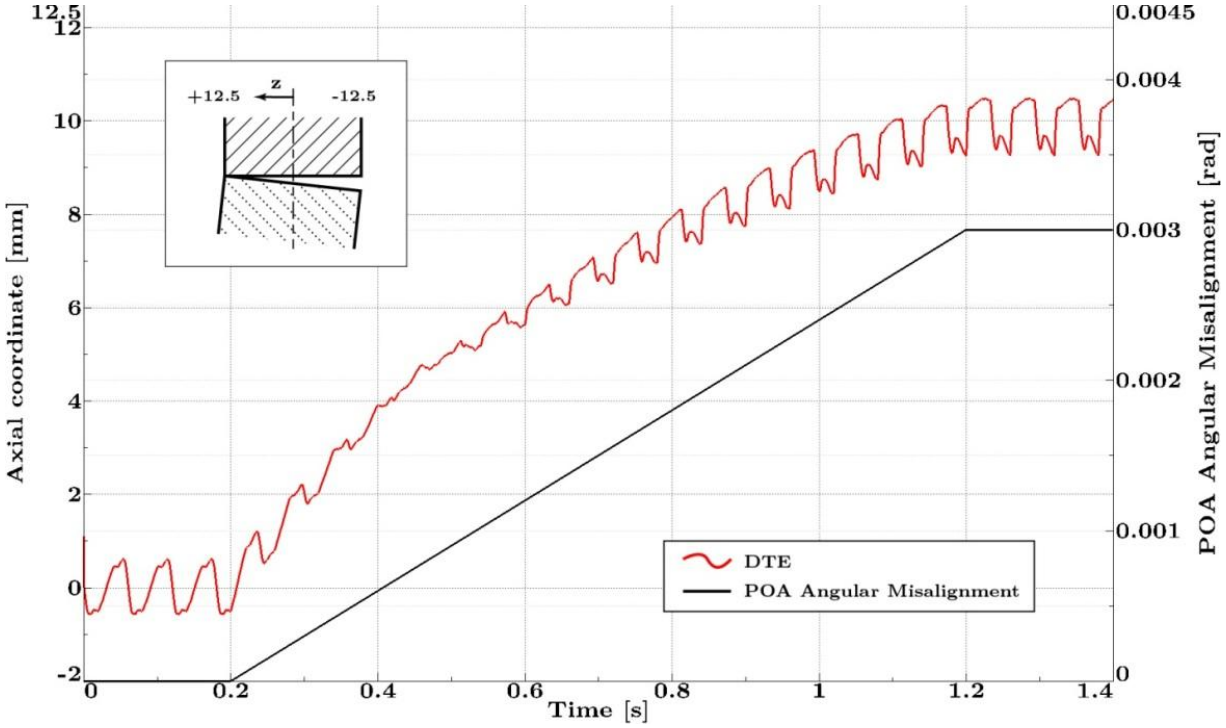

Figure 6.9 – Shift of the axial coordinate for the contact point due to POA angular misalignment.

DTE in case of positive and negative misalignment are compared in *Figure 6.10*. Both misalignments cause an increase in DTE peak-to-peak value. Average values have to be treated separately. Negative misalignment causes only decrease in mesh stiffness and therefore an increase in the average DTE. Positive misalignment also causes a decrease in mesh stiffness since the contact area is reduced, however the offset component in *(4.24)* soon prevails and pushes the driven gear ahead of the driving gear, causing the DTE to become negative. The two curves in *Figure 6.10* also show how misalignment variations can increase the DTE span and therefore become an important source of dynamic excitation.

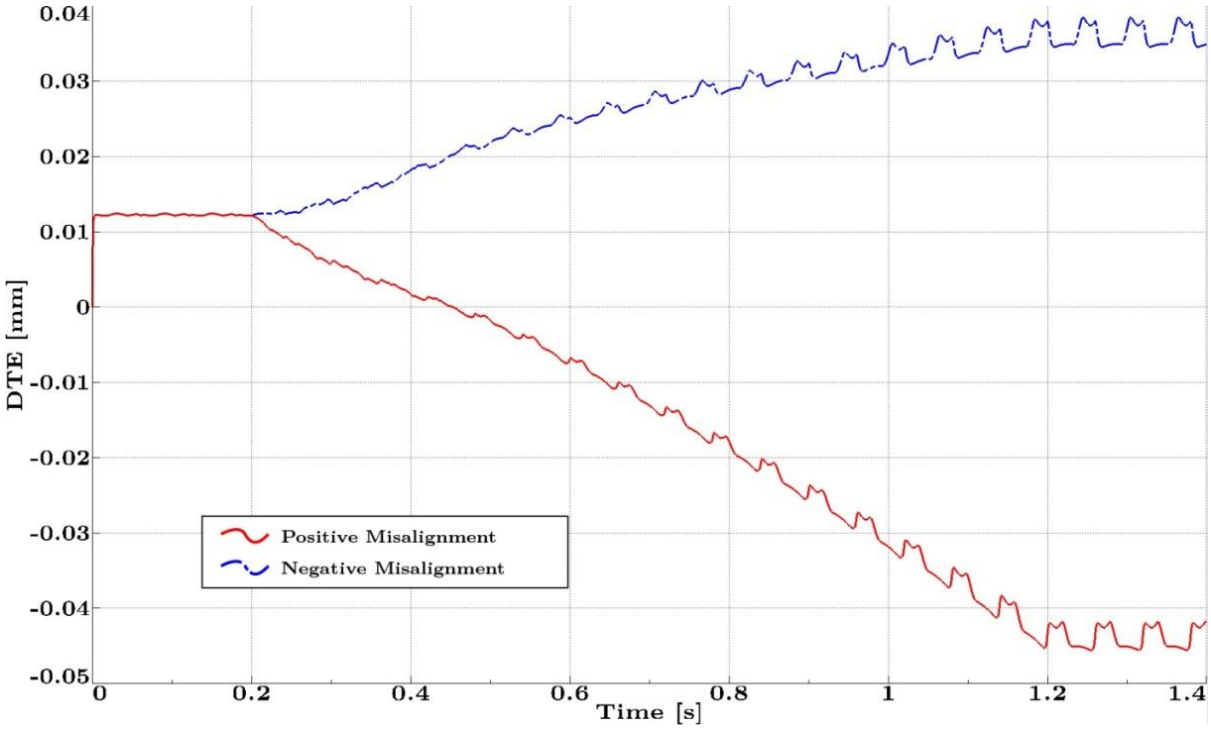

Figure 6.10 – Effects on DTE of positive and negative POA angular misalignment (±3 mrad).

6.2. Planetary gear stage

6.2.1. Three-dimensional effects

During the progress of gear meshing, the axial position of the contact area(s) is not constant. In helical gears contact lines span teeth surfaces moving from one corner to the opposite one. If the resulting contact force is calculated in subsequent moments of a mesh cycle, the axial position of its point of application (hereafter simply the “contact point”) is found to be varying periodically. The term “shuttling” is used to indicate this periodic variation of the contact point axial positioning, which has the same period as a mesh cycle. More generally, the term can be used also in relation to other causes. Besides the geometric properties of meshing in helical gears, another main cause of shuttling is the angular misalignment of teeth surfaces. Angular misalignment displaces the point of contact towards one face of the meshing gears. It is usually dependent on structural deflections caused by the instantaneous contact load. Load variability

therefore translates into a variable misalignment, which causes in turn the contact point to move axially. In both cases, whether it is due to the helix angle or a misalignment, shuttling causes an oscillating load sharing among the bearings which support the gears. The main effect of shuttling due to helix angle is a periodic tilting moment, acting in the plane of action on the gear bodies, with a fundamental frequency equal to mesh frequency. When shuttling is due to the angular misalignment, the tilting moment magnitude depends on the misalignment amplitude and tends to push the gears to the aligned position. The two effects are combined in case of misaligned helical gears.

As it can be seen in *Figure 6.11a*, while in spur gears the progression of contact lines is parallel to the axis of rotation and spans the driving tooth profile from root to tip, in helical gears these contact lines start gradually from one corner and proceed at an angle towards the opposite one (*Figure 6.11b*).

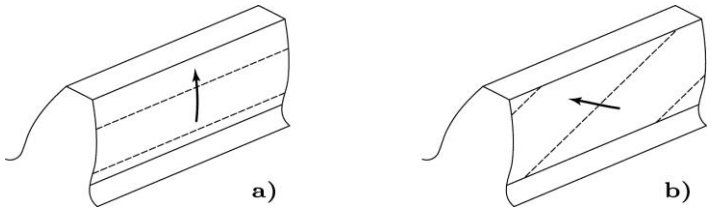

Figure 6.11 – Path of contact lines for a) spur gears, b) helical gears.

The cyclic oscillation of the axial coordinate for the contact point can be observed by plotting the contact lines load distribution for different positions along the mesh cycle. *Figure 6.12* shows how in case of helical gears, the contact point undergoes a cyclic displacement in the axial direction, while for spur gears the contact point remains centred at half the active face width of the gear pair.

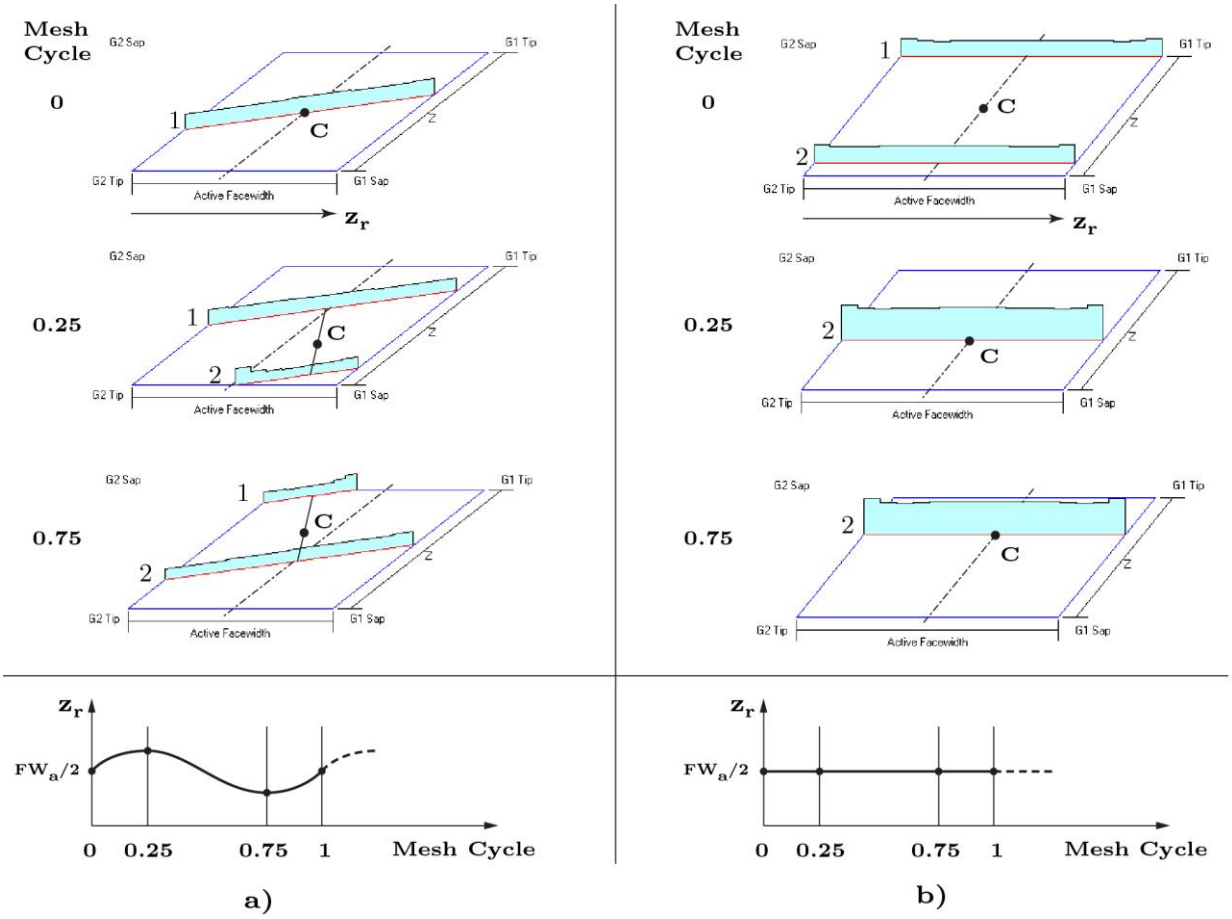

Figure 6.12 – Position of the contact point and contact lines with load distribution in the plane of action at different positions along the mesh cycle for a) Helical gear pair; b) Spur gear pair.

This example is drawn for aligned gear pairs and shows how shuttling intrinsically happens for helical gears due to geometric characteristics of their meshing. However the position along the mesh cycle is not the only operating condition which affects shuttling. More in general shuttling happens whenever the load distribution varies in the axial direction.

Angular POA misalignment is a major cause of load distribution variation in the axial direction. Angular POA misalignment can be constant or variable in time along with the operating conditions. In case it is constant, typically when it is due to assembly errors, the axial position of the contact point is displaced but does not cause extra excitation. In case of variable misalignment, typically when it is due to shaft deflections, it is depending on the instantaneous load and introduces a tilting moment excitation for the affected gear pair (*Figure 6.13*).

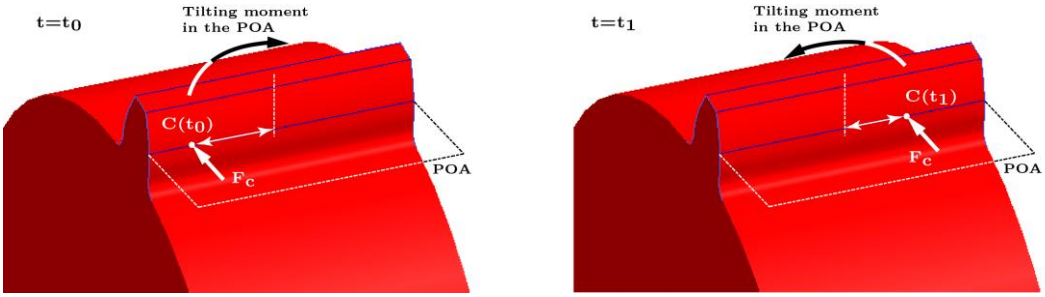

Figure 6.13 – Different tilting moments at different time instants due to shuttling of the contact point.

Both spur and helical gears are sensitive to such a misalignment. Therefore, while shuttling happens intrinsically for helical gears, when POA angular misalignment is variable, it is possible to have shuttling phenomena also for spur gears.

The effects of shuttling become more important when supporting bearings are very close to each other and under the gear bodies, since their load sharing becomes more sensitive to contact load distribution on the gear teeth and to gear-tilting modes. Planet bearings in planetary gear stages are a widespread example in this direction. Displaced contact distribution towards one of the gear faces causes an increase in the fraction of the resultant contact force carried by one bearing and a decrease on the other bearing (*Figure 6.14*), with significant reduction of the overloaded bearing life. Moreover, if the planet has helical teeth, an additional tilting moment is introduced by the axial components of the contact forces acting on opposite teeth (*Figure 6.15*). This moment represents an additional cause of POA angular misalignment and introduces two opposite radial forces on the bearings.

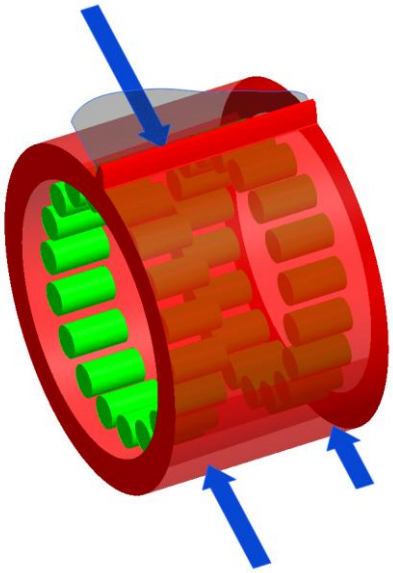

Figure 6.14 – Schematic of a loaded tooth on a spur planet gear with typical integrated cylindrical roller bearings. A displaced contact load distribution causes an uneven load sharing on the bearings.

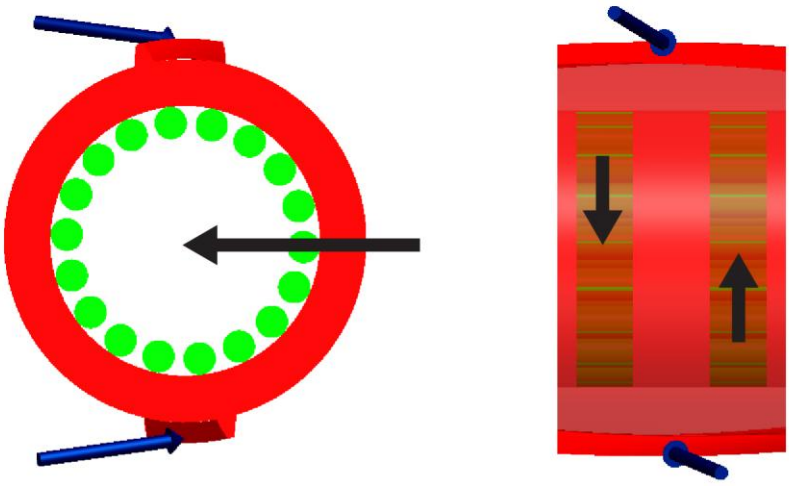

Figure 6.15 – Schematic of a loaded helical planet gear. a) Radial contact force components cancel, while tangential components add up and are compensated by the bearings. b) Axial contact force components cancel but generate a tilting moment which is balanced by bearing radial forces.

6.2.2. Specifications

Unequal load sharing in planet bearings is a major concern for durability in wind turbines gearboxes [152]. The proposed models are applied to an example planetary gear set case study taken from the wind turbine field. Aim of the investigation is to analyse how three-dimensional effects are captured by the proposed multibody gear element. Macro-geometry parameters for the gears were taken from [152] as outlined in *Table 6.3*. Helix angle and gears face width were chosen arbitrarily. Teeth proportions were taken as standard (addendum equal to 1.25 times and dedendum one time the transverse module). A three-dimensional representation for the analysed planetary stage is reported in *Figure 6.16*.

Parameter name	Sun	Planet	Ring
Number of teeth	39	21	99
Helix angle	10°	-10°	-10°
Normal Pressure angle	20°		
Normal Module	10 mm		
Face width	200 mm		
Centre line Sun-Planet, Planet-Ring	304.63 mm		

Table 6.3 – Macro-geometry parameters for the analysed planetary stage.

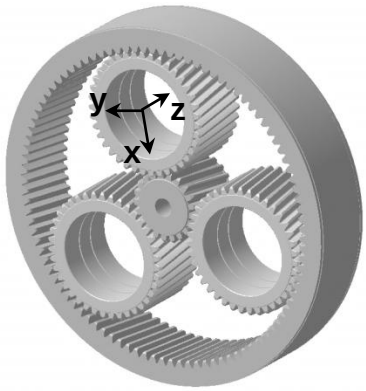

Figure 6.16 – Analysed planetary gear stage and reference system for planet bearing forces.

Real-case values for gear micro-geometry modifications were not available and taken arbitrarily equal to zero. While the hypothesis of unmodified teeth leads to higher sensitivity to misalignment and higher TE excitation, the obtained results are qualitatively valid without loss of generality.

The planet considered by the analysis is supported by bearings spaced at 75 mm from half the face width in the axial direction, having radial stiffness of $10^9 N/m$ and axial stiffness of $10^6 N/m$, in the same order of magnitude of typical wind applications [154]. Contact nonlinearities are not taken into account for bearings. Linear viscous damping coefficients were estimated to obtain a modal damping ratio close to 5% [53]. The ring is held fixed, while the sun, the carrier and the

other two planets are placed on rigid revolute joints. Loads were chosen as 50% of the rated design values reported in [155], leading to a torque of 150 kNm applied on the carrier. Thresholds for the angular POA misalignment-based shuttling model are found to be $\alpha_{0.1} = +1\, mrad$, $\alpha_{0.5} = 0\, mrad$ and $\alpha_{0.9} = -1\, mrad$.

Modal analysis, linearizing the system around the nominal operating conditions, shows a tilting mode for the planet at a frequency of 367 Hz with a damping factor of 5.7%. The sun angular speed which determines a mesh frequency matching this resonance frequency is 1050 rpm. A run-up simulation crossing the resonance is performed from 0 rpm linearly increasing to 1500 rpm in 10 seconds.

6.2.3. Results

Results for planet bearing forces are discussed first in the frequency domain to highlight the interaction between excitation and resonances by means of Campbell diagrams (two-dimensional waterfall plots) and then in the time domain to highlight bearing overloads. Observations will be highlighted in a qualitative way, since crucial parameters for the model were chosen arbitrarily (e.g. micro-geometry, damping coefficients).

Campbell diagrams for the tangential component of the planet bearing force F_y, which is caused by the tangential components of the contact force and is responsible for transmitting power, are plotted in *Figure 6.17*. Diagrams are displayed for each of the two bearings and for three cases: shuttling not taken into account, misalignment-based shuttling and contact-based shuttling. Units are taken in Decibel to better highlight the excitation orders and resonance frequencies, using as a reference value a force of 1 Newton. All the diagrams show clearly an excitation at the 21st order and integer multiples of the sun rotation, corresponding to the tooth-passing order. All the diagrams also show a resonance frequency above 500 Hz, in correspondence of a planet torsional mode of vibration (from the modal analysis: 582 Hz, modal damping ratio of 4.5%). The tilting mode for the planet is not excited for the case of no shuttling, since no significant amplification can be seen in correspondence of its resonance frequency of 367 Hz. On the contrary, the tilting mode is excited for both cases of misalignment-based and contact-based shuttling, with higher force amplification

for the latter case. Similar observations can be drawn for the radial component F_x, which is caused by the tilting moment applied on the planet in an axial plane due to axial component of the contact force acting on opposite teeth, plotted in *Figure 6.18*. Axial bearing forces F_z are zero as expected following the discussion from the previous sub-paragraph. It is worthwhile to point out an asymmetry in the dynamic response for the two bearings: the dynamic tangential force on the bearing number 2 exhibits higher amplification than the one on bearing number 1 (compare rows in *Figure 6.17*). Such behaviour no longer happens for the radial forces (compare rows in *Figure 6.18*). This phenomenon can be observed more in detail in the time traces for the bearing forces, which are discussed later.

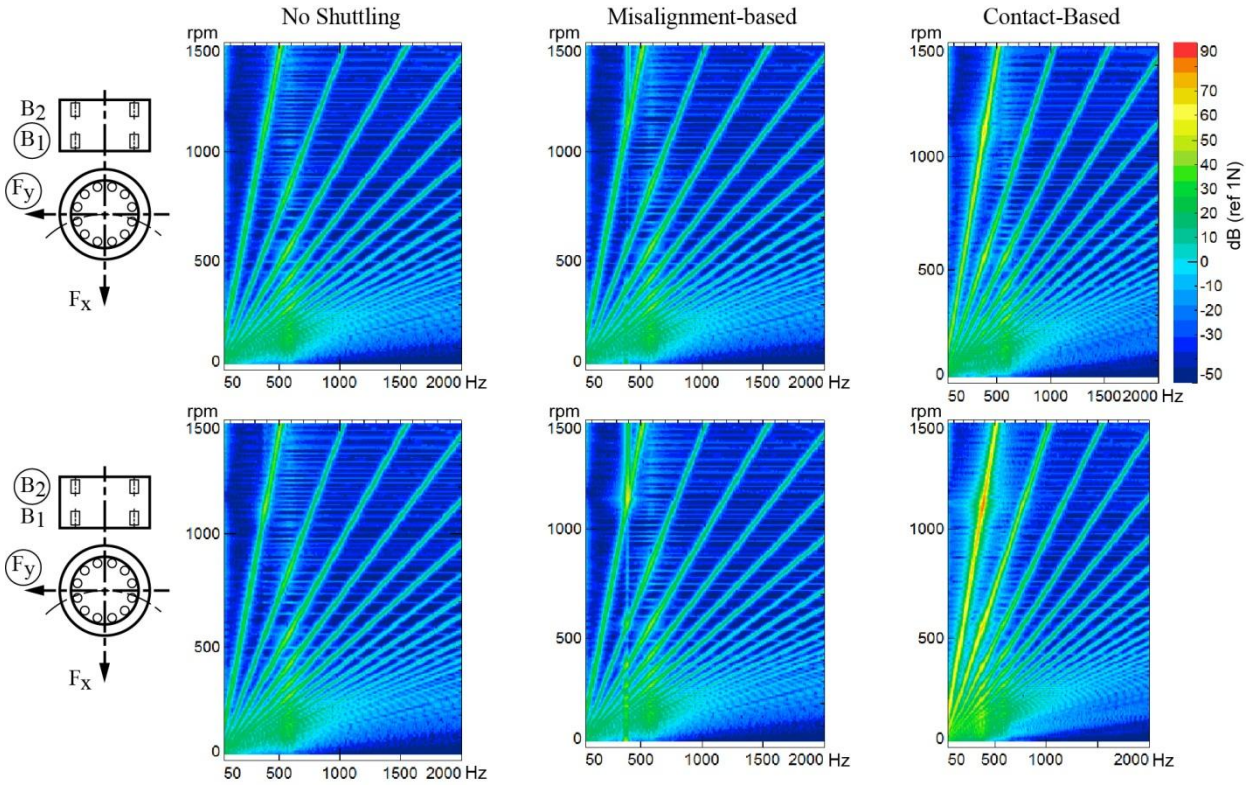

Figure 6.17 – Campbell diagrams for the tangential component of the planet bearing force, for each of the two planet bearings and for the cases of no shuttling, misalignment-based shuttling and contact-based shuttling. Planet projection schemes on the left.

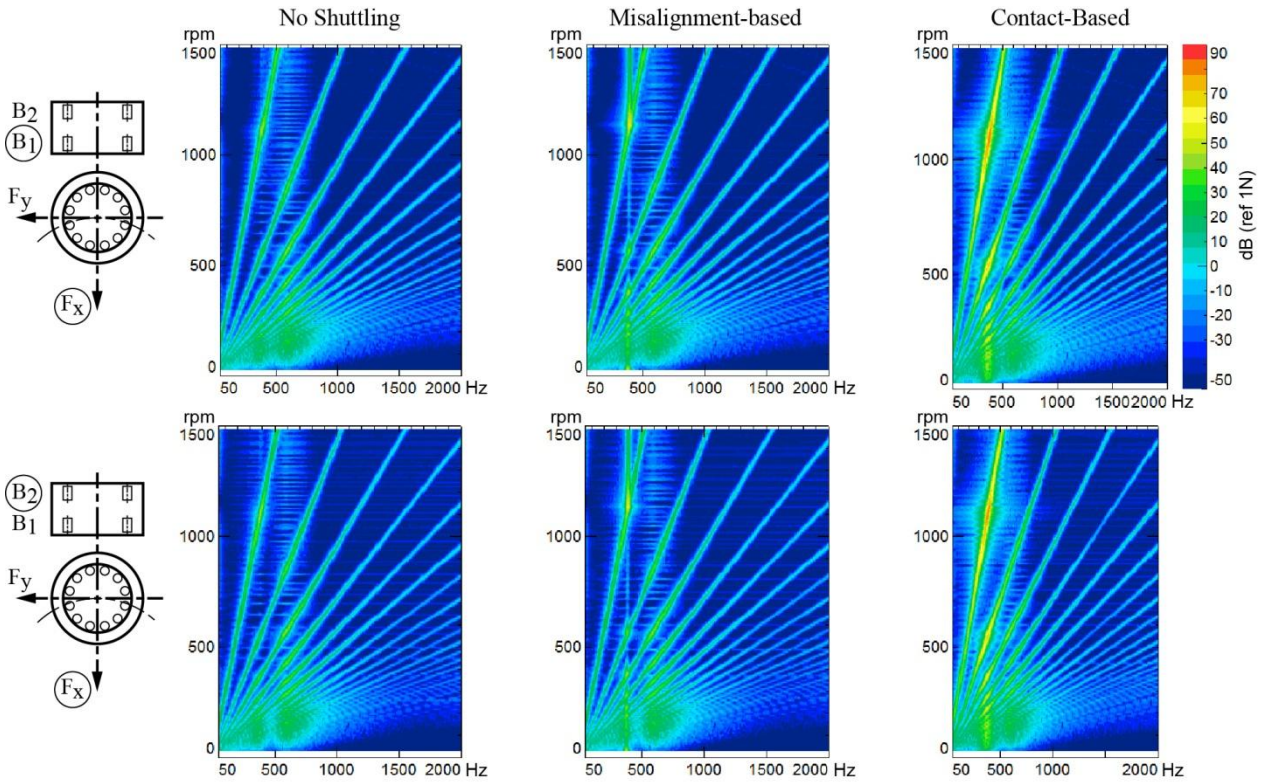

Figure 6.18 – Campbell diagrams for the radial component of the planet bearing force, for each of the two planet bearings and for the cases of no shuttling, misalignment-based shuttling and contact-based shuttling. Planet projection schemes on the left.

The tilting mode for the planet has an effect on the contact force exerted on the gear teeth and on the misalignment. *Figure 6.19* shows the Campbell diagrams for the dynamic normal contact force and the POA angular misalignment relative to the sun-planet gear mesh. Amplification is revealed in correspondence of the tilting mode resonance frequency if shuttling is taken into account, and in correspondence of the torsional mode resonance frequency for all the cases.

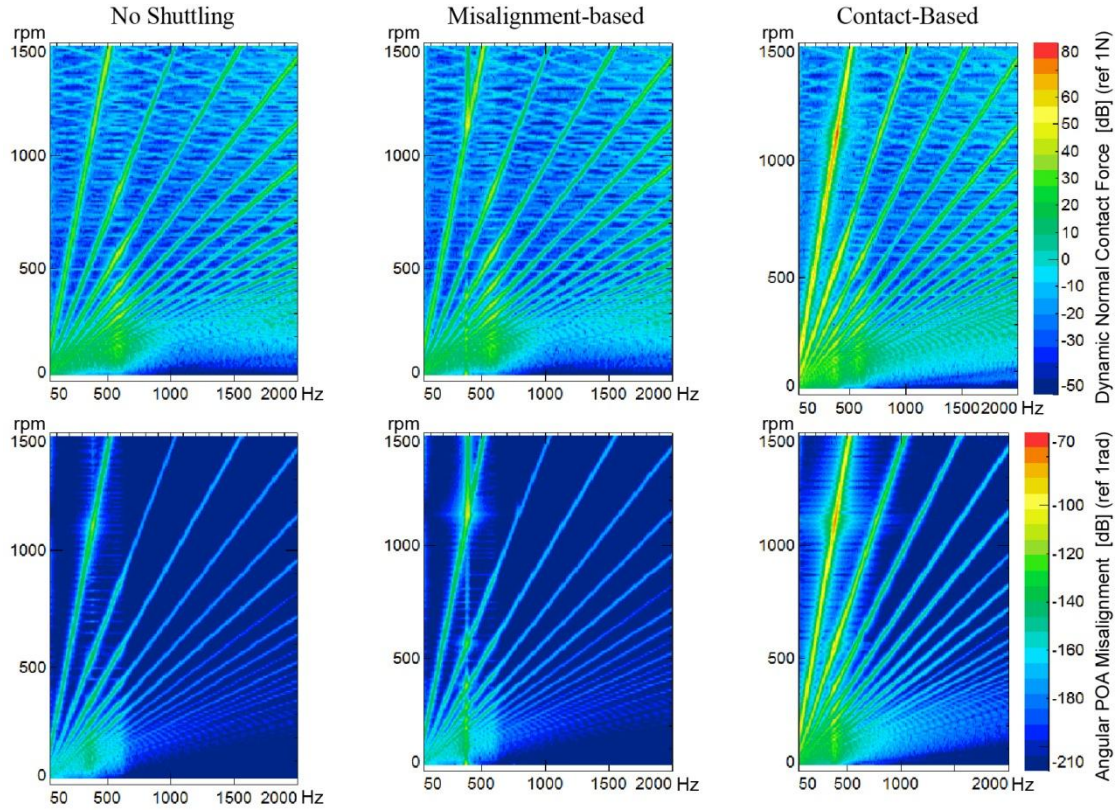

Figure 6.19 – Campbell diagrams for the dynamic normal contact force and the POA angular misalignment, between the sun and the analysed planet for the cases of no shuttling, misalignment-based shuttling and contact-based shuttling.

Comparing the tangential bearing forces in time domain allows the asymmetry in the dynamic response to become more evident (*Figure 6.20*). When shuttling is taken into account, force amplification for the bearing number 2 is considerably higher than for the bearing number 1. This phenomenon happens on the less loaded bearing, as load sharing is altered by the POA misalignment.

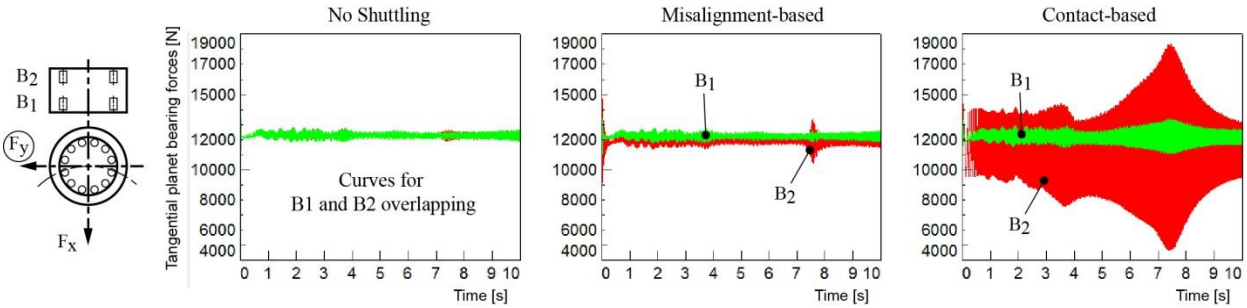

Figure 6.20 – Time traces for the tangential planet bearing forces on bearing number 1 and 2, compared by shuttling case on the same scale. Planet projection schemes on the left.

Radial forces (*Figure 6.21*) have opposite sign and same magnitude, since they are caused by the tilting moment due to the axial contact force components. Their dynamic behaviour is symmetric for bearing number 1 and 2. Significant force amplification occurs if shuttling is taken into account, being more severe for the contact-based formulation.

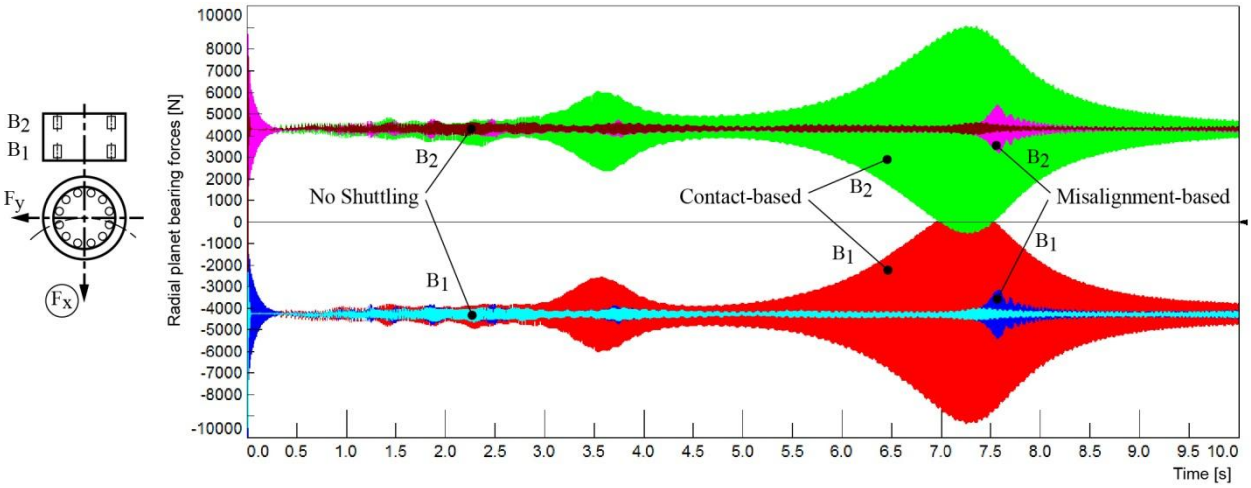

Figure 6.21 – Time traces for the radial planet bearing forces on bearing number 1 and 2 for all the shuttling cases. Planet projection schemes on the left.

The simulation completed in circa 6 minutes in each of the three cases, calculating circa 5×10^5 time steps (2×10^{-5} average time step size) using a PECE solver in the commercial multibody simulation software LMS Virtual.Lab Motion, running on a mobile workstation Intel Core i7 Q740 (1.73 GHz) having 4 GB RAM.

Conclusions on the results are to be considered based on the assumptions of each shuttling formulation. The contact-based shuttling formulation is accounting for instantaneous operating conditions and three-dimensional contact between the teeth. A faster, but simplified, way to account for shuttling is using the formulation based on the angular POA misalignment. In this case the shuttling excitation is connected to the gear contact load variations, which trigger variations in the bearing deflections and the misalignment itself. This formulation can be used for preliminary assessment of shuttling sensitivity.

Simulations show how the excitation of planet tilting modes does not happen when shuttling is not considered in the simulation. In relation to this aspect, planet bearing forces, which are sensitive to tooth load distribution, show significantly higher variation when shuttling phenomena are taken into account. Aside the dynamic effects on bearing forces, an average POA angular misalignment is caused by a tilting moment which is arising when the gears are helical. This misalignment moves the contact point towards one of the faces and makes uneven the planet bearing load sharing (fraction of the gear contact force carried by each of the two bearing).

An asymmetry in the dynamic behaviour of the tangential component for the bearing forces appeared between bearing number 1 and 2. The less loaded bearing shows considerably higher force amplification when the excitation frequency matches the one of the planet tilting mode. This phenomenon does not happen for the radial component of the bearing forces. Further investigation will be performed to better understand this asymmetry.

Chapter 7.
Conclusions

In this PhD disseration an efficient element accounting for 3D effects of gear contact has been proposed in multibody environment for the simulation of internal and external spur and helical gears. Gears are modelled taking into account the instantaneous operating conditions, defined as relative positioning and instantaneous transmitted load, in a scalable way. Ranges for the operating conditions are discretised and mesh stiffness is calculated for each combination, in a pre-processing step, using a 3D static contact analysis tool. The LDP software from the OSU Gearlab [141] has been adopted to execute this pre-processing step, although several other specialized tools or FE packages can be used to perform similar calculations. The generated dataset is stored in look-up tables which are interpolated during the multibody dynamic simulation. This proposed approach proved to have high computational efficiency due to the hypothesis of rigid bodies and since contact must not be solved, but only interpolated, at each timestep of the simulation. Since the complexity of a fully-flexible approach, as it happens for FE approaches, would be prohibitive for the simulation time, the rigid-body hypothesis is currently needed to efficiently allow speed-sweep simulations and simulate dynamic interactions between the gears, the structure and the power source/user at the assembly level. Considering the dynamic response which can be obtained for the full assembly, two additional main advantages of the proposed element can be highlighted. Firstly, the level of detail for the proposed element is scalable depending on the simulation purposes, since dynamic effects of each operating condition and shuttling can be enabled or disabled independently, allowing to perform sensitivity analyses to the operating conditions. Secondly, the proposed element can be used in a general multibody model which has no a-priori restriction, as instead happens with analytical models. Simulation cases have been discussed based on a reference helical gear pair. Results showed: the dynamic effects due to inertia and

damping, the non-linear load-dependent effects of microgeometric modifications and misalignment influences on DTE, axial positioning of the contact point (shuttling). The results are in line with theoretical predictions. Future steps are the validation of the methodology based on experimental results, friction modelling and single-tooth loading calculation and accounting for unequal tooth spacing (index error). Dedicated focus will be also reserved to the complex gear interactions arising for planetary gear systems, which represent a widespread configuration for transmitting mechanical power.

Chapter 8.

Publications list

International peer-reviewed journal articles

A. Palermo, D. Mundo, R. Hadjit, W. Desmet, Multibody element for spur and helical gear meshing based on detailed three-dimensional contact calculations, *Mechanism and Machine Theory*, [accepted]

Full papers in proceedings of international conferences

A. Palermo, D. Mundo, R. Hadjit, P. Mas, W. Desmet, Multibody modelling of shuttling excitation in spur and helical geared transmissions, *Proceedings of the ISMA 2012 Conference*, Leuven, 2012.

A. Palermo, D. Mundo, R. Hadjit, A. S. Lentini, Effects of variable loads and misalignments on gear noise and vibration through multibody simulation based on transmission error, *Proceedings of the ECCOMAS Conference on Multibody Dynamics*, Bruxelles, 2011.

A. Palermo, D. Mundo, A. S. Lentini, R. Hadjit, W. Desmet, Gear noise evaluation through multibody TE-based simulations, *Proceedings of the ISMA 2010 Conference*, Leuven, 2010.

Oral presentations at international conferences

A. Palermo, D. Mundo, R. Hadjit, A.S. Lentini, W. Desmet, Effects of real-case parameters on gear N&V through efficient multibody TE-based simulations, *LMS European Vehicle Conference*, Munich, 2011.

Chapter 9.

References

[1] P. Velex, A. Singh, Top gear, *Journal of Mechanical Design*, 132, (2010) 060301-1-2.

[2] K. Efstathiou, A. Basiakoulis, M. Efstathiou, M. Anastasiou, J.H. Seiradakis, Determination of the gears geometrical parameters necessary for the construction of an operational model of the Antikythera Mechanism, *Mechanism and Machine Theory*, 52 (2012) 219–231.

[3] T. Freeth, Y. Bitsakis, X. Moussas, J. H. Seiradakis, A. Tselikas, H. Mangou, M. Zafeiropoulou, R. Hadland, D. Bate, A. Ramsey, M. Allen, A. Crawley, P. Hockley, T. Malzbender, D. Gelb, W.Ambrisco, M. G. Edmunds, Decoding the ancient Greek astronomical calculator known as the Antikythera Mechanism, *Nature*, 444 (2006) 587-591.

[4] J. Helsen, The Dynamics of High Power Density Gear Units with Focus on the Wind Turbine Application, *PhD dissertation, Katholieke Universiteit Leuven, Department of Mechanical Engineering, Division PMA*, Leuven (2012).

[5] J. L. M. Peeters, Simulation of dynamic drive train loads in a wind turbine, *PhD dissertation, Katholieke Universiteit Leuven, Department of Mechanical Engineering, Division PMA*, Leuven (2006).

[6] D. Appleyard, Assessing drivetrain reliability, Renewable Energy World - Wind Technology, November 2011.

[7] US National Renewable Energy Laboratory, Gearbox Reliability Collaborative, www.nrel.gov/wind/grc/

[8] H. N. Ozguven, D. R. Houser, Mathematical models used in gear dynamics – A review, *Journal of Sound and Vibration*, 121, 3 (1988) 383-411.

[9] P. Velex, M. Ajmi, On the modelling of excitations in geared systems by transmission errors, *Journal of Sound and Vibration*, 290 (2006) 882–909.

[10] T. Eritenel, R. G. Parker, Modal properties of three-dimensional helical planetary gears, *Journal of Sound and Vibration*, 325 (2009) 397–420.

[11] V. K. Tamminana, A. Kahraman, S. Vijayakar, A Study of the Relationship Between the Dynamic Factors and the Dynamic Transmission Error of Spur Gear Pairs, *Journal of Mechanical Design*, 129 (2007) 75-84.

[12] R. G. Parker, S. M. Vijayakar, T. Imajo, Non-linear dynamic response of a spur gear pair: modelling and experimental comparisons, *Journal of Sound and Vibration*, 237, 3 (2000) 435-455.

[13] G. Liu, R. G. Parker, Dynamic Modeling and Analysis of Tooth Profile Modification for Multimesh Gear Vibration, *Journal of Mechanical Design*, 130 (2008) 121402-1-13.

[14] S. L. Harris, Dynamic loads on the teeth of spur gears, *Proceedings of the IMechE,* 172 , 1 (1958) 87-112*.*

[15] R. W. Gregory, S. L. Harris, R. G. Munro, Dynamic Behaviour of Spur Gears, *Proceedings of the IMechE, 178 (1963) 207–226.*

[16] J.D. Smith, Gear noise and vibration, *CRC Press*, 2003.

[17] F. L. Litvin, A. Fuentes, Gear Geometry and Applied Theory, *Cambridge University Press*, 2004.

[18] S. P. Radzevich, Dudley's handbook of practical gear design and manufacture*, CRC Press,* 2012.

[19] J. Helsen, F. Vanhollebeke, B. Marrant, F. De Coninck, D. Vandepitte, W. Desmet, Updated wind turbine gearbox multibody model with optimized flexible housing to deliver inputs for acoustic calculations, *Multibody dynamics 2011, ECCOMAS Thematic Conference*, Bruxelles (Belgium).

[20] J. L. Dion, S. Le Moyne, G. Chevallier, H. Sebbah, Gear impacts and idle gear noise: Experimental study and non-linear dynamic model, *Mechanical Systems and Signal Processing*, 23 (2009) 2608–2628.

[21] P. Ziegler, P. Eberhard, B. Schweizer, Simulation of impacts in geartrains using different approaches, *Archive of Applied Mechanics*, 76 (2006) 537–548.

[22] A. Kahraman, R. Singh, Non-linear dynamics of a spur gear pair, *Journal of Sound and Vibration*, 142, 1 (1990) 49-75.

[23] H. N. Ozguven, D. R. Houser, Dynamic analysis of high speed gears by using loaded static transmission error, *Journal of Sound and Vibration*, 125, 1 (1988) 71–83.

[24] J. A. Morgan, M. R. Dhulipudi, R. Y. Yakoub, A. D. Lewis, Gear Mesh Excitation Models for Assessing Gear Rattle and Gear Whine of Torque Transmission Systems with Planetary Gear Sets, *SAE Technical Paper* (2007) 2007-01-2245.

[25] O.J. Harris, M. Douglas, B.M. James, A.M. Wooley, L.W. Lack, Predicting the effects of transmission housing flexibility and bearing stiffness on gear mesh misalignment and transmission error, *2nd MSC Worldwide Automotive Conference (2000)*, Dearborn, MI (USA).

[26] B. Campbell, W. Stokes, G. Steyer, M. Clapper, Gear Noise Reduction of an Automatic Transmission Trough Finite Element Dynamic Simulation, *SAE Technical Paper* (1997) 971966.

[27] K. Umezawa, T. Suzuki, T. Sato, Vibration of Power Transmission Helical Gears (Approximate Equation of Tooth Stiffness), *Bulletin of the JSME*, 251, 29 (1986) 1605-1611.

[28] Y. Cai, T. Hayashi, The Linear Approximated Equation of Vibration of a Pair of Spur Gears (Theory and Experiment), *Journal of Mechanical Design*, 116 (1994) 558-564.

[29] Y. Cai, Simulation on the Rotational Vibration of Helical Gears in Consideration of the Tooth Separation Phenomenon (A New Stiffness Function of Helical Involute Tooth Pair), *Journal of Mechanical Design*, 117 (1995) 460-469.

[30] V. K. Ambarisha, R. G. Parker, Nonlinear dynamics of planetary gears using analytical and finite element models, *Journal of Sound and Vibration*, 302 (2007) 577-595.

[31] P. Velex, M. Ajmi, On the modelling of excitations in geared systems by transmission errors, *Journal of Sound and Vibration*, 290 (2006) 882–909.

[32] T. Eritenel, R. G. Parker, Modal properties of three-dimensional helical planetary gears, J. Sound Vib. 325 (2009) 397–420.

[33] T. Nishino, Vibration analysis of the helical gear system using the integrated excitation model, *Journal of Advanced Mechanical Design, Systems, and Manufacturing*, 4, 1 (2007) 541-552.

[34] M. Kubur, A. Kahraman, D. M. Zini, K. Kienzle, Dynamic Analysis of a Multi-Shaft Helical Gear Transmission by Finite Elements: Model and Experiment, *Journal of Vibration and Acoustic*, 126 (2004) 398-406.

[35] T. Lin, H. Ou, R. Li, A finite element method for 3D static and dynamic contact/impact analysis of gear drives, *Computer Methods in Applied Mechanics and Engineering*, 196 (2007) 1716–1728.

[36] S. Li, Experimental investigation and FEM analysis of resonance frequency behavior of three-dimensional thin-walled spur gears with a power-circulating test rig, *Mechanism and Machine Theory*, 43 (2008) 934–963.

[37] R. R. Craig, M. C. C. Bampton, Coupling of Substructures for Dynamic Analysis, *Journal of AIAA*, 7, 6 (1968) 1313-1319.

[38] R. R. Craig, Coupling of substructures for dynamic analysis, *AIAA Journal*, 6 (1968) 1313-1319.

[39] A. Cardona, Three-dimensional gears modelling in multibody systems analysis, *International Journal for Numerical Methods in Engineering*, 40 (1997) 357-381.

[40] S. Ebrahimi, P. Eberhard, Rigid-elastic modeling of meshing gear wheels in multibody systems, *Multibody System Dynamics*, 16 (2006) 55–71.

[41] S. Mahalingam, R. E. D. Bishop, Dynamic loading of gear teeth, *Journal of Sound and Vibration*, 36, 2 (1974) 179-189.

[42] Umezawa K.: Fundamental investigation on the design of power transmission helical gears, *Doctoral dissertation, Tokyo Institute of Technology*, 1972.

[43] Umezawa K., Deflection and moments due to a concentrated load on a rack-shaped cantilever plate with finite width for gears, *Bulletin of JSME*, 15, 79 (1972) 116.

[44] Umezawa K., Ishikawa J., Deflection due to contact between gear teeth with finite width, *Bulletin of JSME*, 16, 97 (1973) 1085.

[45] Umezawa K., The meshing test on helical gears under load transmission (3rd report: the static behaviours of driven gear), *Bulletin of JSME*, 17, 112 (1974) 1348.

[46] G. W. Blankenship, A. Kahraman, Steady state forced response of a mechanical oscillator with combined parametric excitation and clearance type non-linearity, *Journal of Sound and Vibration*, 185, 5 (1995) 743-765

[47] G. W. Blankenship, A. Kahraman, Interactions between commensurate parametric and forcing excitations in a system with clearance, *Journal of Sound and Vibration*, 194, 3 (1996) 317-336.

[48] A. Andersson, L. Vedmar, A dynamic model to determine vibrations in involute helical gears, *Journal of Sound and Vibration*, 260 (2003) 195–212.

[49] H. H. Lin, F. B. Oswald, D. P. Townsend, Dynamic loading of spur gears with linear or parabolic tooth profile modifications, *Mechanism and Machine Theory*, 29, 8 (1994) 1115-1129.

[50] M. Faggioni, F. S. Samani, G. Bertacchi, F. Pellicano, Dynamic optimization of spur gears, *Mechanism and Machine Theory*, 46 (2011) 544–557.

[51] G. Bonori, M. Barbieri, F. Pellicano, Optimum profile modifications of spur gears by means of genetic algorithms, *Journal of Sound and Vibration*, 313 (2008) 603–616.

[52] M. R. Kang, A. Kahraman, Measurement of vibratory motions of gears supported by compliant shafts, *Mechanical Systems and Signal Processing*, 29 (2012) 391–403.

[53] H. N. Ozguven, A non-linear mathematical model for dynamic analysis of spur gears including shaft and bearing dynamics, *Journal of Sound and Vibration*, (1991) 145(2), 239-260.

[54] L. Walha, T. Fakhfakh, M. Haddar, Nonlinear dynamics of a two-stage gear system with mesh stiffness fluctuation, bearing flexibility and backlash, *Mechanism and Machine Theory*, 44 (2009) 1058–1069.

[55] C. Siyu, T. Jinyuan, L. Caiwang, W. Qibo, Nonlinear dynamic characteristics of geared rotor bearing systems with dynamic backlash and friction, *Mechanism and Machine Theory*, 46, 4 (2011) 466–478.

[56] A. Kahraman, Dynamic analysis of a multi-mesh helical gear train, *Journal of Mechanical Design*, 116 (1994) 706-712.

[57] M. Kubur, A. Kahraman, D. M. Zini, K. Kienzle, Dynamic Analysis of a Multi-Shaft Helical Gear Transmission by Finite Elements: Model and Experiment, *Journal of Vibration and Acoustics*, 126 (2004) 398-406.

[58] P. Velex, M. Maatar, A mathematical model for analyzing the influence of shape deviations and mounting errors on gear dynamic behaviour, *Journal of Sound and Vibration*, 191, 5 (1996) 518-559.

[59] S. Baud, P. Velex, Static and Dynamic Tooth Loading in Spur and Helical Geared Systems-Experiments and Model Validation, *Journal of Mechanical Design*, 124 (2002) 334-346.

[60] M. Ajmi, P. Velex, A model for simulating the quasi-static and dynamic behaviour of solid wide-faced spur and helical gears, *Mechanism and Machine Theory*, 40 (2005) 173–190.

[61] T. Eritenel, R. G.Parker, Modal properties of three-dimensional helical planetary gears, *Journal of Sound and Vibration*, 325 (2009) 397–420.

[62] T. Eritenel, R. G.Parker, An investigation of tooth mesh nonlinearity and partial contact loss in gear pairs using a lumped-parameter model, *Mechanism and Machine Theory*, 56 (2012) 28–51.

[63] J. Lin, R. G. Parker, Planetary gear parametric instability caused by mesh stiffness variation, *Journal of Sound and Vibration*, 249 ,1 (2002) 129-145.

[64] R. G. Parker , J. Lin, Mesh Phasing Relationships in Planetary and Epicyclic Gears, *Journal of Mechanical Design*, 126 (2004) 365-370.

[65] A. Al-shyyab, A. Kahraman, A non-linear dynamic model for planetary gear sets, *Proceedings of the IMechE, Part K*, 221 (2007) 567-576.

[66] A. Singh, Load sharing behavior in epicyclic gears: Physical explanation and generalized formulation, *Mechanism and Machine Theory*, 45 (2010) 511–530.

[67] A. Kahraman, Natural modes of planetary gear trains, *Journal of Sound and Vibration*, 173, 1 (1994) 125-130.

[68] D. L. Seager, Conditions for the neutralization of excitation by the teeth in epicyclic gearing, *Journal of Mechanical Engineering Science*, 17, 5 (1975) 293-198.

[69] J. Lin, R. G. Parker, Analytical characterization of the unique properties of planetary gear free vibration, *Journal of Vibration and Acoustics*, 121 (1999) 316-321.

[70] J. Lin, R. G. Parker, Structured vibration characteristics of planetary gears with unequally spaced planets, *Journal of Sound and Vibration*, 233, 5 (2000) 921-928.

[71] F. Chaari, T. Fakhfakh, R. Hbaieb, J. Louati, M. Haddar, Influence of manufacturing errors on the dynamic behavior of planetary gears, *International Journal of Advanced Manufacturing Technology*, 27 (2006) 738–746.

[72] A. Kahraman, Planetary gear train dynamics, *Journal of Mechanical Design*, 116 (1994) 713-720.

[73] P. Velex, L. Flamand, Dynamic Response of Planetary Trains to Mesh Parametric Excitations, *Journal of Mechanical Design*, 118 (1996) 7-14.

[74] T. F. Conry, A. Seireg, A mathematical programming technique for the evaluation of load distribution and optimal modifications for gear systems, *Journal of Engineering for Industry*, (1973) 1115-1122.

[75] M. E. Stegemiller, D. R. Houser, A Three-Dimensional Analysis of the Base Flexibility of Gear Teeth, *Journal of Mechanical Design*, 115 (1993) 186-192.

[76] J. Wang, I. Howard, Finite Element Analysis of High Contact Ratio Spur Gears in Mesh, *Journal of Tribology*, 127 (2005) 469-483.

[77] S. Li, Effects of machining errors, assembly errors and tooth modifications on loading capacity, load-sharing ratio and transmission error of a pair of spur gears, *Mechanism and Machine Theory*, 42 (2007) 698–726.

[78] J. I. Pedrero, M. Pleguezuelos, M. Artés, J. A. Antona, Load distribution model along the line of contact for involute external gears, *Mechanism and Machine Theory*, 45, 5 (2010) 780–794.

[79] P. Sainsot, P. Velex, O. Duverger, Contribution of Gear Body to Tooth Deflections – A New Bidimensional Analytical Formula, *Journal of Mechanical Design*, 126 (2004) 748-752.

[80] T. Eritenel, R. G. Parker, A static and dynamic model for three-dimensional, multi-mesh gear systems, *ASME 2005 International Design Engineering Technical Conferences and Computers and Information in Engineering Conference*.

[81] T. Lin, H. Ou, R. Li, A finite element method for 3D static and dynamic contact/impact analysis of gear drives, *Computational Methods in Applied Mechanics and Engineering*, 196 (2007) 1716–1728.

[82] P. Ziegler, P. Eberhard, B. Schweizer, Simulation of impacts in geartrains using different approaches, *Archive of Applied Mechanics*, 76 (2006) 537–548.

[83] P. Ziegler, P. Eberhard, Simulative and experimental investigation of impacts on gear wheels, *Computational Methods in Applied Mechanics and Engineering*, 197 (2008) 4653–4662.

[84] G. H. K. Heirman, T. Tamarozzi, W. Desmet, Static modes switching for more efficient flexible multibody simulation, *International Journal for Numerical Methods in Engineering*, 87 (2011).

[85] T. Tamarozzi, P. Ziegler, P. Eberhard, W. Desmet, On the Applicability of Static Modes Switching in Gear Contact, *The 2nd Joint International Conference on Multibody System Dynamics*, 2012, Stuttgart, Germany.

[86] V. Abousleiman, P. Velex, A hybrid 3D finite element/lumped parameter model for quasi-static and dynamic analyses of planetary/epicyclic gear sets, *Mechanism and Machine Theory*, 41 (2006) 725–748.

[87] S. M. Vijayakar, A combined surface integral and finite element solution for a three-dimensional contact problem, *International Journal for Numerical Methods in Engineering*, 31 (1991) 524-546.

[88] R. G. Parker, V. Agashe, S. M. Vijayakar, Dynamic Response of a Planetary Gear System using a Finite Element/Contact Mechanics Model, *Journal of Mechanical Design*, 122 (2000) 304-310.

[89] Alberto Cardona, Three-dimensional gears modelling in multibody systems analysis, *International Journal for Numerical Methods in Engineering*, 40 (1997) 357-381.

[90] S. Ebrahimi, P. Eberhard, Rigid-elastic modeling of meshing gear wheels in multibody systems, *Multibody System Dynamics*, 16 (2006) 55–71.

[91] J. Pears, S. Curtis, A. Poon, A. Smith, D. Poon, D. Palmer, Investigation of Methods to Predict Parallel and Epicyclic Gear Transmission Error, *2005 SAE World Congress Detroit*, Michigan, (2005-01-1818).

[92] S. Mulski, Simpack modeling elements, *Simpack Wind and Drivetrain Conference*, 2010.

[93] B. K. Han, M. K. Cho, C. Kim, C. H. Lim, J. J. Kim, Prediction of vibrating forces on meshing gears for a gear rattle using a new multi-body dynamic model, *International Journal of Automotive Technology*, 10, 4 (2009) 469−474.

[94] Z. Neusser, M. Sopouch, T. Schaffner, H. H. Priebsch, Multi-body Dynamics Based Gear Mesh Models for Prediction of Gear Dynamics and Transmission Error, *SAE Technical Paper 2010-01-0897*.

[95] G. Lethé, J. De Cuyper, J. Kang, M. Furman, D. Kading, Simulating dynamics, durability and noise emission of wind turbines in a single CAE environment, *Journal of Mechanical Science and Technology*, 23 (2009) 1089-1093.

[96] B. James, M. Douglas, Development of a gear whine model for the complete transmission system, *SAE Technical Paper 2002-01-0700*.

[97] B. Schlecht, State-of-the-Art Techniques used for Determining Reliable Load Assumptions in Wind Turbines using SIMPACK, *SIMPACK Conference: Wind and Drivetrain 2010*.

[98] Contact Analysis in the Cylindrical Gear Calculation, *KissSoft AG*, 2011.

[99] B. R. Höhn, P. Oster, S. Radev, T. Griggel, Tooth flank corrections against noise excitation of spur gears in theory and practice. Designing low-noise gears with the computer program DZP. Transmission Vibration Meeting 2006 VDI Reports (2006) 235-250. (*In German*)

[100] H. Vinayak,R. Singh, Multi-body dynamics and modal analysis of compliant gear bodies, *Journal of Sound and Vibration*, 210, 2 (1998) 171-214.

[101] O. Lundvall, N. Stromberg, A. Klarbring, A flexible multi-body approach for frictional contact in spur gears, *Journal of Sound and Vibration*, 278 (2004) 479–499.

[102] P. Velex, M. Ajmi, Dynamic tooth loads and quasi-static transmission errors in helical gears – Approximate dynamic factor formulae, *Mechanism and Machine Theory*, 42 (2007) 1512–1526.

[103] I. Gonzalez-Perez, J. L. Iserte, A. Fuentes, Implementation of Hertz theory and validation of a finite element model for stress analysis of gear drives with localized bearing contact, *Mechanism and Machine Theory*, 46, 6 (2011) 765–783.

[104] J.J. Zhanga, I.I. Esat, Y.H. Shi, Load analysis with varying mesh stiffness, *Computers and Structures*, 70 (1999) 273-280.

[105] P. Davoli, E. Conrado, K. Michaelis, Recognizing gear failures, *Machine Design*, 06/2007 Issue.

[106] A. Raad, J. Antoni, M. Sidahmed, Indicators of cyclostationarity: Theory and application to gear fault monitoring, *Mechanical Systems and Signal Processing*, 22 (2008) 574–587.

[107] G. Dalpiaz, A. Rivola, R. Rubini, Effectiveness and sensitivity of vibration processing techniques for local fault detection in gears, *Mechanical Systems and Signal Processing*, 14, 3 (2000) 387-412.

[108] N. Baydar, A. Ball, Detection of gear failures via vibration and acoustic signals using wavelet transform, *Mechanical Systems and Signal Processing*, 17, 4 (2003) 787–804.

[109] F. Chaari, W. Baccar, M. S. Abbes, M. Haddar, Effect of spalling or tooth breakage on gearmesh stiffness and dynamic response of a one-stage spur gear transmission, *European Journal of Mechanics A/Solids*, 27 (2008) 691–705.

[110] C. Brecher, C. Gorgels, C. Carl, M. Brumm, Benefit of Psychoacoustic Analyzing Methods for Gear Noise Investigation, *Gear Technology*, August 2011.

[111] M. S. Abbes, S. Bouaziz, F. Chaari, M. Maatar, M. Haddar, An acoustic–structural interaction modelling for the evaluation of a gearbox-radiated noise, *International Journal of Mechanical Sciences*, 50 (2008) 569–577.

[112] B. James, M. Douglas, Development of a Gear Whine Model for the Complete Transmission System, *SAE Technical Paper 2002-01-0700*.

[113] Y. Cheng, T. Abe, B. K. Wilson, Automatic Transmission Gear Whine Simulation and Test Correlation, *SAE Technical Paper 2005-01-2290*.

[114] J. L. Dion, S. Le Moyne, G. Chevallier, H. Sebbah, Gear impacts and idle gear noise: Experimental study and non-linear dynamic model, *Mechanical Systems and Signal Processing*, 23 (2009) 2608-2628.

[115] R. Y. Yakoub, M. Corrado, A. Forcelli, T. Pappalardo, S. Dutre, Prediction of System-Level Gear Rattle Using Multibody and Vibro-Acoustic Techniques, *SAE Technical Paper 2004-32-0063*.

[116] N. C. Otto, R. Simpson, J. Wiederhold, Electric Vehicle Sound Quality, *SAE Technical Paper 1999-01-1694*.

[117] M. Bodden, R. Heinrichs, Analysis of the time structure of gear rattle, *INTERNOISE, New Zealand Acoustical Society*, 2 (1998) 1273-1278.

[118] R. Seebacher, Dual mass flywheel, *LuK Symposium* 1998.

[119] http://auto.howstuffworks.com/transmission4.htm

[120] International Standard IEC 61400 for Wind turbine generator systems, Part 11 - Acoustic noise measurement techniques, 2006.

[121] ZF 8HP 8-Speed Automatic Transmission, Product Brochure.

[122] Toyota USA Newsroom, *http://pressroom.toyota.com/*

[123] W. Musial, S. Butterfield, B. McNiff, Improving Wind Turbine Gearbox Reliability, *European Wind Energy Conference 2007*, Milan, Conference Paper NREL/CP-500-41548.

[124] A. Greenhill, Global Trends and Challenges for Driveline Engineers, *Romax European Summit 2011*, Frankfurt.

[125] GE Drivetrain Technologies, Wind Turbine Gearbox Brochure.

[126] J. Coultate, Wind Turbine Gearbox Durability, *Wind Systems Magazine*, July/August 2009 Issue.

[127] R. G. Parker, X. Wu, Parametric Instability of Planetary Gears Having Elastic Continuum Ring Gears, *Journal of Vibration and Acoustics*, 134 (2012) 041011-1-11.

[128] T. C. Lim, R. Singh, Vibration Transmission Through Rolling Element Bearings, Part I: Bearing Stiffness Formulation, *Journal of Sound and Vibration*, 139, 2 (1990) 179-199.

[129] T. C. Lim, R. Singh, Vibration Transmission Through Rolling Element Bearings, Part II: System Studies, *Journal of Sound and Vibration*, 139, 2 (1990) 201-225.

[130] T. C. Lim, R. Singh, Vibration Transmission Through Rolling Element Bearings, Part III: Geared Rotor System Studies, *Journal of Sound and Vibration*, 151, 1 (1991) 31-54.

[131] Y. Guo, R. G. Parker, Stiffness matrix calculation of rolling element bearings using a finite element/contact mechanics model, *Mechanism and Machine Theory*, 51 (2012) 32–45.

[132] A. Gunduz,J. T. Dreyer, R. Singh, Effect of bearing preloads on the modal characteristics of a shaft-bearing assembly: Experiments on double row angular contact ball bearings, *Mechanical Systems and Signal Processing*, 31 (2012) 176–195.

[133] M. Arra, L'elicottero, *Hoepli editore*, 2001 (In Italian)

[134] R. B. Randall, State of the Art in Monitoring Rotating Machinery – Part 1, *Sound and Vibration*, March 2004 Issue, 14-20.

[135] R. B. Randall, State of the Art in Monitoring Rotating Machinery – Part 2, *Sound and Vibration*, May 2004 Issue, 10-16

[136] P. D. Samuel, D. J. Pines, A review of vibration-based techniques for helicopter transmission diagnostics, *Journal of Sound and Vibration*, 282 (2005) 475–508.

[137] E. Mucchi, A. Vecchio, Acoustical signature analysis of a helicopter cabin in steady-state and run up operational conditions, *Proceedings of the ISMA Conference 2008*, Leuven, 1345-1358.

[138] AgustaWestland AW101 VVIP Helicopter, Product Brochure.

[139] A. Rezaei, A. Dadouche, Development of a turbojet engine gearbox test rig for prognostics and health management, *Mechanical Systems and Signal Processing*, 33 (2012) 299–311.

[140] Rolls-Royce, The Jet Engine, *Key Publishing*, 2005.

[141] R. Guilbault, S. Lalonde, M. Thomas, Nonlinear damping calculation in cylindrical gear dynamic modeling, Journal of Sound and Vibration, 331 (2012) 2110–2128.

[142] Load Distribution Program, User's Manual, *Ohio State University GearLab* (2002).

[143] C. Weber, The deformations of loaded gears and the effect on their load-carrying capacity, *Sponsored research, British Dept. of Scientific and Industrial Research*, Report No. 3. (1949).

[144] D. Yakubek, Plate bending and finite element analysis of spur and helical gear tooth deflection, *AGMA paper No. 85FTM4* (1985).

[145] H. Yau, Analysis of shear effect on gear tooth deflections using Rayleigh-Ritz energy method, *Master's Thesis, The Ohio State University* (1987).

[146] M.E. Stegemiller, The effects of base flexibility on thick beams and plates used in gear tooth deflection models, *Master's Thesis, The Ohio State University* (1986).

[147] M. W. Berry, K. S. Minser, Algorithm 798: High-Dimensional Interpolation Using the Modified Shepard Method, *ACM Transactions on Mathematical Software*, 25, 3 (1999) 353–366.

[148] S. Li, Experimental investigation and FEM analysis of resonance frequency behavior of three-dimensional, thin-walled spur gears with a power-circulating test rig, *Mechanism and Machine Theory*, 43 (2008) 934–963.

[149] D.R. Houser, J. Harianto, D. Talbot, Gear mesh misalignment, *Gear Solutions*, 6 (2006) 34-43.

[150] R.W. Cornell, Compliance and Stress Sensitivity of Spur Gear Teeth, *Journal of Mechanical Design*, 103 (1981) 447.

[151] H. Akima, A new method of interpolation and smooth curve fitting based on local procedures, *Journal of the ACM*, 17, 4 (1970) 589-602.

[152] F. Oyague, Gearbox Reliability Collaborative Experimental Data Overview and Analysis, *NREL Presentation,* PR-500-48176, (2010).

[153] F. Oyague, Gearbox Reliability Collaborative Description and Loading, *NREL Technical Report*, TP-5000-47773, (2011).

[154] J. L. M. Peeters, D. Vandepitte, P. Sas, Analysis of Internal Drive Train Dynamics in a Wind Turbine, *Wind Energy*, 9, 1 (2006) 141-161.

[155] F. Oyague, C. P. Butterfield, S. Sheng, Gearbox Reliability Collaborative Analysis Round Robin, *Proceedings of the Windpower Conference*, Chicago (2009), NREL Conference Paper CP-500-45325.